8 The Neoarchaean Limpopo Orogeny: Exhumation and Regional-Scale Gravitational Crustal Overturn Driven by a Granulite Diapir

Dirk D. van Reenen, C. Andre Smit, Alexei L. Perchuk, Jan M. Huizenga, Oleg G. Safonov, and Taras V. Gerya

Abstract

Integrated geological, geochronological and geophysical data from the Neoarchaean Limpopo Complex (LC) and adjacent granite-greenstone terrane of the Northern Kaapvaal Craton (NKVC) demonstrates the following three key features. (1) The LC-NKVC tectonic boundary defined by the Hout River Shear Zone (HRSZ) played a fundamental role in establishing high-grade metamorphic domains in the Southern Marginal Zone (SMZ) of the LC. These domains are characterized by their specific retrograde *P-T* evolution, (2) Near-isobaric southward thrusting of a hot allochthonous SMZ nappe with imbedded steeply plunging folds and steep shear zones against and over the NKVC along the HRSZ before ca. 2.68 Ga occurred as a consequence of steep exhumation within the Central Zone (CZ) at 2.72–2.62 Ga. (3) Initial exhumation of the CZ to mid-crustal levels before ca. 2.68 Ga was associated with isoclinal folding and melt-weakened domes and directed the southwards channelling of the hot nappe. Final exhumation of the CZ to the upper crust at 2.65–2.62 Ga was driven by granitic diapirism and the formation of shear-related, mega-scale closed structures. These features favour an intracrustal Neoarchaean Limpopo orogeny as the result of a granulite diapir triggered by mantle heat-fluid flow underneath the CZ at 2.72–2.62 Ga. The data is neither compatible with continent collisional models nor with an Archean accretionary orogen along the northern edge of the Kaapvaal Craton that is linked to the collision of the Pietersburg Block with the CZ.

Keywords

Limpopo orogeny • Granulite diapir • Granitic diapirism • Regional-scale gravitational crustal overturn • High-temperature retrograde hydration

D. D. van Reenen (✉) · C. A. Smit · A. L. Perchuk · J. M. Huizenga · O. G. Safonov
Department of Geology, University of Johannesburg, P.O. Box 524 Auckland Park, Johannesburg, 2006, South Africa
e-mail: dirkvr@uj.ac.za

A. L. Perchuk · O. G. Safonov · T. V. Gerya
Geological Faculty, Moscow State University, Leninskie Gory, Moscow, 119234, Russia

J. M. Huizenga
Economic Geology Research Institute (EGRU), College of Science and Engineering, James Cook University, Townsville, QLD 4811, Australia

A. L. Perchuk · O. G. Safonov
Institute of Experimental Mineralogy, Russian Academy of Sciences, Chernogolovka, 142432, Russia

T. V. Gerya
Department of Earth Sciences, Swiss Federal Institute of Technology, 8092 Zurich, Switzerland

8.1 Introduction

Developing a tectono-metamorphic model that explains the evolution of the Neoarchaean Limpopo granulite-facies terrane (the Limpopo Complex) located between the more ancient Kaapvaal and Zimbabwe granite-greenstone cratons of Southern Africa (Fig. 8.1) poses special challenges to researchers dealing with Archaean geology. The following principal features of the high-grade Limpopo Complex (LC) complicate this task. First, original stratigraphic relationships have been completely destroyed by intense deformation, high-grade metamorphism and associated magmatism (e.g. van Reenen et al. 1987; Roering et al. 1992b), and most of the upper crustal cap has been removed (e.g. Roering et al. 1992b). Second, there is no record of the prograde *P-T* path of the high-grade rocks, and no geological evidence for a geological process that might have been associated with the initial formation of the granulite-facies rocks at depth (e.g. van Reenen 1983; van Reenen et al. 1987, 1990; Perchuk et al. 2000a; Smit et al. 2011; Belyanin et al. 2014). Thirdly, the high-grade Central Zone (CZ) of the LC is a polymetamorphic terrane that was extensively overprinted in the Palaeoproterozoic by a younger mainly

A. Kröner and A. Hofmann (eds.), *The Archaean Geology of the Kaapvaal Craton, Southern Africa*, Regional Geology Reviews, https://doi.org/10.1007/978-3-319-78652-0_8

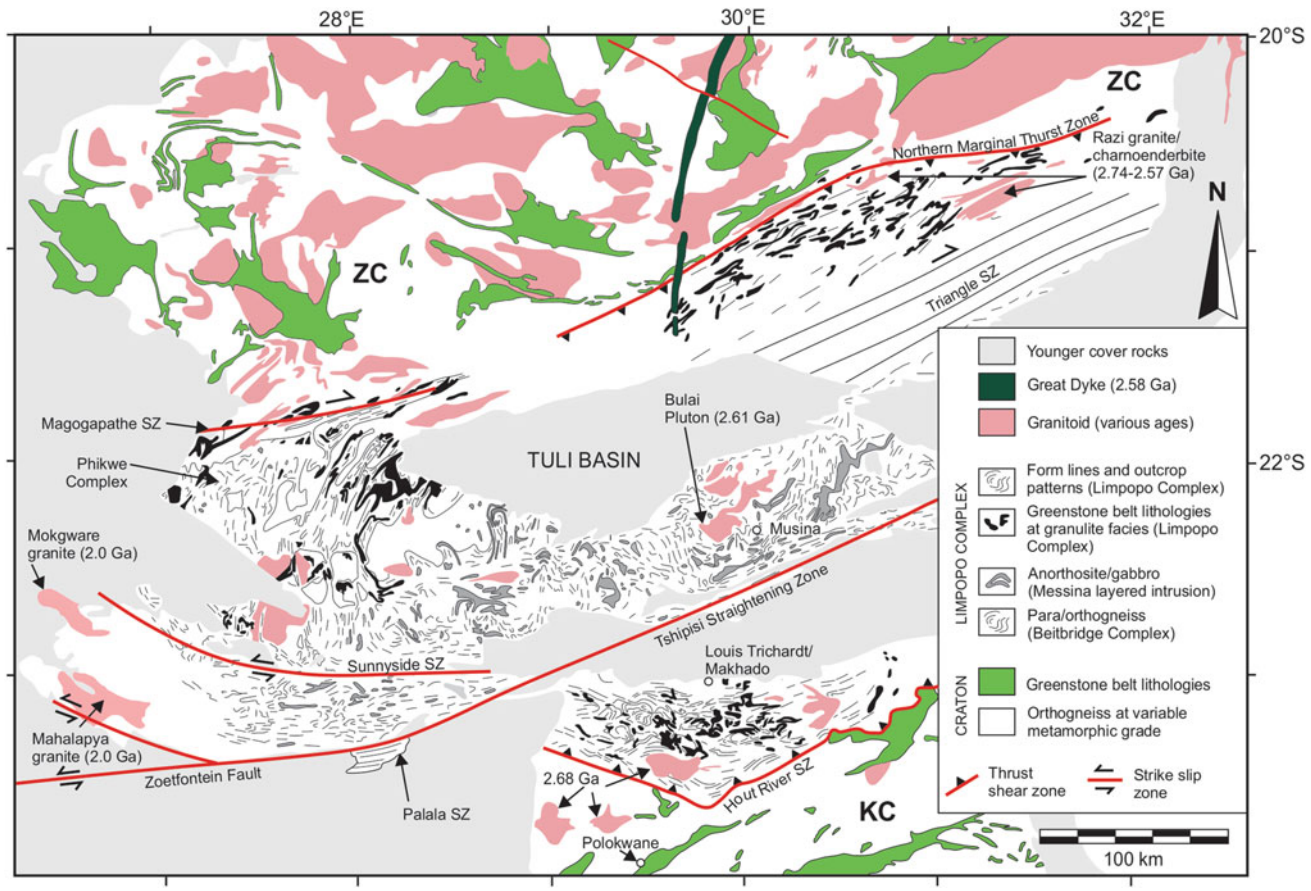

Fig. 8.1 Regional geological map of the Limpopo complex (after Smit et al. 2011) emphasizing the coherent structural style that characterizes the entire granulite-facies terrane, which is in strong contrast with the low-grade linear, greenstone belts on the adjacent cratons. Neoarchaean inward-dipping thrusts separate the granulite-facies terrane from the adjacent low-grade Kaapvaal (KC) and Zimbabwe (ZC) Cratons. The central zone is bounded in the south and the north by Neoarchaean dip-slip shear zones, Triangle SZ in the north and Tshipise Straightening Zone in the south, that were reactivated as strike-slip shear zones in the Palaeoproterozoic

thermal event associated with the formation of discrete shear zones (e.g. van Reenen et al. 2008; Mahan et al. 2011; Smit et al. 2011).

A credible orogenic building model for the LC not only depends on the geological controls imposed by this high-grade rock mass, but also by an understanding of the tectonic relationship with the juxtaposed granite-greenstone terranes, and especially the relationship of the Southern Marginal Zone (SMZ) with the Northern Kaapvaal Craton (NKVC) (e.g. McCourt and van Reenen 1992; Roering et al. 1992a, b; Perchuk et al. 1996, 2000b; van Reenen et al. 2011; Smit et al. 2014).

Kramers et al. (2011) appraised the diversity of published models that have been proposed for the evolution of the LC (Fig. 8.1) since the early 1980s including continent collisional models and gravitational redistribution models linked to the action of granulite diapirs. They concluded that only the model involving Archaean collision of the Kaapvaal and Zimbabwe Cratons (KVC and ZC, respectively) (e.g. van Reenen et al. 1987; De Wit et al. 1992c; Roering et al. 1992a; Treloar et al. 1992; Kramers et al. 2011; Smit et al. 2011) remains a viable working hypothesis. Kramers et al. (2011) further stated that gravitational redistribution in the context of crustal thickening (Gerya et al. 2000; Perchuk and Gerya 2011) is compatible with Neoarchaean collision and can explain important features at the contact of the LC with the granite-greenstone terrane of the NKVC (e.g. van Reenen et al. 2011; Smit et al. 2014).

However, if the LC was formed as the result of a collisional orogeny, a large volume of sediments (ca. 5 million km^3), should have accumulated within 2.72–2.65 Ga as result of erosion of the Limpopo Highland (Gerya et al. 2000; Perchuk and Gerya 2011; Dorland et al. 2004). These sediments have not been documented within the Precambrian successions on either the NKVC or the ZC. No Archaean age zircons were found within the Mesoproterozoic sedimentary formations on the adjacent NKVC, whereas ca. 2.0 Ga detrital zircons are very common in these

rocks (Dorland et al. 2004). These observations imply that no voluminous mountains existed or were eroded above the Neoarchaean Limpopo Complex (Perchuk and Gerya 2011).

Smit et al. (2014) further proposed a link between crustal thickening and gravitational redistribution in the context of Neoarchaean collision by suggesting that southwards channelling of a hot SMZ nappe against and over the adjacent NKVC was controlled by a tectonic 'conveyor belt' mechanism. This concept, as it especially pertains to the SMZ and the relationship with the CZ and with the NKVC, is derived from studies of younger orogens such as the Himalayan–Tibetan and Variscan orogens (e.g. Jamieson et al. 2011 and references therein), and, in particular, the Bohemian Massif (Lexa et al. 2011; Schulmann et al. 2008). These studies suggest that thickened crust heated by radioactive decay would result in partial melting at mid to lower levels, producing melt-rich weakened migmatitic crust. This weakened crust is able to flow outwards onto the lower foreland areas through a process described as mid-crustal heterogeneous channel flow (e.g. Schulmann et al. 2008; Jamieson et al. 2011; Lexa et al. 2011).

Coupled petrological thermomechanical numerical modelling of Precambrian ultrahot orogenies (Perchuk et al. 2018) addresses the issue of the formation of granulite-facies rocks at the base of the crust, including granulites with ultrahigh-temperature (UHT) signatures (e.g. Belyanin et al. 2014; Rajesh et al. 2014). Numerical modelling thus provides a possible source for UHT granulites and a solution to a long-standing question on how granulite-facies terranes developed within moderately thickened crust (e.g. Ellis 1987; Thompson 1990), as has, for instance, been suggested for the LC (e.g. van Reenen et al. 1987; Roering et al. 1992a; Kramers et al. 2011; Smit et al. 2014).

8.1.1 Aims of This Study

The goal of this paper is to demonstrate, based on a large published geological, geochronological, and geophysical database (e.g. van Reenen et al. 1990, 2011, 2014; Kramers et al. 2006, 2011, 2014 and references therein) that exhumation of the LC as a geotectonic entity at 2.72–2.62 Ga was probably controlled by the action of a crustal-scale granulite diaper. This diaper was triggered by deep crustal fluid-heat flow that penetrated the upper crust (e.g. England and Thompson 1984; Pili et al. 1997; Perchuk and Gerya 2011) underneath the present CZ. We propose that this intracrustal process controlled exhumation of granulite-facies rocks that were formed at the base of the crust as the result of an earlier ultrahot orogeny. This caused a two-stage steep exhumation of the CZ at 2.72–2.62 Ga and regional-scale gravitational crustal overturn of complex morphology and dynamics that controlled the southwards channelling of a hot SMZ nappe against and over the adjacent NKVC before ca. 2.68 Ga (the conveyor belt tectonic mechanism of Smit et al. 2014). This gravity-driven tectonic model links the post-peak metamorphic exhumation of the SMZ, CZ and NMZ (Northern Marginal Zone) at 2.72–2.61 Ga and is adapted from gravitational redistribution models first considered by Gerya et al. (2000) and Perchuk and Gerya (2011). We thus propose that the formation and exhumation of the LC granulite-facies rocks should no longer be considered within the context of a collisional orogeny involving crustal thickening at ca. 2.72 Ga (e.g. van Reenen et al. 1987; De Wit et al. 1992c; Roering et al. 1992a; Treloar et al. 1992; Kramers et al. 2011; Smit et al. 2014) but rather a process driven by diapirism.

This paper takes recent publications by Vezinet et al. (2019) and Laurent et al. (2019) in consideration. These authors argue in favour of an Archean accretionary orogen at 2.95–2.75 Ga along the northern edge of the Kaapvaal Craton that involves collision of a proposed Pietersburg Block that includes the SMZ, with the CZ of the LC. Their model depends on a revised lithotectonic model for the SMZ of the LC in which the Nthabalala Shear Zone and not the Hout River Shear Zone (HRSZ) (Fig. 8.2) is taken as the tectonic boundary of the granulite-facies SMZ with the low-grade Pietersburg Block in the south (Laurent et al. 2019). We will demonstrate that the proposed revised lithotectonic model for the SMZ (Vezinet et al. 2018) is in complete disagreement with a large published geological, geochronological, and geophysical dataset showing (1) that the Nthabalala Shear Zone is totally developed within the granulite-facies domain of the SMZ, and (2) that the SMZ is separated from the NKVC in the south by the ca. 2.72 Ga HRSZ (Figs. 8.1, 8.2 and 8.3). We will show that there is no conflict between peak metamorphism dated at ca. 2.72 Ga in the SMZ and the time of a metamorphic event in the CZ that was recently dated at 2.64–2.62 Ga (Kröner et al. 2018). Finally, we will demonstrate that a proposed counterclockwise *P-T* path for the CZ based mainly on the interpretation of pseudosection modelling (Brandt et al. 2018) Ga and linked with burial and prograde heating at 2.64–2.62 Ga (Kröner et al. 2018), is not supported by published data. Integrated field, structural, metamorphic and geochronological data show that the CZ at this time was steeply exhumed towards the northeast (e.g. Smit et al. 2011).

8.1.2 Terminology

To avoid confusion, it is necessary that we explain the specific terminology used in this paper to describe important major geological features related to the evolution of the Limpopo Complex.

The term 'Limpopo Complex' was proposed by van Reenen and Du Toit (1977) to describe the crustal block referred to as the Limpopo Mobile Belt by Mason (1973). The rationale being that the rocks produced by the Limpopo orogeny covered a much bigger area than the linear zone (belt) between the (Palaeoproterozoic) Triangle and Palala Shear Zones as defined by Mason (1973). The Limpopo Belt of Mason (op cit) being the Central Zone of the Limpopo Complex.

The term 'orogeny' used in the context of the 'Limpopo Complex' has to be explained. Orogeny is used to describe the processes affecting continental lithosphere in convergent settings. In Phanerozoic orogens such processes are linked to horizontal shortening and significant topography, but for the Precambrian the term has been used in a broader sense to identify episodes of intense crustal deformation and tectono-magmatic reworking characterized by vertical tectonics and in places (e.g. Eastern Darwar Craton) flat topography (e.g. Chardon et al. 2009; Cagnard et al. 2011).

The term 'crustal-scale granulite diapir' (Perchuk and Gerya 2011) refers to the orogenic process triggered by mantle heat-fluid flow that in the context of the LC directed steep exhumation of the Central Zone of the LC and regional-scale gravitational crustal overturn of complex morphology and dynamics that controlled the southwards channelling of a hot SMZ nappe against and over the adjacent granite-greenstone craton before emplacement of the Matok pluton at ca. 2.68 Ga (Fig. 8.1) (Laurent et al. 2013, 2019; Smit et al. 2014).

The term 'melt-weakened domes' proposed by Jamieson et al. (2011) refers to large dome-like structural features cored by migmatites that were formed at deep crustal levels without evidence for significant segregation of the melt. In contrast, the term 'melt-cored domes' (e.g. Brown 2007; Rey et al. 2009) refers to the situation where larger volumes of melt are present and segregated, leading to emplacement of melt-cored domes in the upper crust. In this paper the term 'granitic diapirism' is equivalent to the term 'melt-cored domes'.

The term 'conveyor belt mechanism' was coined by Smit et al. (2014) to explain a tectonic mechanism linked to near-vertical tectonics in the CZ that controlled the southwards channelling of a hot SMZ nappe along the near-horizontal section of the Hout River Shear Zone (HRSZ), against and over the adjacent NKVC.

The term 'mega closed structures' refers to mega-scale structures in the CZ that are circular in outcrop pattern, and that were initially mapped as sheath folds (Roering et al. 1992a).

Finally, we use the term 'TSZ' in this paper to describe the Tshipise Straightening Zone, and not the Triangle Shear Zone, as is normally done (Fig. 8.1).

8.2 Regional Geological Setting of the Limpopo Complex of Southern Africa

The ca. 2.72 Ga LC of southern Africa (Fig. 8.1; van Reenen et al. 2011 and references therein) is a classic example of a Neoarchaean granulite-facies gneiss complex situated between two cratons. It provides a well-exposed crustal section from the low-grade granite-greenstone terrane of the NKVC in the south across the entire high-grade terrane of the LC and into the low-grade granite-greenstone terrane of the ZC in the north. The LC (Fig. 8.1) comprises three distinct high-grade zones namely NMZ, SMZ and CZ, which are separated from each other and from the juxtaposed cratons by complex inward-dipping Neoarchaean reverse-sense crustal-scale shear zones. Some elements of this Neoarchaean thrust sense system have been overprinted by strike-slip/transpressive activity during the Palaeoproterozoic (ca. 2.0 Ga) and are now represented by the Triangle and Palala Shear Zones (e.g. Kramers et al. 2011; Smit et al. 2011; van Reenen et al. 2011).

The major geological features of NMZ, CZ, SMZ, as well as those of the juxtaposed NKVC that collectively define the regional tectonic setting of the Limpopo Complex have been discussed in detail in numerous publications (e.g. van Reenen et al. 1990, 2011; Kröner et al. 1999; Kramers et al. 2006 and references therein). The following section presents a brief overview to explain important geological features of the LC high-grade terrane and adjacent cratons and serves as a general background for the main part of this paper.

8.2.1 The Northern Kaapvaal Craton (NKVC)

The NKVC comprises >3 Ga greenschist- to amphibolite-facies greenstone belts (Pietersburg, Giyani, Rhenosterkoppies) and associated granitoids located at the northern edge of the KVC (Fig. 8.1) (e.g. De Wit et al. 1992a; Vezinet et al. 2018; Laurent et al. 2019). It is separated from the ca. 2.72 Ga granulite-facies SMZ of the LC by the north-dipping reverse-sense Hout River Shear Zone (HRSZ) (Fig. 8.1).

Two post ca. 3.0 Ga tectono-metamorphic events are documented in the northern part of the NKVC: (1) the ca. 2.86 Ga Pietersburg greenstone belt-Lwaji (PGB-Lwaji) orogeny (Kramers et al. 2014) that affected much of the NKVC between the Giyani and Pietersburg greenstone belts (Figs. 8.1, 8.2 and 8.3), and (2) the ca. 2.72 Ga Limpopo orogeny that only affected a narrow zone in the footwall of the north-dipping HRSZ (e.g. McCourt and van Reenen 1992; Roering et al. 1992a, b; van Reenen et al. 2011, 2014; Kramers et al. 2014). Laurent et al. (2019) discuss a

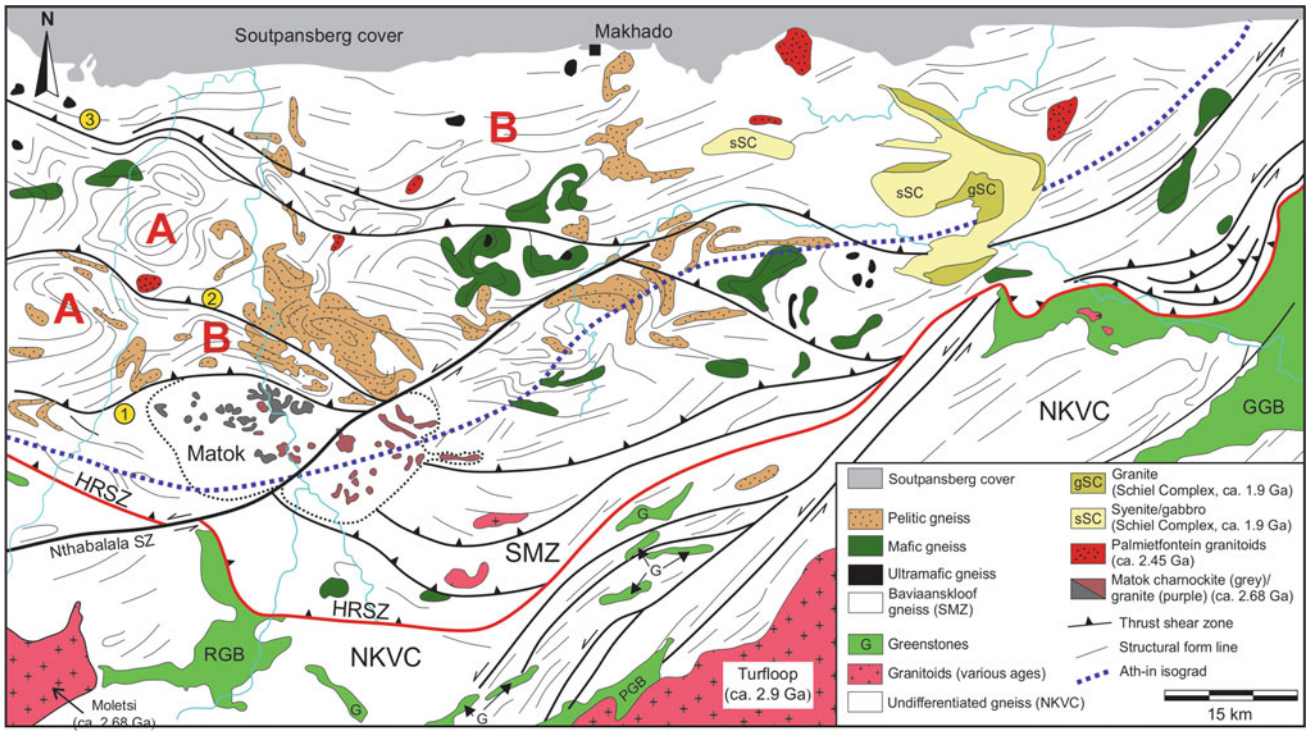

Fig. 8.2 Geological map of the SMZ (after van Reenen et al. 2011) showing: (1) North-dipping HRSZ that bounds the SMZ in the south, and presence of steeply dipping high-grade shear zones that internally subdivide the high-grade terrane into several large crustal blocks. (2) Ath-in isograd superimposed onto major folds that subdivides the SMZ into a northern granulite zone and a southern zone of retrograde hydrated granulite. (3) Crustal-scale blocks bounded by steeply dipping shear zones characterized by complex fold patterns depicting large migmatitic domes (**a**) and steeply plunging isoclinal folds (**b**). (4) Outcrop pattern of the Matok granitic complex comprising granitic (purple) and charnockitic (grey) rocks (compare with Fig. 8.3). (5) Large volumes of tonalitic orthogneisses (Baviaanskloof gneiss) with intercalated deformed slivers of Bandelierkop Formation lithologies comprising metapelitic, mafic and ultramafic gneisses characterize the SMZ. 1–3 (yellow circles) respectively refer to the Matok-, Petronella- and Annaskraal Shear Zones

geodynamic model for the Paleao- to Mesoarchaean evolution of the NKVC, which they also extends to the Neoarchaean involving the SMZ.

8.2.2 The Southern Marginal Zone (SMZ)

The SMZ of the LC (Figs. 8.2 and 8.3) occupies the hanging wall section of the north-dipping HRSZ that separates it from the NKVC and comprise intensely deformed granulite-facies gneisses that document evidence only for a high-temperature decompression-cooling metamorphic history (e.g. Roering et al. 1992b; van Reenen et al. 1990, 2011, 2014). The SMZ mainly comprises metasedimentary and mafic/ultramafic gneisses of the ca. 3.0 Ga Bandelierkop Formation structurally folded and intercalated with the volumetrically significant, enderbitic, Baviaanskloof Gneiss (Fig. 8.2) (van Reenen et al. 2011, 2014 and references therein). Granulite-facies metamorphism and deformation occurred between 2.72 and 2.68 Ga (e.g. Roering et al. 1992b; van Reenen et al. 2011, 2014), followed between ca. 2.68 Ga and ca. 2.64 Ga by emplacement of anatectic granitoids including diorite, granodiorite and monzogranite of the ca. 2.68 Ga Matok complex (e.g. Laurent et al. 2013; Figs. 8.2 and 8.3). Emplacement of the post-tectonic Palmietfontein granite (ca. 2.46 Ga) (Barton and van Reenen 1992) manifests the end of tectono-metamorphic activity related to the Neoarchaean Limpopo event.

The SMZ has been subdivided into a northern granulite domain separated from a southern domain of retrograde hydrated granulite by an anthophyllite-in (Ath-in) isograd (Figs. 8.2 and 8.3) (e.g. van Reenen 1986; van Reenen et al. 2014). The northern granulite domain comprises large crustal blocks characterized by complex fold deformation patterns separated from each other by steeply north-dipping high-grade shear zones (the Matok, Petronella and Annaskraal Shear Zones in Figs. 8.2 and 8.3) (Smit et al. 1992). The northern granulite domain is subdivided (Fig. 8.3) into a northern subdomain characterized by decompression-cooling pressure–temperature (*P-T*) paths and a southern

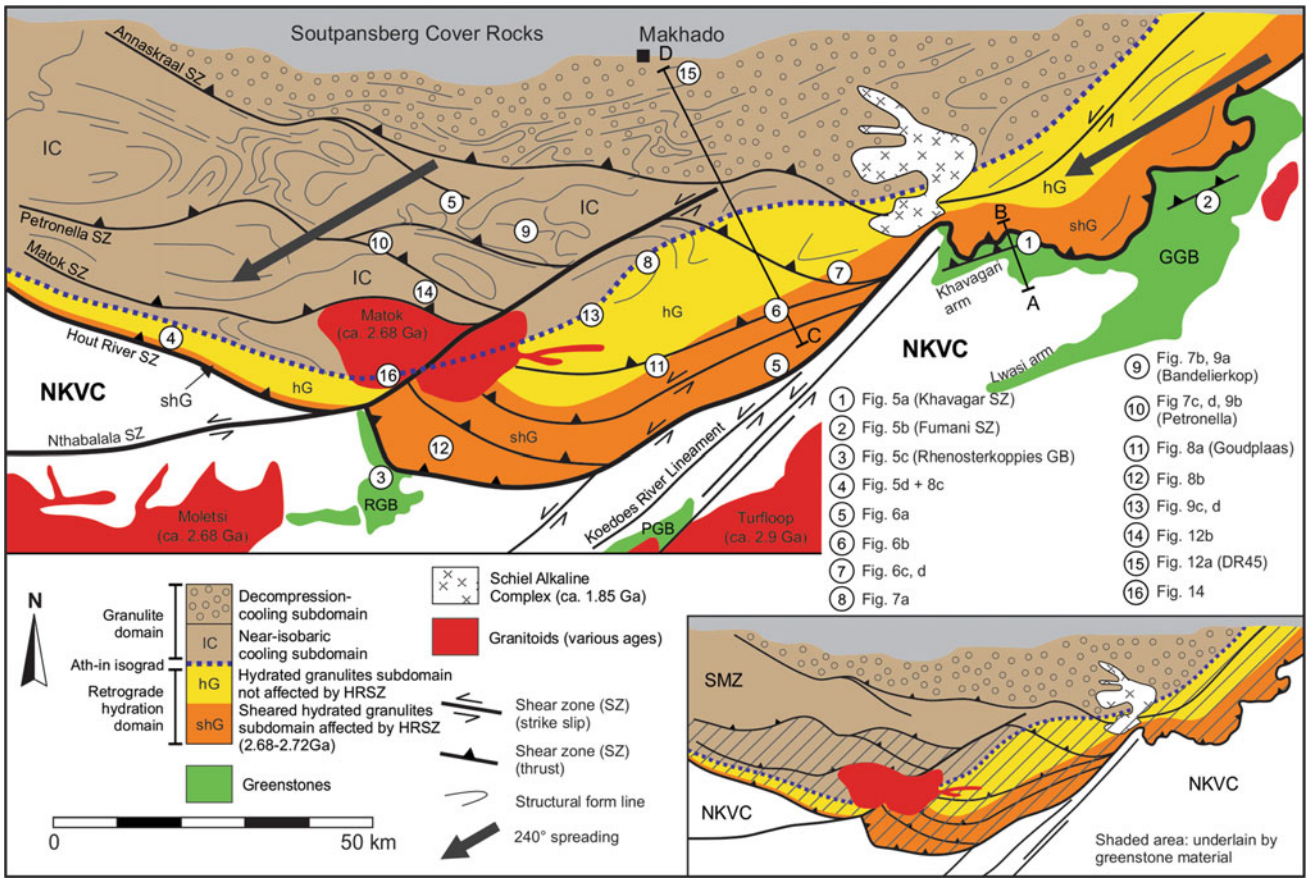

Fig. 8.3 SMZ metamorphic map (after van Reenen et al. 2014) showing (1) localities 1–16 referred to in the text; (2) two south–north-oriented traverses, A–B and C–D along which the SMZ crustal section (Fig. 8.4) has been constructed; (3) subdomain showing the flat section of the Hout River Shear Zone exposed in the deeply eroded Lowveld (orange); (4) subdomain of folded retrograde hydrated granulite exposed in the escarpment (yellow), (5) subdivision of the granulite domain exposed on the plateau (brown) into a northern subdomain characterized by decompression-cooling *P-T* paths, and a southern subdomain characterized by near-isobaric cooling *P-T* paths. The inset map shows the surface area (cross-hatched) of the Southern Marginal Zone that is underlain by greenstone belt material based on geophysical data (after De Beer and Stettler 1992)

subdomain characterized by near-isobaric cooling *P-T* paths (e.g. Perchuk et al. 2000a; Smit et al. 2001, 2014; van Reenen et al. 2011, 2014).

Additional important characteristics of the SMZ should be emphasized. First, syn-metamorphic granitoid diapirism is notably absent in the SMZ, whereas this phenomenon occurs extensively both in the CZ and the NMZ (see below). Secondly, the SMZ, like the NMZ, is dominated by magmatic rocks (i.e. tonalitic Baviaanskloof Gneiss), whereas meta-basic, meta-ultrabasic, and metasedimentary rocks of the Bandelierkop Formation (Fig. 8.2) are a minor constituent of the SMZ. This is in strong contrast with the CZ, which is characterized by a much larger volume of metasedimentary lithologies (see below). Third, metasedimentary rocks of both the Bandelierkop Formation (SMZ) (e.g. Rajesh et al. 2014) and the Beit Bridge Complex (CZ) (e.g. Kröner et al. 1999) record evidence for protolith ages greater than ca. 3.0 Ga.

8.2.3 The Central Zone (CZ)

The CZ (e.g. Hofmann et al. 1998; Kröner et al. 1999; Kramers et al. 2006; Smit et al. 2011, 2014 and references therein) forms the largest core portion of the LC (Fig. 8.1). It includes large volumes of metasedimentary granulite-facies rocks very different in character from those of either the SMZ or the NMZ. The ca. 3.3 Ga old Beit Bridge Complex is the most dominant unit in the CZ and comprises meta-quartzites, Mt-bearing quartzites (mineral abbreviations after Whitney and Evans 2010), marbles, and calc-silicate gneisses, mafic and ultramafic gneisses, metamorphosed iron formation and various Grt-Bt paragneisses interfolded with quartzofeldspathic orthogneisses. Precursors of the ca. 3.3 Ga Messina Suite and Sand River tonalite-trondhjemite orthogneisses intruded metasedimentary rocks of the Beit Bridge Complex. At 2.69–2.62 Ga this association was intruded by a number of tonalitic granitoids (precursors of

the Verbaard and Alldays gneisses) and leucocratic quartzofeldspathic granitoids (precursors of the collectively termed Singelele-type granitoids). Singelele-type granitoids are considered to be the product of crustal anatexis (Bahnemann 1972; Fripp et al. 1979; Watkeys et al. 1983). The close association of the leucocratic granitoids with km-scale, steeply plunging closed structures mapped as sheath folds (e.g. Roering et al. 1992b; Perchuk et al. 2008a, b; Smit et al. 2011) support the concept of extensive granitic diapirism that accompanied final exhumation of the CZ. The slightly deformed Bulai pluton comprises a porphyritic phase dated at ca. 2.61 Ga (Millonig et al. 2008) and is an important time marker. It intruded high-grade metamorphic gneisses of the Beit Bridge Complex at the end of the Neoarchaean high-grade tectono-metamorphic event in the CZ. A second high-grade metamorphic event that is mainly expressed by a regional thermal overprint at ca. 2.0 Ga and associated with discrete linear ductile shear zones (e.g. van Reenen et al. 2008; Smit et al. 2011; Kramers and Mouri 2011) will not be further discussed since this paper only focuses on the Neoarchaean evolution of the LC.

8.2.4 The Northern Marginal Zone (NMZ)

The NMZ (Fig. 8.1) (e.g. Blenkinsop et al. 2004; Blenkinsop 2011 and references therein) consists mainly of charnoenderbites that diapirically intruded metasedimentary and meta-mafic rocks between 2.74 and 2.57 Ga, coeval with granulite-facies metamorphism. Similar to the proposed relationship of the SMZ with the NKVC, the NMZ exhibits lithologies that are geochemically similar to that of the ZC (Kreissig et al. 2000). Pervasive Neoarchaean horizontal shortening that occurred in association with the exhumation of the NMZ is expressed by steep to near-vertical gneissic banding striking in general east–northeast, parallel to the strike of the NMZ (Fig. 8.1) (e.g. Blenkinsop 2011). The highly radiogenic nature of the rocks of the NMZ, supplemented by heat from mantle melts, triggered heating and diapirism that culminated in the intrusion of distinctive porphyritic charnockites and granites (Blenkinsop 2011). This author proposed that crustal thickening during horizontal shortening and steep extrusion of the NMZ was limited by high geothermal gradients, in contrast with overthickening and gravitational collapse that characterizes younger orogens. The contact of the ZC with the NMZ (the North Marginal Thrust Zone) is a moderately south-dipping thrust along which NMZ granulites were thrust onto the ZC (Light 1982; Blenkinsop et al. 1995; Blenkinsop 2011). The NMZ was also affected by lower grade retrogression and transpressive deformation in localized shear zones at ca. 2.0 Ga, mainly in the southern part. Emplacement of the Great Dyke of Zimbabwe at 2.58 Ga (Armstrong and Wilson 2000) across the contact of the ZC with the NMZ (Fig. 8.1) signifies the end of all tectono-metamorphic activity related to the Neoarchaean Limpopo event in the NMZ.

8.2.5 The Zimbabwe Craton (ZC)

The south-dipping Neoarchaean North Marginal Thrust Zone (NMTZ) (Fig. 8.1) separates the NMZ from the ZC, which comprises low-grade greenstone belts and granitoids. The geometry of the south-dipping NMTZ is evidence for thrusting the NMZ against and over the ZC.

The rest of the paper focuses on a detailed discussion of published geological, geochronological, and geophysical data that forms the basis for the construction of a south–north crustal section (Fig. 8.4) along two linked traverses (sections A–B and C–D in Fig. 8.3) that connect the northern part of the Giyani greenstone belt in the south with the SMZ and CZ of the LC to the north (Fig. 8.1). The crustal section (Fig. 8.4) is the foundation for the analyses of the geological characteristics of the SMZ and its relationship with the NKVC in the south, and the CZ in the north. It also elucidates the arguments used to promote a gravity-driven diapiric model for the 2.72–2.62 Limpopo orogeny.

8.3 Northern Kaapvaal Craton—Southern Marginal Zone Relationship at ca. 2.72 Ga

Studies in the Giyani and Rhenosterkoppies greenstone belts located on the NKVC in the immediate footwall of the HRSZ (Figs. 8.1, 8.2 and 8.3) have proven to be critical to understanding the relationship between the NKVC and the SMZ, which is a major constraint on any geodynamic model proposed for the evolution of the LC at 2.72–2.62 Ga. The Giyani greenstone belt consists of a continuous central-northeastern part that in the west (Fig. 8.3) bifurcates into a northern (Khavagari) and a southern (Lwaji) arm separated by granitoid gneisses (McCourt and van Reenen 1992). The northern arm is dominated by ultramafic schists intercalated with minor mafic and metasedimentary rocks including BIF, ferruginous quartzite and metapelitic schist, but due to structural complexity, no stratigraphic sequence can be defined (McCourt and van Reenen 1992). In contrast, both the central section of the belt and the southern Lwaji arm, are characterized by metavolcanics of which mafic schists dominates (e.g. McCourt and van Reenen 1992; Kramers et al. 2014).

Kramers et al. (2014) recently showed that garnet-bearing mafic schists from the Lwaji arm (Fig. 8.3) document metamorphic ages of ca. 2.86 Ga that overlap with ages of 2.85–2.87 Ga for younger zircons in syntectonic granitic

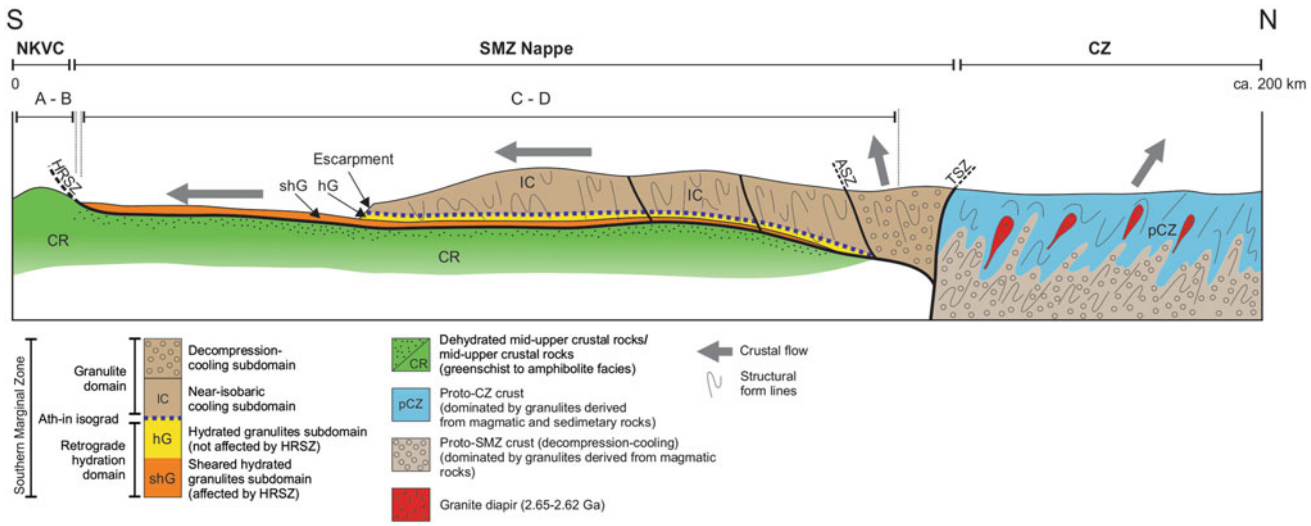

Fig. 8.4 Schematic south-north crustal section constructed along two linked traverses (A–B) and C–D (Fig. 8.3) respectively across the Khavagari arm of the Giyani greenstone belt (A–B) and through the central part of the SMZ (C–D). The section also includes the southern part of the CZ. ASZ: Annaskraal Shear Zone, HRSZ: Hout River Shear Zone; TSZ: Tshipise Straightening Zone. Decompression-cooling *P-T* paths (DR 45 in Fig. 8.11) in the decompression-cooling subdomain (brown coloured area with open circles) are in synchronicity with steeply plunging folds and steeply dipping shear zones that collectively document evidence for steep exhumation. In contrast, near-isobaric cooling *P-T* paths (B, C, and D in Fig. 8.11) in the near-isobaric cooling subdomain (brown coloured area) are not in synchronicity with the steep tectonic features, but documents metamorphic evidence that support spreading along the underlying sub-horizontal section of the HRSZ. See text for further discussion

intrusions within the Giyani and Pietersburg greenstone belts (Kröner et al. 2000; Jaguin et al. 2012; Laurent et al. 2013, 2019; Zeh et al. 2013; Kramers et al. 2014). Kramers et al. (2014) interpreted these ages to reflect a Pietersburg greenstone belt (PGB)-Lwaji orogeny that affected the Lwaji arm of the Giyani greenstone belt as well as the NKVC (Fig. 8.3) (also Vezinet et al. 2018; Laurent et al. 2019).

Ages of 2.85–2.87 Ga obtained from much of the NKVC are significantly older than peak metamorphic ages of 2.72–2.69 Ga obtained from the north-dipping Khavagari Shear Zone in the Khavagari arm (Kreissig et al. 2001; Kramers et al. 2014) of the Giyani greenstone belt (Fig. 8.3) and from the Rhenosterkoppies greenstone belt also located in the footwall of the HRSZ to the west of the Giyani greenstone belt (Figs. 8.2 and 8.3) (Miyano et al. 1992; Passeraub et al. 1999; Kramers et al. 2014). These younger ages have been interpreted as the timing of hot-iron metamorphism related to emplacement of SMZ granulites against and over the Giyani greenstone belt during the ca. 2.72 Ga Limpopo orogeny (McCourt and van Reenen 1992; Roering et al. 1992a; Perchuk et al. 1996, 2000b; Kramers et al. 2014) (see Sect. 8.4.3.3 and *P-T* path A in Fig. 8.11). Kramers et al. (2014) concluded that the ca. 120 Ma age difference between the ca. 2.86 Ga PGB-Lwaji orogeny and the ca. 2.72 Ga Limpopo orogeny 'precludes any causal link between these two events'.

8.4 Tectono-Metamorphic Characteristics of the SMZ and NKVC Linked to the North-Dipping HRSZ

8.4.1 Subdivision of the NKVC and Adjacent SMZ into Distinct Domains

The SMZ and juxtaposed granite-greenstone terrane of the NKVC (Fig. 8.3) comprise distinct structural and metamorphic domains that are relevant for the geodynamic models proposed for the evolution of the LC. The subdivision of the NKVC (Fig. 8.3) into a domain older than 2.85–2.86 Ga and a 2.72–2.69 Ga domain that occupies the footwall of the steep north-dipping crustal-scale HRSZ has already been discussed. The geological map (Figs. 8.2 and 8.3) (van Reenen et al. 2011, 2014; Smit et al. 2014) further shows that the SMZ is subdivided into a northern granulite domain separated from a southern domain of retrograde, hydrated, former granulite by a well-established Ath-in retrograde isograd. Both these domains can further be subdivided. The granulite domain with steeply plunging folds and steep dipping high-grade shear zones (Fig. 8.3) is subdivided into a northern subdomain characterized by decompression-cooling *P-T* paths preserved in metapelitic granulite, and a southern subdomain that abuts against the

Ath-in retrograde isograd characterized by near-isobaric cooling *P-T* paths, also preserved in metapelitic granulite.

The southern retrograde domain (Fig. 8.3) can also be subdivided into a northern and southern subdomain. The northern subdomain bordering the Ath-in retrograde isograd (yellow area in Fig. 8.3) is like the adjacent granulite domain characterized by steeply plunging folds and steep dipping shear zones but these structures deform retrograde, hydrated, former granulite. In contrast, the southern subdomain (orange area in Fig. 8.3) comprises flat-lying sheared retrograde hydrated former granulites that are considered to be closely associated with the underlying HRSZ as will be discussed. It is important to note that more than 60% of the SMZ surface area (inset map in Fig. 8.3) is underlain by rocks with a geophysical signature indistinguishable from the granite-greenstone material that characterizes the adjacent NKVC (De Beer and Stettler 1992).

Construction of a south–north crustal section (Figs. 8.3 and 8.4) explains the observed tectono-metamorphic characteristics of the SMZ (Fig. 8.3) and the relationship with the NKVC and CZ at 2.72–2.69 Ga as a direct consequence of the fundamental role that the HRSZ has played in the evolution of the SMZ. The crustal section (Fig. 8.4) is constructed along two linked south–north traverses (A–B and C–D) (Fig. 8.3). The short A–B traverse runs through the Khavagari arm to the steep north-dipping HRSZ demonstrating the interaction of the northern part of the Giyani greenstone belt with the SMZ at ca. 2.72 Ga.

The longer traverse C–D runs across the central part of the SMZ up to Makhado in the north (Fig. 8.3). The vertical topographical difference of ca. 600 m (Smit et al. 2014) between the plateau (Highveld) in the north (shown in brown in Fig. 8.3) and the Lowveld (shown in orange in Fig. 8.3) at the base of the escarpment (shown in yellow in Fig. 8.3) in the south allowed the reliable construction of this important crustal section (Fig. 8.4). Traverse C–D explains the regional distribution of metamorphic subdomains within the SMZ and their relationship with the underlying HRSZ (Fig. 8.3).

The construction and interpretation of the C–D crustal section is based on (1) *Field, structural and petrological data* (van Reenen 1983, 1986; van Reenen et al. 1990, 1995, 2008, 2011, 2014; van Reenen and Hollister 1988; Baker et al. 1992; De Wit et al. 1992c; McCourt and van Reenen 1992; Mahan et al. 2011; Miyano et al. 1992; Perchuk et al. 1996, 2000a, b, 2008a, b; Roering et al. 1992a, b, 1995; Van Schalkwyk and van Reenen 1992; Smit et al. 1992, 2011, 2014; Huizenga et al. 2014; Tsunogae and van Reenen 2014; Koizumi et al. 2014); (2) *Geochronological data* (Passeraub et al. 1999; Kreissig et al. 2001; Laurent et al. 2013; Belyanin et al. 2014, 2015; Kramers and Mouri 2011; Kramers and Zeh 2011; Kramers et al. 2014, *Oxygen isotope data* (Hoernes et al. 1995; Dubinina et al. 2015); (3) *Geophysical data* (De Beer and Stettler 1992 and references therein), and (4) *Numerical modelling data* (Gerya et al. 2000; Perchuk and Gerya 2011; Perchuk et al. 2018).

8.4.2 Steep North-Dipping HRSZ in Contact with the NKVC

8.4.2.1 Field and Structural Data

The HRSZ (Figs. 8.1, 8.2 and 8.3) in contact with the NKVC has a fault pattern that varies from steep southwest-verging thrust faults with steep dip-slip kinematics against both the Rhenosterkoppies (Fig. 8.5c) and Giyani (Fig. 8.5a, b) greenstone belts, to near-vertical southwest-verging sinistral strike-slip faults (Figs. 8.2 and 8.3). This typical frontal–lateral ramp geometry defines southwest (240°) movement of high-grade SMZ material against and over the NKVC (Fig. 8.3) (Smit et al. 1992, 2014).

Structural evidence for intense tectonic activity associated with steep north-over-south thrusting along the HRSZ against and over the Giyani greenstone belt is well documented by kinematic data acquired from underground workings at the Fumani Mine (locality 2 in Fig. 8.3) (Pretorius 1988; McCourt and van Reenen 1992) and the Klein Letaba and Frankie (Gan and van Reenen 1995, 1997) gold mines. Gold deposits in these gold mines occur in large structural shoots, respectively, associated with the steep north-dipping Fumani (locality 2 in Fig. 8.3) and Khavagari (locality 1 in Fig. 8.3) shear zones located in the immediate footwall of the HRSZ. The structural shoots hosting gold deposits plunge to the northeast, which is the same direction as the HRSZ.

Fault segments in the central part of the contact area with the NKVC (Figs. 8.2 and 8.3) display strike-slip kinematics characterized by left-lateral displacement (e.g. the Koedoes River Lineament, Figs. 8.2 and 8.3). They are particularly well exposed at the extreme western tip of the Khavagari arm of the Giyani greenstone belt near the village of Babango (see De Wit et al. 1992c). Based on data from surface exposures at the contact with the NKVC, Roering et al. (1992a, b) and Smit et al. (1992) initially interpreted the HRSZ as a steeply north-dipping thrust, even though geophysical data indicate that the shear zone flattens to the north (see Fig. 8.15).

8.4.2.2 Metamorphic Activity Associated with the Steep Section of the HRSZ

Data obtained from Grt-St-Ky (mineral abbreviations after Whitney and Evans 2010) bearing mica schists (Perchuk et al. 1996, 2000b) sampled from the Khavagari shear zone in the footwall of the HRSZ within the Khavagari limb of the Giyani greenstone belt (locality 1 in Fig. 8.3) provide direct evidence for a non-isobaric *P-T* loop comprising prograde

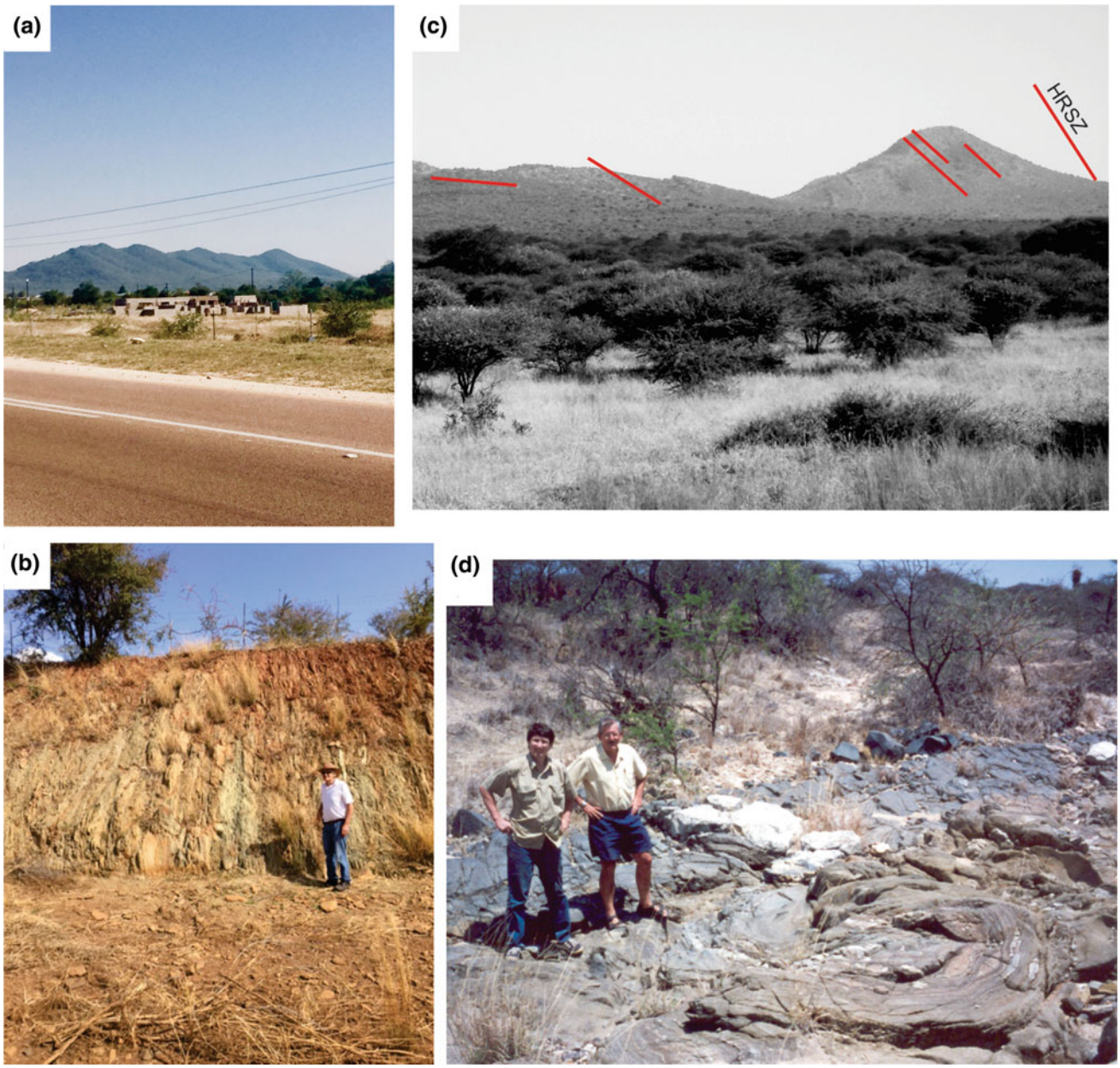

Fig. 8.5 Structural evidence highlighting the steep attitude of the HRSZ at the contact with the NKVC. All localities are shown in Fig. 8.3. **a** Khavagari Hills in the footwall of the HRSZ southwest of the town of Giyani. View to the west. Note the steeply north-plunging thrust duplexes associated with the steep north-dipping section of the HRSZ. **b** Outcrops of the steep north-dipping Fumani Shear Zone exposed in the spillway of the Hudson Ntsanwisi dam (locality 2 in Fig. 8.3) in the northeastern part of the Giyani greenstone belt. The sheared rocks comprise quartz-sericite schists and mafic schists. View is to the west. **c** Rhenosterkoppies greenstone belt (locality 3 in Fig. 8.3) as viewed towards the west. Near-horizontal structures in the central part of the belt (left side of photograph) have been rotated to dip steeply north below the steep north-dipping section of the HRSZ. **d** Steeply north-plunging minor closed folds developed within retrograde hydrated metapelitic gneiss in the Hout River (locality 4 in Fig. 8.3)

and retrograde segments (the 'hot iron effect', see *P-T* path A in Fig. 8.11). The loop shows that prograde and peak metamorphic conditions, reached at 2.72–2.69 Ga within the footwall greenschist, are coeval with attainment of peak metamorphism at ca. 2.72 Ga documented by hot overriding SMZ granulite in the hanging wall (Kreissig et al. 2001; Kramers et al. 2014; Rajesh et al. 2014; Taylor et al. 2014; Nicoli et al. 2015). Data obtained from the central and northern portions of the Rhenosterkoppies greenstone belt (Figs. 8.3 and 8.5c) document a similar scenario in which slightly higher peak *P-T* conditions (ca. 7 kbar and 700 °C) resulted from the thrusting of hot granulites over relatively

cold rocks at ca. 2.72 Ga (Miyano et al. 1992; Passeraub et al. 1999; Kramers et al. 2014). The age of 2.7 Ga provides a constraint on deformation along the HRSZ that is compatible with that obtained by Kreissig et al. (2001) from the Khavagari section of the Giyani greenstone belt.

A minimum age for the juxtaposition of the hot SMZ nappe with the granite-greenstone terrane of the NKVC along the steeply north-dipping HRSZ is also accurately constrained by emplacement at ca. 2.68 Ga (Laurent et al. 2013) of geochemically similar and mainly undeformed Matok- and Moletsi granitic plutons, respectively, on either side of the HRSZ (Figs. 8.2 and 8.3). This data provides unequivocal evidence that the SMZ was already juxtaposed at the position of the HRSZ against the NKVC before ca. 2.68 Ga.

In conclusion, published structural, metamorphic, and geochronological data supported by geophysical data (see Fig. 8.15) confirm the status of the HRSZ as a crustal-scale tectonic feature that bounds the SMZ in the south. These data contradict the revised lithotectonic model proposed for the SMZ in which Vezinet et al. (2018) and Laurent et al. (2019) claims that that the Nthabalala Shear Zone (Fig. 8.2), and not the HRSZ, is the tectonic boundary of the SMZ with what these authors term the low-grade Pietersburg block. With reference to the published geological of the SMZ (Fig. 8.2) it is clear that the Nthabalala Shear Zone is located entirely within the granulite domain of the SMZ, 5 km north of the Ath-in retrograde isograd. Large folds comprising granulite-facies metapelitic gneisses can thus be followed uninterruptedly across this oblique sinistral shear zone with little left-lateral displacement.

8.4.3 Flat-Lying Section of the HRSZ

8.4.3.1 Field and Structural Data

The long south–north traverse (C–D, Fig. 8.3) reveals field and structural data (Figs. 8.5, 8.6, 8.7 and 8.8) demonstrating important features of the SMZ that are critical to understand the concept of a hot SMZ granulite nappe with imbedded steeply plunging folds and steep dipping high-grade shear zones that was thrust southwards along a near-isobaric (ca. 6 kbar) crustal plane defined by the near-horizontal section of the HRSZ (Fig. 8.4) before ca. 2.68 Ga (van Reenen et al. 2011; Smit et al. 2014).

First, it shows that the attitude of the HRSZ (see Fig. 8.4) changes over a short distance from a steep north-dipping dip-slip fault (Fig. 8.5a–d) at the direct contact with the NKVC in the south, through a moderately north-dipping thrust still close to the contact with the NKVC (Fig. 8.6a, locality 5 in Fig. 8.3) into a sub-horizontal thrust (Fig. 8.6b–d, localities 6 and 7 in Fig. 8.3) that underlies the entire Lowveld up to the base of the escarpment in the north (orange area in Fig. 8.3). Flat-lying and intensely sheared and retrograde gneisses that have been shown to represent the retrograde hydrated equivalents of former metapelitic-, mafic-, ultramafic granulite of the Bandelierkop Formation and Opx-bearing tonalitic gneisses (Fig. 8.6b–d) (van Reenen 1986) are considered to be closely linked to the underlying sub-horizontal section of the HRSZ (Fig. 8.3) (Smit et al. 2014). This conclusion follows from the observation that outcrops of flat-lying sheared gneisses occupy large areas in the Lowveld (orange area in Fig. 8.3) up to the base of the escarpment (yellow area in Fig. 8.3) in the north.

Second, traverse C–D (Fig. 8.3) exposes the steeply dipping gneissic foliation (Fig. 8.7a) associated with folded retrograde hydrated granulites that outcrop in the escarpment towards the north (yellow area in Figs. 8.3 and 8.4).

Third, the traverse continuous across the retrograde Ath-in isograd located at the top of the escarpment (Figs. 8.2 and 8.3) and into the overlying northern granulite domain (brown area in Figs. 8.3 and 8.4) of the Highveld. The granulite domain (Fig. 8.3) is also characterized by a steeply dipping gneissic foliation (Fig. 8.7b) associated with steeply plunging folds and steeply dipping high-grade shear zones (Matok-, Petronella, Annaskraal shear zones) (Fig. 8.7c, d).

Gravel roads that connect the Lowveld in the south at an elevation of ca. 660 m (orange area in Figs. 8.3 and 8.4) with the Highveld in the north at an elevation of 1240 m (brown area in Figs. 8.3 and 8.4) demonstrate that the flat-lying shear fabric of gneisses (Fig. 8.6b–d) that outcrop in the deeply eroded Lowveld (Figs. 8.3 and 8.4) is superimposed onto and thus younger, than the steep gneissic fabric of folds and shear zones (Fig. 8.8a–c) exposed in road cuttings through the escarpment in the north (coloured yellow in Figs. 8.3 and 8.4). This observation strongly suggests that the sub-horizontal section of the HRSZ (Fig. 8.4) projects northwards underneath the granulite domain exposed on the plateau (brown area in Fig. 8.3), with its steep tectonic features that include the Matok, Petronella, and Annaskraal Shear Zones (Figs. 8.3, 8.4 and 8.7c).

Our overall conclusion is that the granulite domain of the SMZ underlain by retrograde hydrated granulite both with embedded steeply plunging folds and steep high-grade shear zones (Matok-, Petronella-, Annaskraal-) that respectively occupy the Highveld and the escarpment (Fig. 8.3) represents an allochthonous granulite nappe that is riding on the younger underlying sub-horizontal section of the HRSZ (Fig. 8.4). This proposal is supported by *P-T* and geophysical data (Figs. 8.11 and 8.15) as will be further discussed.

8.4.3.2 Metamorphic Evolution of the Retrograde Hydrated Domain

The Ath-in retrograde isograd overprints major folds located south of the Nthabalala Shear Zone (Figs. 8.2 and 8.3) confirming its status as a true metamorphic feature that reflects the continuous transition from the granulite domain

Fig. 8.6 Structural evidence of the HRSZ changing its attitude from a steep north-dipping shear zone in direct contact with the NKVC into a near-horizontal shear zone that underlies much of the SMZ in the east (Figs. 8.3 and 8.4). Localities are shown in Fig. 8.3. **a** Shallow north-dipping sheared retrograde hydrated tonalitic gneiss exposed in a gravel road cutting immediately north of the HRSZ. View to the east (locality 5 in Fig. 8.3). **b** Flat-lying outcrops of sheared and retrograde hydrated tonalitic gneiss exposed at locality 6 (Fig. 8.3). View is towards the east. **c** Flat-lying outcrops of sheared and hydrated metapelitic, mafic, ultramafic gneisses and BIF of the Bandelierkop Formation exposed in Shiphophi Hill on farm Hartebeesfontein (locality 7 in Fig. 8.3). View is towards the west. **d** Sheared retrograde hydrated outcrops of tonalitic gneiss exposed in a dry river bed between localities 6 and 7 (Fig. 8.3). The thrust dips at 6° to the north. View is towards the west. This locality and localities 6 and 7 are considered type localities for the sub-horizontal section of the HRSZ

in the north to the retrograde domain in the south (van Reenen 1986; van Reenen et al. 2011, 2014). There is no genetic relationship with the Nthabalala Shear Zone (Fig. 8.2) as is demonstrated by the fact that major folds comprising Bandelierkop Formation granulite-facies gneisses continue across the oblique-slip Nthabalala Shear Zone with little left-lateral displacement. Published geological maps thus contradict the claims by Vezinet et al. (2018) and Laurent et al. (2019) that the sinistral oblique-slip Nthabalala Shear Zone (Fig. 8.2) is a tectonic boundary that separates the granulite-facies SMZ from their low-grade Pietersburg Block to the south.

Fig. 8.7 Steeply plunging folds and steeply dipping high-grade shear zones exposed in the folded retrograde hydrated and granulite domains. **a** Steeply dipping migmatitic metapelitic gneisses that outcrop at the position of the Ath-in isograd (locality 8 in Fig. 8.3). Note undeformed leucocratic trondhjemite dykes that intrude the migmatitic gneiss. **b** Steeply dipping pristine foliated migmatitic metapelitic granulite at Bandelierkop quarry (locality 9 in Fig. 8.3). **c** Steeply dipping granulite-facies shear fabric developed within migmatitic metapelitic granulite in the km-wide Petronella Shear Zone (locality 10 in Fig. 8.3). This steep fabric characterizes all shear zones developed within the granulite-facies domain of the SMZ. View is towards the west. **d** Same locality as (**a**), but with view parallel to the steep plunging lineation showing evidence of heterogeneous deformation of metapelitic granulite in which the early folded gneissic fabric is transposed and partly destroyed by the Petronella shear zone

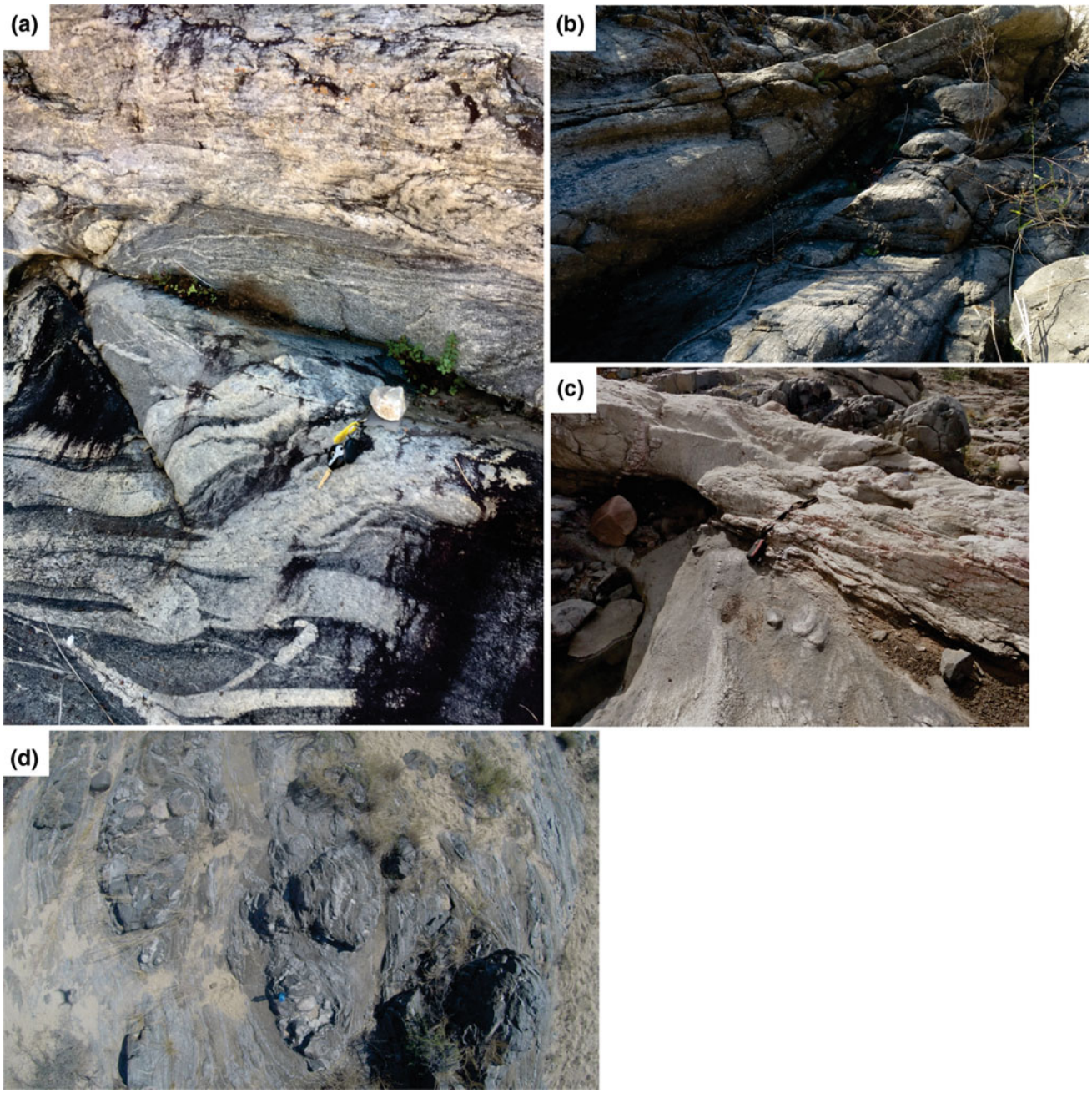

Fig. 8.8 Flat-lying shear zones superimposed onto the steep gneissic fabric of folds exposed near the contact of the zone of hydration with the underlying flat-lying HRSZ (Fig. 8.3). **a** Steeply dipping foliation developed in retrograde hydrated migmatitic tonalitic gneiss cut by near-horizontal shear fabric at the classic Goudplaats locality exposed in a river bed (locality 11 in Fig. 8.3). View to the north. **b** Instructive example in which the early steeply dipping shear fabric and steeply dipping foliation (bottom right side) preserved in retrograde hydrated tonalitic gneiss is cut by the flat-lying shear fabric in the Sand River on farm Breipaal (locality 12 in Fig. 8.3). View is to the east. **c** Steeply dipping foliation of retrograde hydrated tonalitic gneiss (bottom) cut by flat-lying shear fabric (Hout River, locality 4 in Fig. 8.3). **d** Aerial photograph taken with a drone of a steeply dipping high-grade shear zone developed in retrograde hydrated tonalitic and mafic gneiss exposed in the Sand River on farm Breipaal. Heterogeneous deformation reflected by large boudins of folded tonalitic and mafic gneiss wrapped by steep anastomosing shear zones is also reflected on a small scale in Fig. 8.7d

As previously mentioned, the Ath-in retrograde isograd (Figs. 8.2 and 8.3) is a true metamorphic feature that subdivides the SMZ into a northern granulite domain characterized by pristine metapelitic-, mafic- and ultramafic granulite gneisses of the Bandelierkop Formation and large volumes of Opx-bearing tonalitic gneiss (Baviaanskloof gneiss), and a southern domain of retrograde hydrated equivalents of these former granulites. This fact has been thoroughly documented in numerous publications based on field, petrographic, petrological, and O-isotopic studies (e.g. van Reenen 1986; van Reenen et al. 1990, 2011, 2014; Van Schalkwyk 1991; Baker et al. 1992; Van Schalkwyk and van Reenen 1992; Hoernes et al. 1995; Koizumi et al. 2014). Unfortunately, this information is ignored by Vezinet et al. (2018) and Laurent et al. (2019).

Metapelitic granulites at the position of the Ath-in retrograde isograd (Figs. 8.2 and 8.3) are characterized by coexisting Opx + Ath + Qz + Bt + Pl + Qz in Fe-rich (Crd-free) varieties (Fig. 8.9c), and additionally by Ged + Ky after Crd in Mg-rich (Crd-bearing) varieties (Fig. 8.9d) (van Reenen 1986). Retrograde hydrated equivalents of former metapelitic granulites that outcrop south of the Ath-in retrograde isograd are characterized by the complete replacement of Opx + Crd by fine-grained intergrowths of Ged + Ky (Fig. 8.9e). Two major hydration reactions in Opx + Crd + Qz-bearing metapelitic granulites resulted in the production of anthophyllite and gedrite in the same thin sections (Fig. 8.9d) (e.g. van Reenen 1986; Huizenga et al. 2014):

$$3.5\ \mathrm{Opx} + \mathrm{Qz} + \mathrm{H_2O} \rightarrow \mathrm{Ath} \qquad (1a)$$

$$5\ \mathrm{Crd} + 2\ \mathrm{H_2O} \rightarrow 2\ \mathrm{Ged} + 6\ \mathrm{Ky} + 7\ \mathrm{Qz} \qquad (1b)$$

Reaction (1a), which occurs in both Fe-rich Crd-free (Fig. 8.9c) and in Mg-rich Crd-bearing (Fig. 8.9d) granulites is univariant in the subsystem MgO–FeO–SiO_2–H_2O. This feature is evidenced by the fact that Opx − Ath − Qz − bearing metapelitic granulites accurately define the position of the Ath-in isograd in the field (van Reenen 1986; van Reenen et al. 2011, 2014; Huizenga et al. 2014). In contrast, reaction (1b) (Fig. 8.9d) is divariant in the subsystem MgO–FeO–Al_2O_3−SiO_2−H_2O and occurs over a much larger area in the field as is demonstrated by partially hydrated Crd-bearing gneisses that straddles the position of the Ath-in isograd (van Reenen 1986; van Reenen et al. 2011, 2014; Huizenga et al. 2014). The significance of this observation will be further discussed.

Mafic granulite in the zone of hydrated granulite often still contains relict orthopyroxene that is replaced by hornblende (e.g. van Reenen et al. 2011), while tonalitic Baviaanskloof gneiss in the hydrated zone is characterized by the complete absence of orthopyroxene. Ultramafic rocks in the zone of hydration show evidence for extensive interaction of the peak metamorphic assemblage Opx + Ol + Sp + Ca-Amp with H_2O–CO_2 fluids (e.g. Van Schalkwyk 1991; Van Schalkwyk and van Reenen 1992; van Reenen et al. 2011, 2014).

Petrological, fluid inclusion and stable oxygen isotope data show that the fluid responsible for establishing the Ath-in isograd in quartz-bearing metapelites at ca. 6 kbar and 600–630 °C comprised 70–90 mol% CO_2-rich (Fig. 8.10) and 30–10 mol% H_2O and brine fluids (van Reenen 1986; van Reenen and Hollister 1988; Baker et al. 1992; Hoernes and van Reenen 1992; Hoernes et al. 1995; Huizenga et al. 2014; Koizumi et al. 2014; van Reenen et al. 2011, 2014; Koizumi et al. 2014; Smit et al. 2014; Tsunogae and van Reenen 2014). Direct evidence for the passage of an externally derived CO_2-rich fluid through granulites is clearly reflected in granoblastic ultramafic rocks (Van Schalkwyk and van Reenen 1992; van Reenen et al. 2014). Here, the peak assemblage Ol + Hbl-1 + Opx-1 + Spl is partially replaced by the retrograde assemblage Ol + Hbl-2 + Opx-2 + Mgs + Dol + Chl + Tlc at ca. 600 °C and 6 kbar.

Temperature control on the regional hydration of granulite-facies rocks by low H_2O activity fluids (Fig. 8.10) is provided by the observation that at temperatures above ca. 650 °C, fluids moved through the metapelitic granulite rocks without interacting with orthopyroxene. However, when the temperature dropped to 600–630 °C, the infiltrating fluid reacted with orthopyroxene to establish the Ath-in isograd (Fig. 8.3) in metapelitic granulite (Fig. 8.9c, d) (e.g. van Reenen 1986; Baker et al. 1992; Huizenga et al. 2014; Koizumi et al. 2014; Safonov et al. 2014; van Reenen et al. 2014). That water-bearing fluids must have been present at temperatures above ca. 630 °C is evidenced by fluid-inclusion data (van Reenen and Hollister 1988; Huizenga et al. 2014), and by the replacement of cordierite coexisting with orthopyroxene and quartz by gedrite plus kyanite whereas orthopyroxene remains completely stable (Fig. 8.9f) (see also van Reenen et al. 2014, Fig. 8.6a, b).

Additional evidence that hot granulite interacted with cooler infiltrating water-bearing fluids at T ca 620 °C is documented by oxygen isotope data obtained from pristine granulites and their retrograde rehydrated equivalents (Hoernes et al. 1995), and from pristine metapelitic granulite and associated intrusive leucocratic granitoids at different localities that include the Bandelierkop (locality 9 in Fig. 8.3) (Dubinina et al. 2015; Safonov et al. 2018a, b).

As mentioned previously, more than 60% of the SMZ surface area based on their geophysical signature (De Beer and Stettler 1992) is underlain by lower grade greenstone material (inset map in Fig. 8.3). This observation provides a credible source for infiltrating fluids that interacted with the overlying hot granulites to establish the Ath-in retrograde isograd and associated zone of retrograde hydrated granulite. In this scenario the HRSZ acted as a conduit for fluid

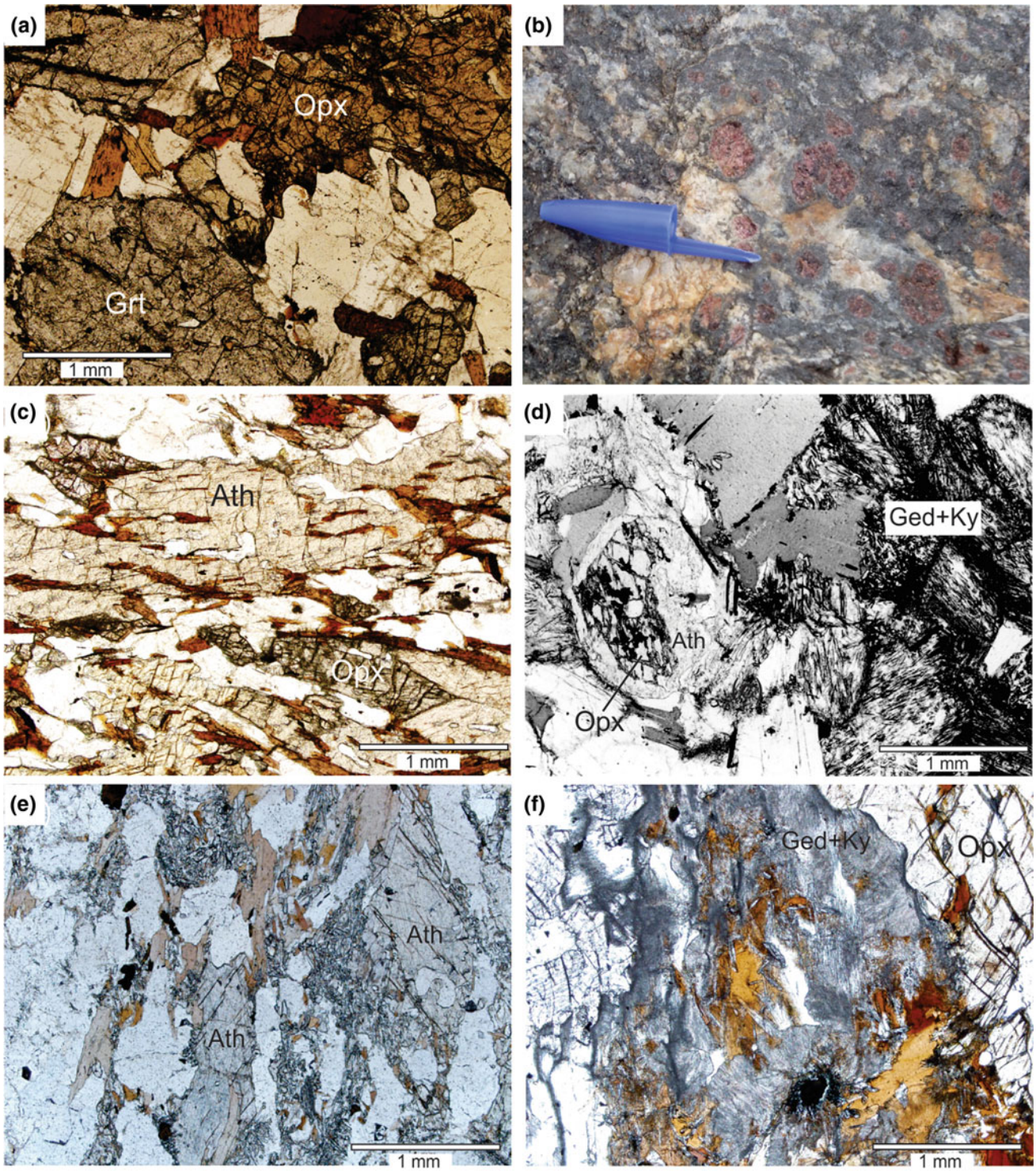

Fig. 8.9 Metamorphic evolution of metapelitic granulite illustrated by photomicrographs (plane-polarized light) (a, c, d, e) and an outcrop photograph (b). **a** Fe-rich (Crd-free) pristine granoblastic Grt-Opx-Bt-Pl-Qz-bearing granulite. **b** Outcrop of pristine granoblastic metapelitic granulite comprising Grt + Crd + Opx at the Petronella locality (locality 7 in Fig. 8.3). Note dark blue cordierite rimming garnet porphyroblasts reflecting evidence for the decompression reaction 2 Grt + 3 Qz → Crd + 2 Opx. **c** Fe-rich Opx-Ath-Qz-bearing equivalent of (a) at the position of the Ath-in isograd, reflecting evidence for the isograd-producing reaction (1a) (see text). Note equilibrium textural relationships of anthophyllite and orthopyroxene. **d** Mg-rich (Crd-bearing) metapelitic granulite at the Ath-in isograd. Orthopyroxene is rimmed by anthophyllite, whereas cordierite is extensively replaced by a fine-grained intergrowth of gedrite and kyanite, reflecting evidence for reaction (1b) (see text). **e** Retrograde hydrated equivalent of (b) and (d) south of the Ath-in isograd. Note large aligned grains of anthophyllite (Ath) and fine-grained intergrowth of gedrite and kyanite completely replacing cordierite in a matrix of quartz and plagioclase. **f** Localized cordierite hydration at Petronella locality (locality 10 in Fig. 8.3) in the granulite domain. Cordierite is replaced by fine-grained intergrowth of gedrite + kyanite, and by coarser grained biotite + kyanite, while orthopyroxene remains unaltered. See text for discussion

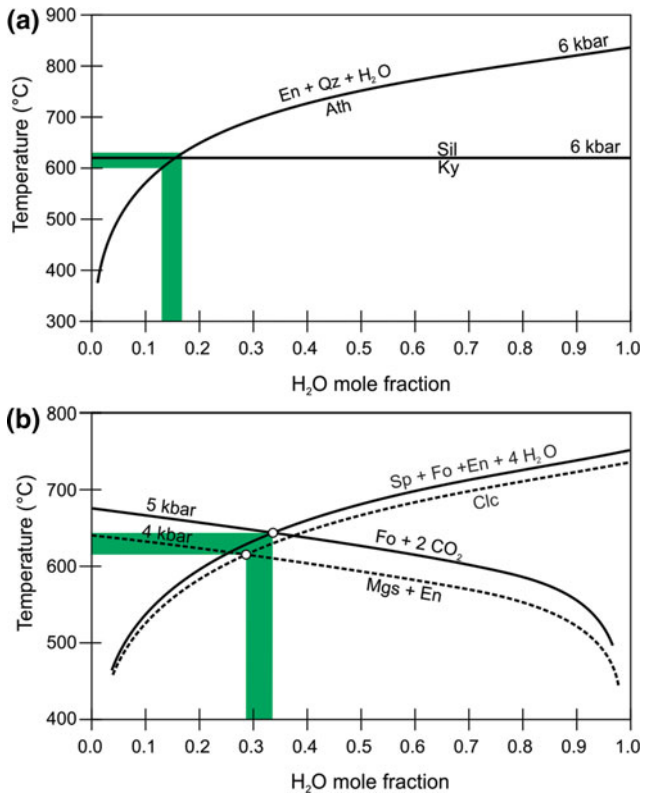

Fig. 8.10 **a** Composition of the hydrating fluid constrained by *P-T* conditions of ca. 6 kbar, 600–630 °C calculated for the retrograde Ath-in isograd assuming Mg-end members. **b** Composition of externally derived fluid phase established from partially hydrated and carbonated ultramafic assemblages. All reaction curves are calculated using the dataset of Holland and Powell (1998). Mineral compositions are given by Van Schalkwyk and van Reenen (1992) (sample DR191). Activities for the end members were calculated using the program AX developed by T. Holland. See text for discussion. Note that the H_2O activity is recalculated to H_2O mole fraction using the H_2O–CO_2 activity-composition model from Aranovich and Newton (1999) (modified after van Reenen et al. 2014)

circulation through the overlying granulite-facies crust at 2.68–2.62 Ga and is manifest in the petrography of the ca. 2.68 Ga Matok granitoid body (Fig. 8.3) (Bohlender et al. 1992; Laurent et al. 2013) and by published age data on fluid events that affected the SMZ up to ca 2.62 Ga (Kreissig et al. 2001; Belyanin et al. 2015).

Evidence that the entire SMZ consisted of granulite-facies rocks prior to ca. 2.68 Ga and before retrograde hydration is demonstrated by partially retrograde hydrated mafic, ultramafic granulite and BIF of the Bandelierkop Formation associated with completely retrograde hydrated metapelitic granulite that outcrop in the Lowveld at locality 7 (Fig. 8.3). De Wit et al. (1992c) also described outcrops of partly retrograde hydrated ultramafic granulite that outcrop at the extreme western tip of the Giyani greenstone belt near Babango (Fig. 8.3) (De Wit et al. 1992c). Partially hydrated ultramafic granulites also outcrop at the extreme western tip of the Rhenosterkoppies greenstone belt (Fig. 8.3).

Finally, it should be noted that the regional retrograde rehydration event that affected large areas of the SMZ in the hanging wall of the sub-horizontal HRSZ occurred after emplacement of Matok pluton at ca 2.68 Ga and reflects the static infiltration of hot water-bearing fluids that reacted with the overlying cooling granulites.

8.4.3.3 Metamorphic Evolution of the Granulite Domain North of the Retrograde Ath-in Isograd

Traverse C–D (Fig. 8.3) continues northwards into the Highveld that exposes steeply foliated pristine granulites (Fig. 8.7b, c) that are subdivided into two distinct metamorphic subdomains located south and north of Annaskraal Shear Zone (Figs. 8.3 and 8.4). Metapelitic assemblages characterized by Grt + Opx + Crd + Bt + Pl + Qz ± Sil in rocks from the southern subdomain document clear evidence for near-isobaric cooling (IC) *P-T* paths superimposed onto earlier decompression-cooling *P-T* paths (DR19 in Fig. 8.11). In contrast, samples with similar mineralogical compositions, but lacking sillimanite and collected from the northern subdomain document only evidence for a two-stage decompression-cooling *P-T* history (DR45 in Fig. 8.11). High-grade gneisses in both subdomains are devoid of kinematic indicators being characterized by macroscopic and microscopic granoblastic textures (Figs. 8.9a, b and 8.12a, b) while only a few rodding structures and small-scale fold axes were identified in the field (Du Toit et al. 1983; Roering et al. 1992b; Smit et al. 1992, 2001, 2011). Steeply north-dipping high-grade shear zones characterized by straight gneisses (Fig. 8.7c) (Smit and van Reenen 1997; Smit et al. 2001) that bound the complexly folded crustal blocks (Figs. 8.2 and 8.3) locally preserve kinematic indicators related to thrust sense shear deformation and record evidence for near-isobaric cooling *P-T* paths similar to that of unsheared granulites (Smit et al. 1992, 2001; Smit and van Reenen 1997). The granoblastic textures of these high-grade gneisses are interpreted to reflect evidence for extensive recrystallization and annealing during initial exhumation to the mid-crustal level as is suggested by metamorphic data (Fig. 8.11) (van Reenen 1983; van Reenen et al. 1987, 1990, 2011, 2014; Roering et al. 1992b; Smit et al. 2001, 2011, 2014).

P-T paths (Fig. 8.11) for rocks from both zones are derived from common Grt + Opx + Crd + Qz ± Sil bearing mineral assemblages, which document evidence for two major net transfer reactions (Fig. 8.12a, b) (Perchuk et al. 1996, 2000a; Smit et al. 2001; van Reenen et al. 2011, 2014):

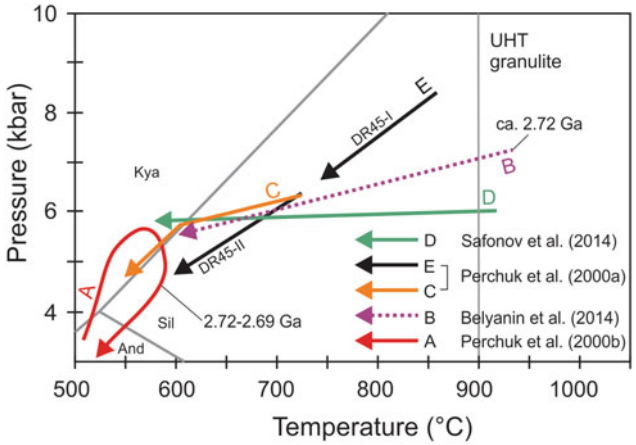

Fig. 8.11 *P-T* paths (A–E) compiled from a large published database (e.g. Perchuk et al. 2000a, b; Smit et al. 2001; Belyanin et al. 2014; Safonov et al. 2014) that highlights important metamorphic features of the SMZ and the juxtaposed Khavagari arm of the Giyani greenstone belt located in the footwall of the steeply north-dipping HRSZ (locality 1 in Fig. 8.3). A: *P-T* loop constructed from Grt-Ky-bearing schists exposed in the Khavagari Shear Zone in the Khavagari arm of the Giyani greenstone belt (locality 1 in Fig. 8.3). B: Near-isobaric cooling *P-T* path that characterizes the southern granulite domain (Figs. 8.3 and 8.4) constructed from MgO–Al_2O_3-rich zones in sample DR19 (Belyanin et al. 2014). C: Near-isobaric cooling *P-T* path that characterizes the southern granulite domain constructed from the common mineral assemblage Grt + Opx + Crd + Qz in sample DR19 (Perchuk et al. 2000a; Smit et al. 2001). This assemblage characterizes metapelitic granulite throughout the granulite subdomain of the SMZ. D: Evidence for ultrahigh-temperature near-isobaric cooling from >900 °C calculated from partially assimilated metapelitic granulite that interacted with intruding ultrahigh-temperature Grt-bearing trondhjemites at the Petronella locality (locality 10 in Fig. 8.3). E: Multi-stage decompression-cooling *P-T* path that characterizes the northern granulite subdomain (DR45) (Figs. 8.3 and 8.4)

$$2\ \mathrm{Grt} - 1 + 3\ \mathrm{Qz} \rightarrow \mathrm{Crd} + 2\ \mathrm{Opx} \qquad (2a)$$

$$3\ \mathrm{Crd} \rightarrow 2\ \mathrm{Grt} - 2 + 4\ \mathrm{Sil} + 5\ \mathrm{Qz} \qquad (2b)$$

Garnet-consuming reaction (2a) (Fig. 8.12a) documents a decompression-cooling history, whereas reaction (2b) (Fig. 8.12b) that is superimposed onto the products of reaction (2a) represents new garnet growth with sillimanite at the expense of cordierite during near-isobaric cooling. For all rocks, *P-T* calculations were done using the same pressure-sensitive reactions (2a) and (2b) combined with temperature-sensitive Fe–Mg cation exchange reactions (Perchuk et al. 2000a; Smit et al. 2001; see Perchuk 2011 for a detailed explanation).

A large number of samples collected throughout the southern granulite subdomain that include straight gneisses sampled from shear zones, show near-isobaric *P-T* paths. These *P-T* paths typically start at a pressure of ca. 6 kbar (ca. 20 km depth) and a temperature of ca. 700 °C, and end at 5.0–5.5 kbar and 570–600 °C (Fig. 8.11) (Perchuk et al. 2000a; Smit et al. 2001). In contrast to the southern granulite zone, metapelitic granulites (e.g. sample DR45, locality 15 in Fig. 8.3) of similar bulk composition and with similar mineral assemblages (but lacking sillimanite) north of the Annaskraal Shear Zone show no evidence for a near-isobaric cooling stage (Perchuk et al. 2000a) and document a two-stage decompression-cooling *P-T* history (DR45 in Fig. 8.11). The rocks record maximum *P-T* conditions of 6.7 kbar and 850 °C, respectively. They were exhumed and emplaced at the mid-crustal level at a pressure of ca. 6 kbar and a temperature of ca. 720 °C (DR45 in Fig. 8.11) (e.g. Perchuk et al. 2000a; Smit et al. 2001; van Reenen et al. 2011). At these *P-T* conditions, the rocks were cooled and annealed before being finally exhumed to 4.5 kbar (ca. 15 km depth). The gap in the decompression-cooling *P-T* path (DR45 in Fig. 8.11) is not recorded by garnet zoning (Perchuk et al. 2000a; Smit et al. 2001) and is interpreted to reflect the time of emplacement of anatectic melts (van Reenen et al. 2011, 2014; Smit et al. 2014) dated at 2.64–2.68 Ga (Kreissig et al. 2001; Belyanin et al. 2014).

The contrasting near-isobaric and decompression-cooling *P-T* paths (compare DR19 and DR45 in Fig. 8.11) suggest that the entire SMZ, with its embedded steeply plunging folds and steeply dipping high-grade shear zones was initially uplifted to the mid-crustal level (ca. 20 km depth), being accompanied by emplacement of leucocratic trondhjemitic magmas at 2.68–2.64 Ga (e.g. Kreissig et al. 2001; Belyanin et al. 2014; Safonov et al. 2014, 2018b; van Reenen et al. 2014), where both granulites and magmas were concomitantly cooled and annealed (Safonov et al. 2014). Consequently, these granoblastic rocks are devoid of mineral lineations (Du Toit et al. 1983; Roering et al. 1992b; Smit et al. 1992).

The presence of near-isobaric cooling *P-T* paths (Fig. 8.11) documented by granulites and their sheared equivalents south of the Annaskraal Shear Zone is in support of structural (Fig. 8.4) and geophysical data (see Fig. 8.15a, b) that a hot SMZ nappe with imbedded steeply plunging folds and steeply dipping shear zones was channelled southwards for a distance of ca. 30 km (inset map in Fig. 8.3) against and onto the adjacent NKVC along a ca. 6 kbar near-isobaric (20 km depth) crustal plane. This plane is represented by the flat-lying HRSZ (Figs. 8.4 and 8.6b, c) and is underlain by lower grade greenstone material (inset map in Fig. 8.3) (De Beer and Stettler 1992; Smit et al. 2014; van Reenen et al. 2014). Near-isobaric cooling *P-T* paths (Fig. 8.11) demonstrate that these rocks had to cool rapidly. The only mechanism to facilitate such cooling of hot rock masses at mid-crustal level and far from the exposed contact with the juxtaposed granite-greenstone craton (Figs. 8.3 and 8.4) is the pervasive and channelled infiltration of large volumes of relatively cold fluids derived from devolatilization of greenstone belt material that underlies much of the

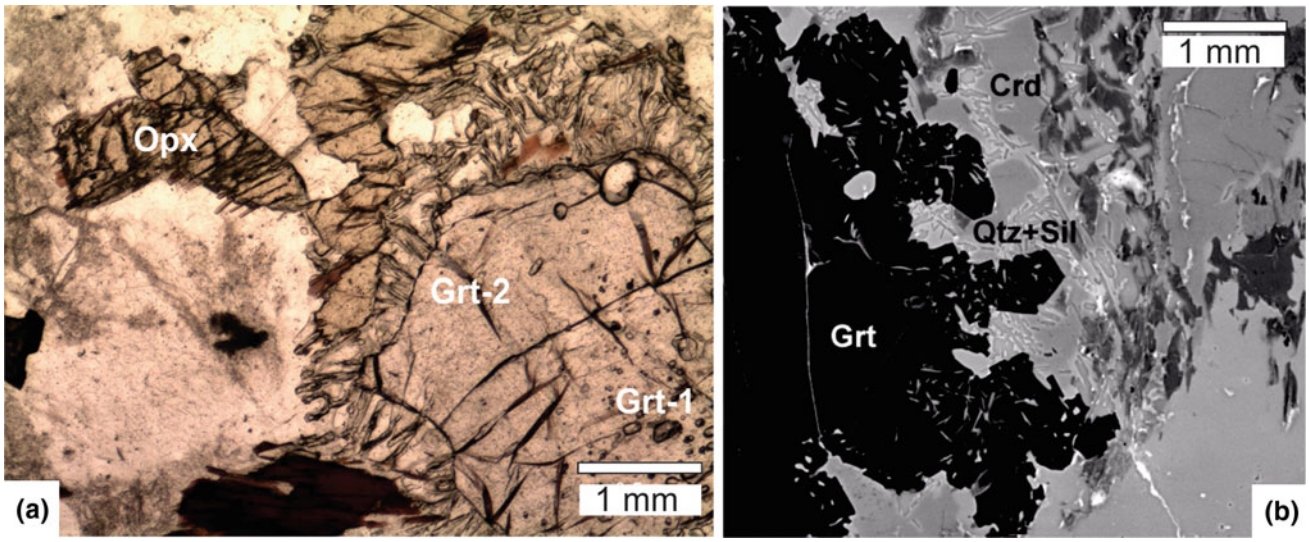

Fig. 8.12 **a** Photomicrograph of reaction (2a): 2 Grt-1 + 3 Qz → Crd + 2 Opx. This reaction documents evidence for a two-stage decompression-cooling *P-T* path (DR45 in Fig. 8.11). The early stage is documented by the poikiloblastic core of Grt-1 in equilibrium with coarse-grained Opx-1 and Crd-1 in the matrix of the rock. The second stage is reflected by the inclusion-free Grt-2 rim in contact with symplectitic intergrowths of Opx-2 and Crd-2 (e.g. Smit et al. 2001). **b** Backscatter electron image of reaction (2b): 3 Crd → 2 Grt-2 + 4 Sil + 5 Qz preserved in sample DV101 (locality 14 in Fig. 8.3). This reaction demonstrates evidence for near-isobaric cooling (e.g. Smit et al. 2001). See text for discussion

SMZ (inset map in Figs. 8.3 and 8.4) (De Beer and Stettler 1992; van Reenen et al. 2011, 2014; Smit et al. 2014).

8.4.3.4 Fluid-Induced Melting and Generation of Granitic Magma at UHT Conditions in the SMZ

High-grade gneisses exposed throughout the SMZ (Figs. 8.2 and 8.3) are migmatitic. This is expressed in outcrops by the presence of small volumes (<10%) of leucocratic Pl + Qz ± perthite/antiperthite anatectic material enhancing the gneissic and shear fabric (e.g. Figs. 8.7a–c and 8.8a) (Du Toit et al. 1983; van Reenen et al. 2014). Migmatization that affected high-grade gneisses is interpreted to have occurred at the deep crustal level during peak metamorphism and deformation (e.g. van Reenen et al. 2011, 2014), resulting in melt-weakened crust from which small amounts of melt were not removed (e.g. Jamieson et al. 2011; Smit et al. 2014).

In addition to the fabric sub-parallel anatectic material, large volumes of mainly discordant and weakly to non-foliated granodioritic-trondhjemitic veins and bodies (Du Toit et al. 1983) also intrude and partially assimilated (Safonov et al. 2014, 2018a) the deformed and metamorphosed granulite at ca. 2.67–2.64 Ga (Kreissig et al. 2001; Belyanin et al. 2014; van Reenen et al. 2011, 2014). These large undeformed bodies (e.g. Fig. 8.13a) reflect a major pulse of anatexis linked to fluid-induced decompression melting that post-date peak metamorphism and deformation at ca. 2.72 Ga and occur at different localities in the SMZ (Dubinina et al. 2015; Safonov et al. 2018b). Safonov et al. (2014, 2018a) studied the large (ca. 30 × 60 m) and almost undeformed granodiorite-trondhjemite body dated at ca. 2.67 Ga that intrude sheared migmatitic granulite (Fig. 8.13a) on the Farm Petronella (locality 10 in Fig. 8.3). The partially assimilated migmatitic gneisses preserve evidence for the near-isobaric cooling of hot magma from >900 to ca. 600 °C (at a pressure of 5.5–6.5 kbar) (D in Fig. 8.11), that also affected the host metapelitic granulite. CO_2 fluid inclusions in quartz and garnet in trondhjemites show that the magma transported CO_2 fluids with densities corresponding to the late stages of magma cooling at 5.5–6.5 kbar and 600–650 °C. CO_2 fluids coexisted with low H_2O activity brine fluids (Safonov et al. 2014). Carbon isotope compositions of graphite and fluid inclusions from different garnet-sillimanite-bearing leucocratic tonalites, trondhjemites and granites associated with orthopyroxene-bearing granulite metapelites (including Bandelierkop, locality 9 in Fig. 8.3) in the SMZ, also indicate that fluids associated with the granitoid magmas of the SMZ originated from a source unrelated to the host metapelites (Safonov et al. 2018b).

Evidence for deep crustal embrittlement (Fig. 8.13b) at the Petronella locality documented by brittle deformation in which granulite-facies breccia are cemented by Opx-bearing leucocratic material (Roering et al. 1995) confirms the action of fluids/melts at near-lithostatic pressures during granulite-facies metamorphism in the SMZ (Roering et al. 1995).

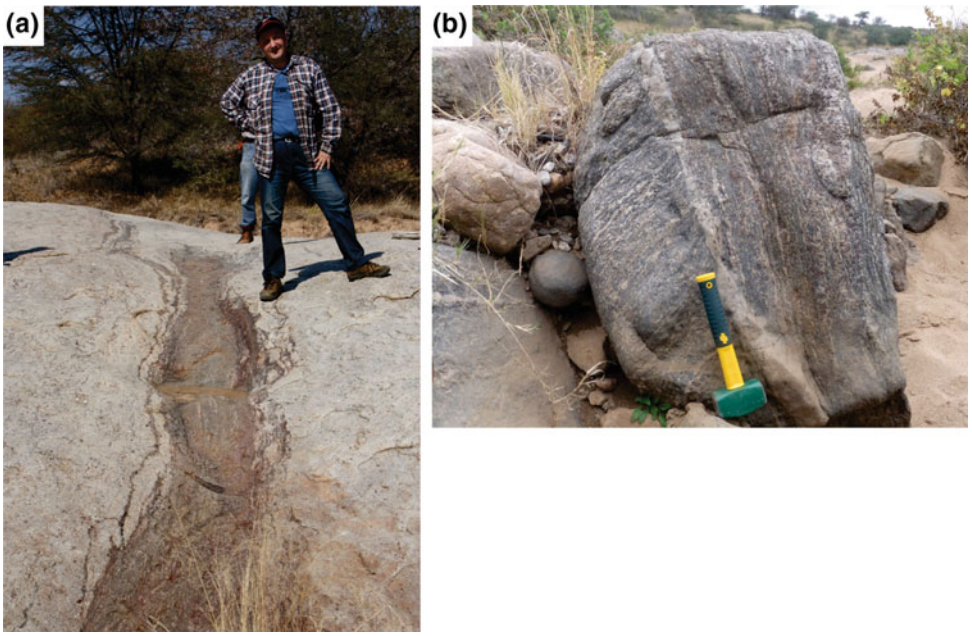

Fig. 8.13 **a** Undeformed leucocratic trondjhemite (ca. 2.67 Ga) with partially assimilated migmatitic metapelite granulite (dated at ca. 2.72 Ga) at Petronella (locality 10 in Fig. 8.3). **b** Exposure of metapelitic granulite that contains two distinct foliation trends at high angles to each other. The leucocratic vein separating the two blocks of foliated granulite is composed of orthopyroxene. The relationship is interpreted as evidence for deep crustal embrittlement under granulite-facies conditions within the Petronella Shear Zone, whereby fractured blocks of granulite gneiss have been cemented together along the orthopyroxene vein (Roering et al. 1995); see text for discussion

Roering et al. (1995) showed that the presence of such fluids/melts along thrust planes resulted in a lubrication effect due to reduction of brittle/plastic strength of rocks subjected to fluid/melt percolation at near-lithostatic pressures. It would have enhanced (and effectively permitted) near-horizontal channelling of a hot granulite nappe for more than 35 km over relatively cold greenstone material by reducing friction along the thrust plane (Roering et al. 1995; Smit et al. 2014). Devolatilization of underlying greenschist material persisted as long as southwards channelling of the hot nappe continued (Koons et al. 1998; Yardley 2009; Smit et al. 2014).

8.4.3.5 Timing of Major Events that Affected the SMZ and Juxtaposed NKVC

Geochronological data obtained by different researchers provide the following important constraints on the timing of major events that affected the SMZ and the juxtaposed NKVC.

(1) Different authors used zircon SHRIMP age data obtained from metamorphic charnockite (Retief et al. 1990) and from metapelitic granulite at different localities in the granulite zone south of the Annaskraal Shear Zone (Rajesh et al. 2014; Taylor et al. 2014; Nicoli et al. 2015) to accurately constrain the timing of the peak metamorphic and deformational event in the SMZ to ca. 2.72 Ga.

(2) Thermal and dynamic interaction of SMZ hanging wall granulite with relatively cold greenstone material in the footwall of the steeply north-dipping HRSZ at the Khavagari arm of the Giyani greenstone belt at 2.72–2.69 Ga accurately dates the age of the HRSZ and the time of emplacement of the SMZ against and over the adjacent NKVC (Figs. 8.3, 8.4 and 8.11) (e.g. Perchuk et al. 2000b; Kreissig et al. 2001; Kramers et al. 2014).

(3) Growth of monazite associated with the common decompression metapelitic assemblage Grt + Crd + Opx + Qz from the Bandelierkop locality at 2.69 Ga accurately dates the early post-peak stage of exhumation (Fig. 8.11) (Kreissig et al. 2001).

(4) Emplacement at ca. 2.67 Ga of the granodioritic-tonalitic body (Fig. 8.13a) into already deformed and sheared migmatitic granulite associated with the steeply dipping Petronella Shear Zone provides a minimum age for peak metamorphism and deformation (van Reenen et al. 2011, 2014; Belyanin et al. 2014; Safonov et al. 2014).

(5) Intrusions of geochemically similar granitoid plutons into the SMZ (Matok) (Figs. 8.2, 8.3 and 8.13) and in the adjacent NKVC (Moletsi) north and south of the HRSZ at ca. 2.68 Ga (Figs. 8.2, 8.3 and 8.14) (Laurent et al. 2013), provide unequivocal evidence that the SMZ nappe was already juxtaposed at ca. 2.72 Ga against and over the NKVC.

Fig. 8.14 Matok granite intrudes a steeply dipping high-grade shear zone developed in sheared Opx-bearing metapelitic granulite on Farm Tarentaaldraai (locality 16 in Fig. 8.3). This high-grade shear zone was subsequently reactivated to produce the oblique-slip upper crustal Nthabalala mylonitic shear zone (e.g. van Reenen et al. 2011) that displaces the Matok pluton (Figs. 8.2 and 8.3). This is shown by superimposition of the younger shear fabric onto the intrusive granite (this figure), by left-lateral displacement of the Matok pluton, and by similar sense displacement of large folds in the area east of the Matok pluton (Fig. 8.2) (van Reenen et al. 2011)

(6) Regional infiltration of aqueous-carbonic fluids into the overlying hot granulite nappe that established the Ath-in retrograde isograd and associated zones of retrograde hydrated granulite (Fig. 8.3) also affected the Matok pluton and occurred at 2.68–2.62 Ga (Kreissig et al. 2001; Laurent et al. 2013).
(7) Emplacement of the post-kinematic Palmietfontein granite into migmatitic granulite at ca. 2.45 Ga indicates the end of major tectono-metamorphic events in the SMZ (Barton and van Reenen 1992).
(8) Rajesh et al. (2014) and Nicoli et al. (2015) reported ages older than 3.0 Ga (as old as 3.44 Ga, Rajesh et al. 2014) for detrital zircon from metapelites of the Bandelierkop Formation, whereas Retief et al. (1990) reported similar ages from zircon in metamorphic charnockite. These ages are consistent with ages reported for greenstone successions on the adjacent NKVC (Zeh et al. 2013).

8.4.4 Geophysical Constraints on the Nature of the SMZ and the Relationship with the NKVC and the CZ

Aeromagnetic-, vibro seismic-, gravity-, and geoelectrical data obtained from the LC and adjacent NKVC (Figs. 8.1, 8.3 and 8.15a, b) (Stuart and Zengeni 1987; Kleywegt et al. 1987; Kleywegt 1988; De Beer and Stettler 1988, 1992; Stettler et al. 1989; Roering et al. 1990; De Beer et al. 1991; Durrheim et al. 1992) provide important information regarding the complex geological relationship of a hot allochthonous SMZ granulite nappe with both the CZ in the north and the NKVC in the south.

Detailed geophysical data (Fig. 8.15a, b) collected across the southern boundary (HRSZ) of the SMZ (Kleywegt et al. 1987; De Beer and Stettler 1988, 1992; De Beer et al. 1991; Klemperer 1992) showed that SMZ granulites were thrust southwards over the low-grade NKVC along the entire lateral length of the HRSZ (Figs. 8.2 and 8.3), confirming the allochthonous nature of the SMZ nappe based on structural and *P-T-t* studies (e.g. Miyano et al. 1992; Roering et al. 1992a; Perchuk et al. 1996, 2000b; Kreissig et al. 2001; Kramers et al. 2014). Furthermore, geoelectrical data (inset map in Fig. 8.3; De Beer and Stettler 1992) show that more than 60% of the surface area of the SMZ is underlain at depth by a material with physical characteristics identical to those of greenstone material on the NKVC. In addition, geoelectrical, seismic, gravity and aeromagnetic data from the NKVC, LC, and ZC allowed modelling the crust with three distinct units (Fig. 8.15a) (e.g. De Beer and Stettler 1992). These units comprise (1) the two granite-greenstone cratons (NKVC and ZC) with similar lithologies and gravity signatures, (2) the SMZ and NMZ both consisting mainly of meta-igneous rocks with identical gravity signatures, and (3) the CZ dominated by metasedimentary rocks with gravity properties that differ significantly from that of the two marginal zones, but that are identical to that of the two cratons (De Beer et al. 1992).

The following section is a detailed discussion of the two-stage steep exhumation of the CZ at 2.72–2.62 Ga that is interpreted to have directed southwards channelling of a hot allochthonous SMZ nappe by means of a conveyor belt mechanism as previously discussed by Smit et al. (2014).

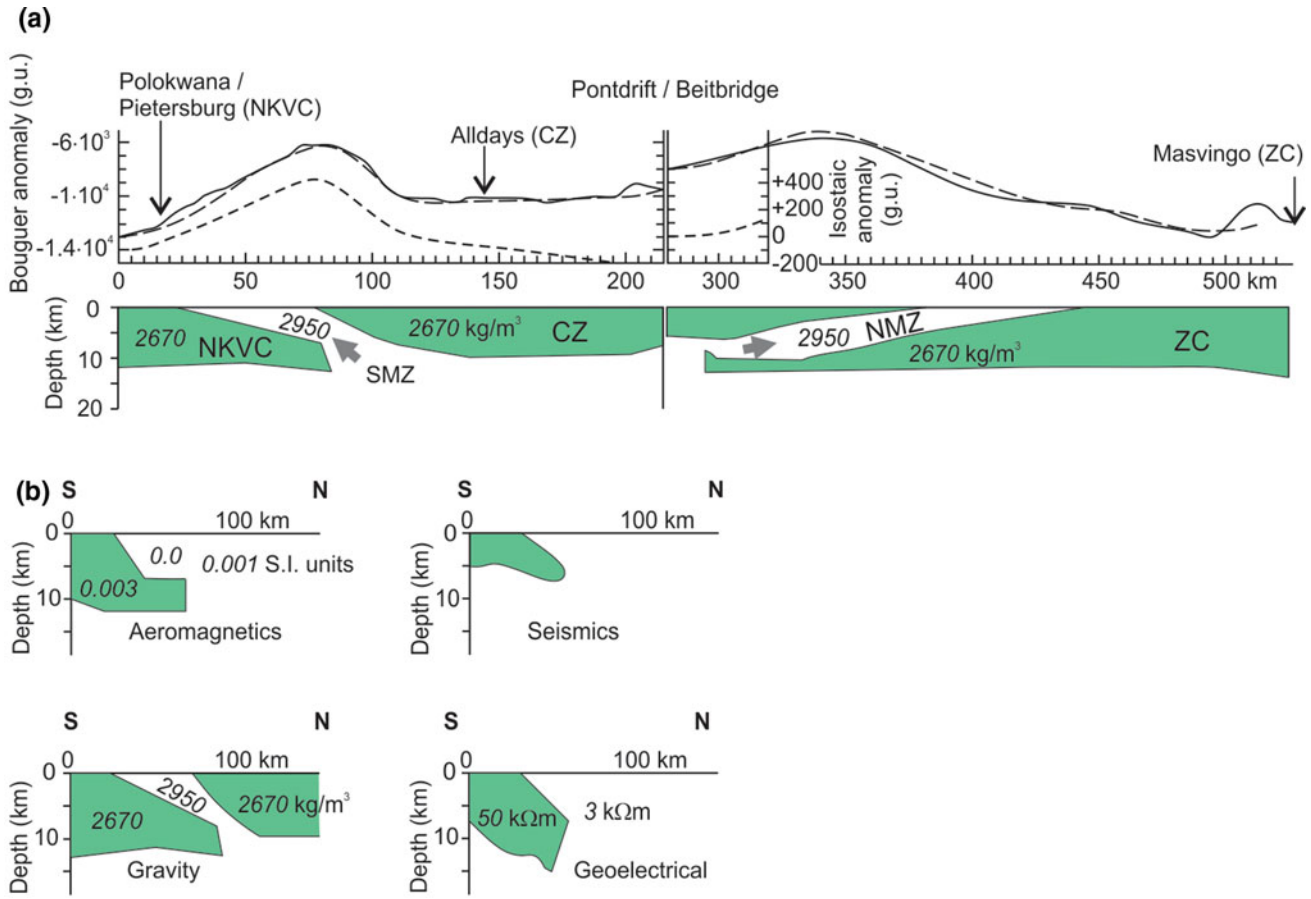

Fig. 8.15 Geophysical data obtained from the Limpopo Complex and adjacent KVC and ZC cratons (modified after De Beer and Stettler 1992). **a** Bouguer gravity models for the Limpopo complex and adjacent granite-greenstone cratons (Fig. 8.1). Densities are in kg/m^3 and Bouguer (solid line) and isostatic (broken line) anomalies are in gravity units (1 g.u. = 10^{-6} m/s^2 = 0.1 mgal). **b** Comparison of the geoelectrical, gravity, aeromagnetic, and seismic reflection data across the SMZ of the LC. Density and susceptibility are expressed in kg/m^3 and S.I. units, respectively, the resistivity is expressed in kΩ·m. See text for discussion

8.5 Two-Stage Exhumation History of the CZ at 2.72–2.61 Ga

The two-stage exhumation of the CZ at ca. 2.72–2.62 Ga is discussed by considering the most relevant published regional structural, magmatic, metamorphic, and geochronological features of the CZ (e.g. Roering et al. 1992a, b; Perchuk et al. 2008a, b; van Reenen et al. 2008; Kramers and Mouri 2011; Kramers and Zeh 2011; Kramers et al. 2011; Smit et al. 2011; Smit et al. 2014; Kröner et al. 2018).

Decompression-cooling *P-T-t* paths constructed for metapelitic gneisses (of which sample TOV13 in Fig. 8.17 is a prime example) that are associated with distinct regional structural features (isoclinal folds and closed structures) of the CZ confirmed the two-stage steep *P-T* evolution of this high-grade gneiss terrane in the Neoarchaean (e.g. Smit et al. 2011). Steeply plunging isoclinal folds and melt-weakened domes were initially emplaced at the mid-crustal level before ca. 2.65 Ga. This was followed by emplacement at the upper crustal level of steeply southwest-plunging mega closed structures at 2.65–2.62 Ga (Figs. 8.17, 8.18, 8.19, 8.23, 8.24a).

P-T-t paths for these distinct major structural features are derived from Grt − Crd − Sil − Bt − Kfs − Qz ± Opx-bearing metapelites of comparable bulk chemical compositions and based on the concept of local chemical equilibrium (e.g. Perchuk et al. 2008a, b; Perchuk and van Reenen 2008; Smit et al. 2011). This approach also recognizes the important role of heterogeneous deformation, which resulted in the formation and preservation of discrete Neoarchaean (and Palaeoproterozoic) high-grade events on scales that vary from the regional scale (Fig. 8.19) to outcrop scale (Fig. 8.20a–c) and also the thin section scale in the CZ (Perchuk and van Reenen 2008; Perchuk et al. 2008a; Mahan et al. 2011; Smit et al. 2011). *P-T-t* paths (Fig. 8.17) linked to

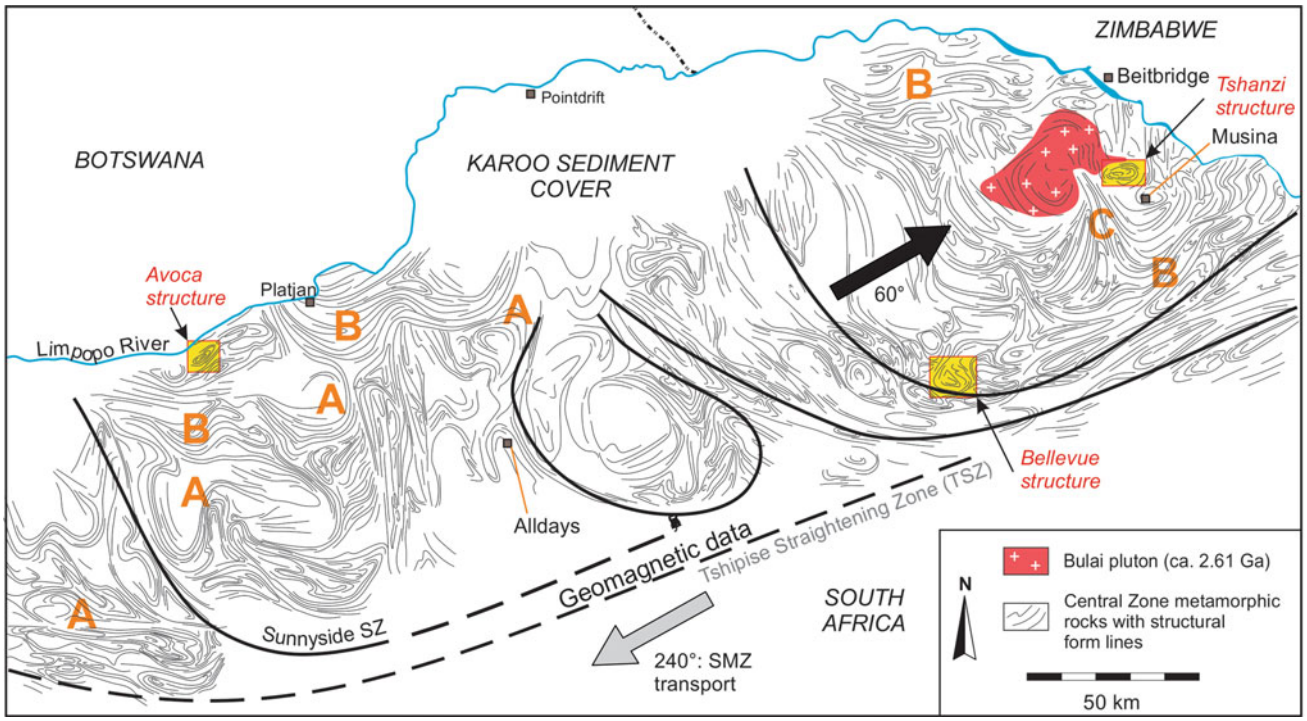

Fig. 8.16 Structural map of the central zone (CZ) based on aerial photographic interpretation (after Smit et al. 2011). Structural form lines (thin black lines) highlight large melt-weakened migmatitic domes (A) and regional-scale isoclinal folds developed in granoblastic gneisses that collectively reflect the oldest deformational features of the CZ (B). These early structural features are overprinted by large north–south trending fold structures referred to as cross folds (C), and by large closed structures mapped as sheath folds (Roering et al. 1992b), of which the Avoca, Tshanzi, and Bellevue structures (highlighted in yellow) have been studied in detail. Note the presence of a large number of closed structures developed in the vicinity of the Bellevue structure. The southwest–northeast-trending Tshipise Straightening Zone (here termed TSZ) bounds and truncates the CZ in the south. Also shown is the position of the post-tectonic ca. 2.61 Ga Bulai granitic pluton as well as the northeast direction of exhumation of CZ rocks. The SMZ was channelled in the exact opposite direction (Roering et al. 1992b). North–south trending shear zones related to the TSZ (thick black lines) subdivide the CZ into large crustal blocks

discrete fabric-forming events associated with the formation of regional isoclinal folds and with mega-scale closed structures (Fig. 8.16) provided, for the first time, unequivocal evidence for the high-grade polymetamorphic evolution of the CZ. This complex evolutionary history is reflected by a multi-stage high-grade tectono-metamorphic event at ca. 2.72–2.62 Ga in the Neoarchaean (Fig. 8.17, TOV13-1 and TOV13-2) followed by a high-grade and mainly thermal overprint associated with discrete (metres wide) shear zones in the Palaeoproterozoic at ca. 2.0 Ga (Perchuk and van Reenen 2008; van Reenen et al. 2008; Kramers and Mouri 2011; Kramers and Zeh 2011; Kramers et al. 2011; Mahan et al. 2011; Smit et al. 2011). Kröner et al. (2018) recently published detailed U-Pb age data obtained from deformed high-grade gneisses preserved as a large enclave in the ca. 2.61 Ga Bulai pluton that we interpret to provide direct evidence for the timing of the second stage of exhumation of the CZ (Fig. 8.17, TOV13-2) in the Neoarchaean at ca. 2.62 Ga. This new metamorphic data finally put to rest the conclusion of a single Palaeoproterozoic Limpopo orogeny at ca. 2.0 Ga as has been argued for by different researchers (e.g. Zeh and Klemd 2008 and references therein). However, the proposal by Brandt et al. (2018) that the Neoarchaean high-grade event at 2.64–2.62 Ga (Kröner et al. 2018) is linked to a counterclockwise *P-T* path is not in accordance with our structural-metamorphic and magmatic data as will be further discussed in Sect. 8.5.2.

Evidence for the steep two-stage exhumation of CZ granulites in the interval 2.72–2.61 Ga is demonstrated by linking specific stages of two-stage *P-T-t* paths (TOV13-I and TOV13-II in Fig. 8.17) to the successive evolution of major fold- and shear-deformational events in the CZ (Figs. 8.18, 8.19 and 8.22). Granoblastic metapelitic granulite associated with regionally developed steeply plunging isoclinal folds and dome-like structures cored by migmatitic gneisses (Fig. 8.16) are associated with decompression-cooling *P-T* paths (TOV13-1 in Fig. 8.17) that accompanied the initial exhumation of the CZ at the mid-crustal level

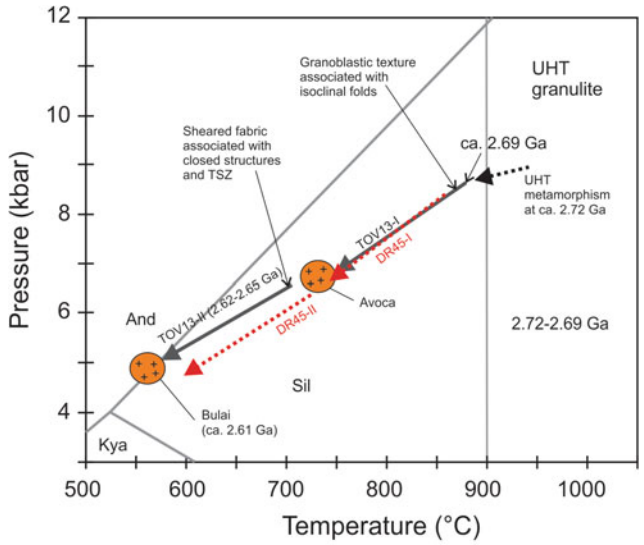

Fig. 8.17 *P-T-t* path constructed for metapelitic sample TOV13 in the rim of the Tshanzi closed structure (Fig. 8.16) is an example of the two-stage decompression-cooling (DC) metamorphic evolution that characterizes the CZ (Perchuk et al. 2008b; Smit et al. 2011). The first stage of the *P-T-t* path (TOV13-I) is constructed from a Grt-1 + Crd-1 + Sil-1 + Bt-1 + Qtz assemblage preserved in a relict granoblastic portion of sample TOV13. TOV13-I demonstrates the initial exhumation of early isoclinal folds and dome-like structures at the mid-crustal level before ca. 2.65 (emplacement of Avoca closed structure). The second stage of the *P-T-t* path (TOV13-II) is constructed from a Grt-2 + Crd-2 + Sil-2 + Bt-2 + Qtz-bearing assemblage preserved in the superimposed shear fabric developed in sample TOV13 (Smit et al. 2011). TOV13-II reflects the subsequent decompression-cooling *P-T* evolution of sheared gneisses associated with formation of closed structures (and with the TSZ) at 2.65–2.62 Ga, prior to emplacement of the Bulai pluton at ca. 2.61 Ga. Note the close similarity of *P-T* paths constructed for metapelitic granulite from the granulite subdomain north of the Annaskraal Shear Zone in the SMZ (DR45 in Fig. 8.11), and *P-T* paths constructed for CZ metapelitic granulite (TOV13 in Fig. 8.17). TSZ: Tshipise Straightening Zone. See text for discussion

before ca. 2.65 Ga. In turn, shear deformation is reflected by large closed structures cored by granitoids and previously mapped as steeply southwest-plunging mega sheath folds (Figs. 8.16, 8.19 and 8.22) (Roering et al. 1992b). These structures record evidence for granitic diapirism that accompanied the steep NE-directed exhumation of the CZ at 2.65–2.62 Ga (Perchuk et al. 2008a; Smit et al. 2011). *P-T* evidence presented for the multi-stage decompression-cooling evolution of the CZ (Fig. 8.17) is discussed with reference to the prime example of sample TOV13 collected from the rim of the Tshanzi closed structure (Fig. 8.16). The reader might also consult publications that discuss similar *P-T* data collected from other localities in the CZ that are up to 150 km apart (e.g. Perchuk et al. 2008a; Huizenga et al. 2011; Smit et al. 2011).

8.5.1 *P-T-t* Paths and the Evolution of Isoclinal Folds and Dome-like Structures

Small-scale to kilometre-scale isoclinal folds and closely associated dome-like structures cored by migmatitic gneisses occur throughout the CZ (Fig. 8.16). These folds deform a steep gneissic/migmatitc foliation (e.g. Smit et al. 2011) that trends in general in an east–west direction sub-parallel to the regional structural trend of the CZ (Figs. 8.1 and 8.16). High-grade gneisses within complexly deformed isoclinal folds and dome-like structures are granoblastic in hand specimen and under the microscope and characterized by the absence of mineral stretching lineations (e.g. Smit et al. 2011). The only kinematic elements visible in such gneisses in the field are quartz rodding and minor fold axes (e.g. Smit et al. 2011). This situation is similar to that of the granulite domain of the SMZ (Figs. 8.2 and 8.3) where granulites associated with isoclinal folds and dome-like structures of similar scale are also characterized by granoblastic textures (Figs. 8.9a, b and 8.12a, b) and the general absence of kinematic indicators. These features allow areas underlain by isoclinal folds and dome-like structures to be easily distinguished in the field from areas underlain by large closed structures with abundant kinematic indicators (compare Figs. 8.16, 8.20a–c and 8.21).

Isoclinal folds are developed in all rocks comprising the Beit Bridge Complex, the Messina Layered Complex, the Sand River Gneiss, and the Alldays/Verbaard gneiss. They provide metamorphic evidence for the early stage of the two-stage exhumation history of the CZ. Peak metamorphism has been reached in the core of the orogen at ca. 2.72 Ga (Fig. 8.17). This was followed by the early decompression-cooling stage, which is reflected by a decompression-cooling *P-T* path constructed for granoblastic metapelitic granulite (TOV 13-I in Fig. 8.17). Decompression-cooling ended concomitant with the onset of granitic diapirism at 2.65–2.63 Ga (Fig. 8.17) and the formation of major closed structures typified by a high-grade shear fabric (Figs. 8.20c and 8.21) (e.g. Smit et al. 2011). *P-T* conditions during the early exhumation stage of the decompression-cooling history calculated from the common metapelitic assemblage Grt + Crd + Sil + Qz + Kfs (Fig. 8.17) range from ca. 6.3 kbar and ca. 830 °C to 6.5 kbar and 700 °C. Timing of peak metamorphism in the CZ has not been accurately established, due to the almost pervasive superimposed thermal event that affected the CZ at ca. 2.01 Ga (van Reenen et al. 2008; Kramers and Mouri 2011; Smit et al. 2011) (see also discussion by Kröner et al. 2018). However, Kröner et al. (1998, 1999) provided accurate age data obtained from two samples of quartzofeldspathic granitoids collected from road cuttings

southwest of Musina (TR115 and TR130, Fig. 8.2; Kröner et al. 1999) that constrain the minimum age of peak metamorphism and deformation in the CZ. The first sample (TR115) described as a well layered, fine-grained, biotite-rich quartzofeldspathic gneiss with granoblastic texture, gave a SHRIMP age of 2717 ± 3 Ma considered by Kröner et al. (1999) to reflect the formation age of the gneiss protolith. The second sample (TR130) considered by these authors to represent anatectic Singelele-type gneiss, gave a SHRIMP age of 2681 ± 8 Ma. Similar rocks also considered as anatectic granitoids have at numerous localities in the CZ been shown to intrude already deformed and metamorphosed supracrustal rocks. Singelele-type granitoids, in general, show little or no evidence of deformation after emplacement (e.g. Fig. 8.18), comparable to similar field relationships described in the SMZ (e.g. Fig. 8.13a). These results, and similar results obtained from similar anatectic granitoids in the SMZ, constrain the minimum time of peak metamorphism and deformation that affected both domains at ca. 2.68 Ga. In fact, the time of peak metamorphism in the CZ based on the age of sample TR115 (2717 ± 3 Ma) is the same as the time of peak metamorphism in the SMZ dated at ca. 2.72 Ga. The proposed linked evolution of these two geotectonic domains is thus strongly supported by geochronological data obtained from intrusive granitoids.

High-grade gneisses associated with steeply plunging isoclinal folds seldomly show evidence of intense deformation on the outcrop scale (Fig. 8.20a) but are always granoblastic in hand specimen and under the microscope (e.g. van Reenen et al. 2008; Mahan et al. 2011; Smit et al. 2011). This suggests, as the case is in the SMZ, that hot granulites were exhumed before ca. 2.65 Ga and emplaced at the mid-crustal level (ca. 20 km depth) (DR45-I, II in Fig. 8.11, and TOV13-I, II in Fig. 8.17), where the rocks were cooled and annealed before being further exhumed along decompression-cooling *P-T* paths.

8.5.2 *P-T-t* Paths and the Evolution of Mega Closed Structures

Mega-scale steeply southwest-plunging folds (Figs. 8.19 and 8.22) that are characteristically circular or eye-shaped in the plan have been recognized throughout the CZ (Fig. 8.16) (e.g. Roering et al. 1992b). Closed structures deforming early isoclinal folds (Figs. 8.19 and 8.20a–c) were initially mapped as sheath folds (Roering et al. 1992b) due to the fact that such well-defined structural features are characterized by identical steeply northeast-verging kinematic indicators (Figs. 8.19 and 8.22). High-grade gneisses located in the

Fig. 8.18 Undeformed Singelele-type leucogranite (dated at 2627 ± 2.5 Ma) that intrudes migmatitic metapelitic granulite directly north of the Bulai Pluton (Fig. 8.15) (Boshoff et al. 2006; Smit et al. 2011). This body has the same age as the tonalitic L-tectonite (2626.8 ± 5.4 Ma) that intrudes the core of the Avoca circular structure (Fig. 8.23a, c), located more than 150 km to the west. Note also the similarity with undeformed leucocratic trondjhemite that intruded the SMZ (Fig. 8.13a)

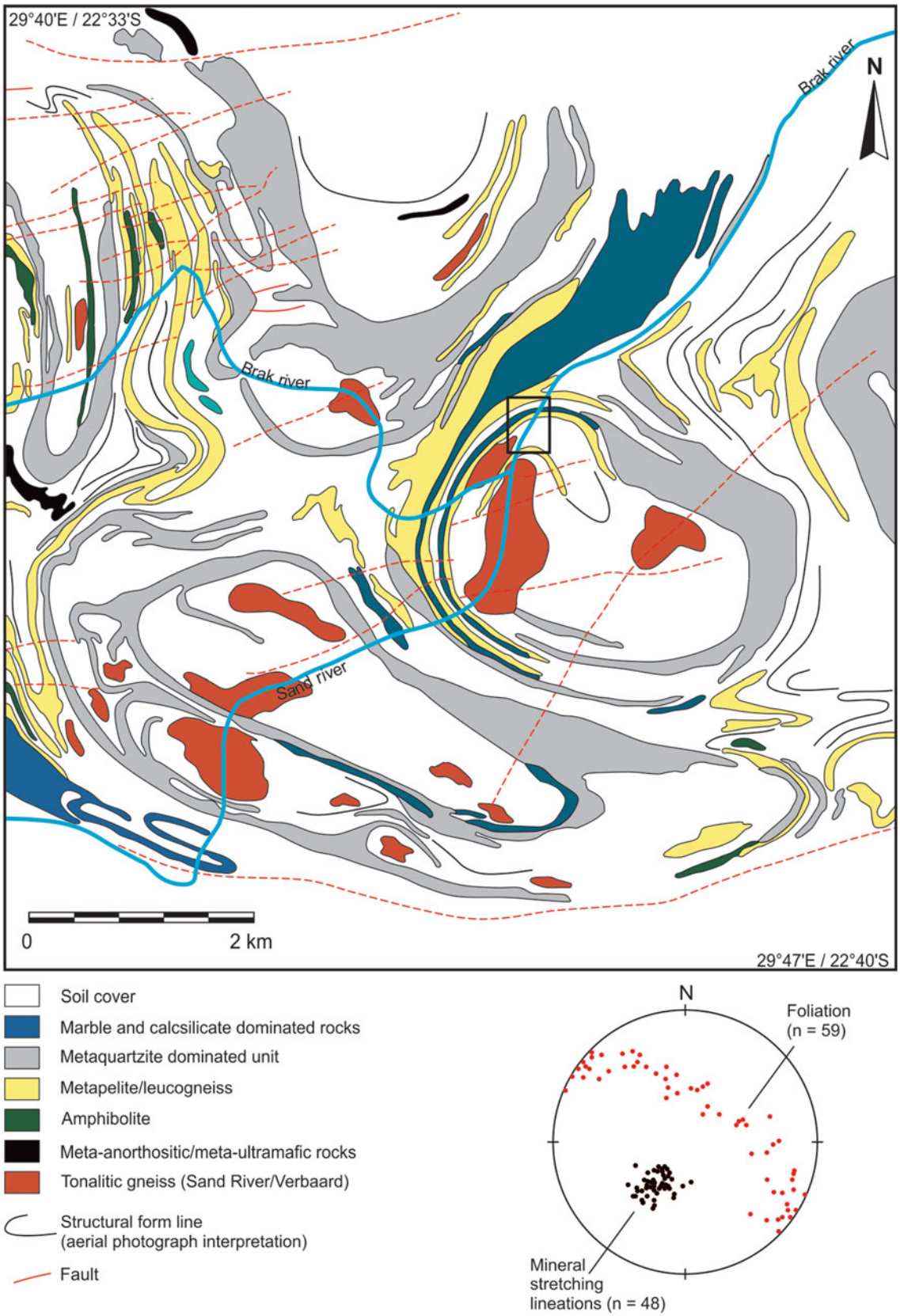

Fig. 8.19 Geological map of the steep southwest-plunging (inset: lower hemisphere stereonet projection) Bellevue closed structure developed on Farm Bellevue southwest of Musina in the CZ (Fig. 8.16) (after Roering et al. 1992b). The map clearly shows transposition of regional-scale isoclinal folds into parallelism with the shear fabric in the rim of the closed structure (Fig. 8.20a–c). Also shown is the location of a well-exposed traverse (rectangular box) through the rim of the structure along the Brak River (Fig. 8.19)

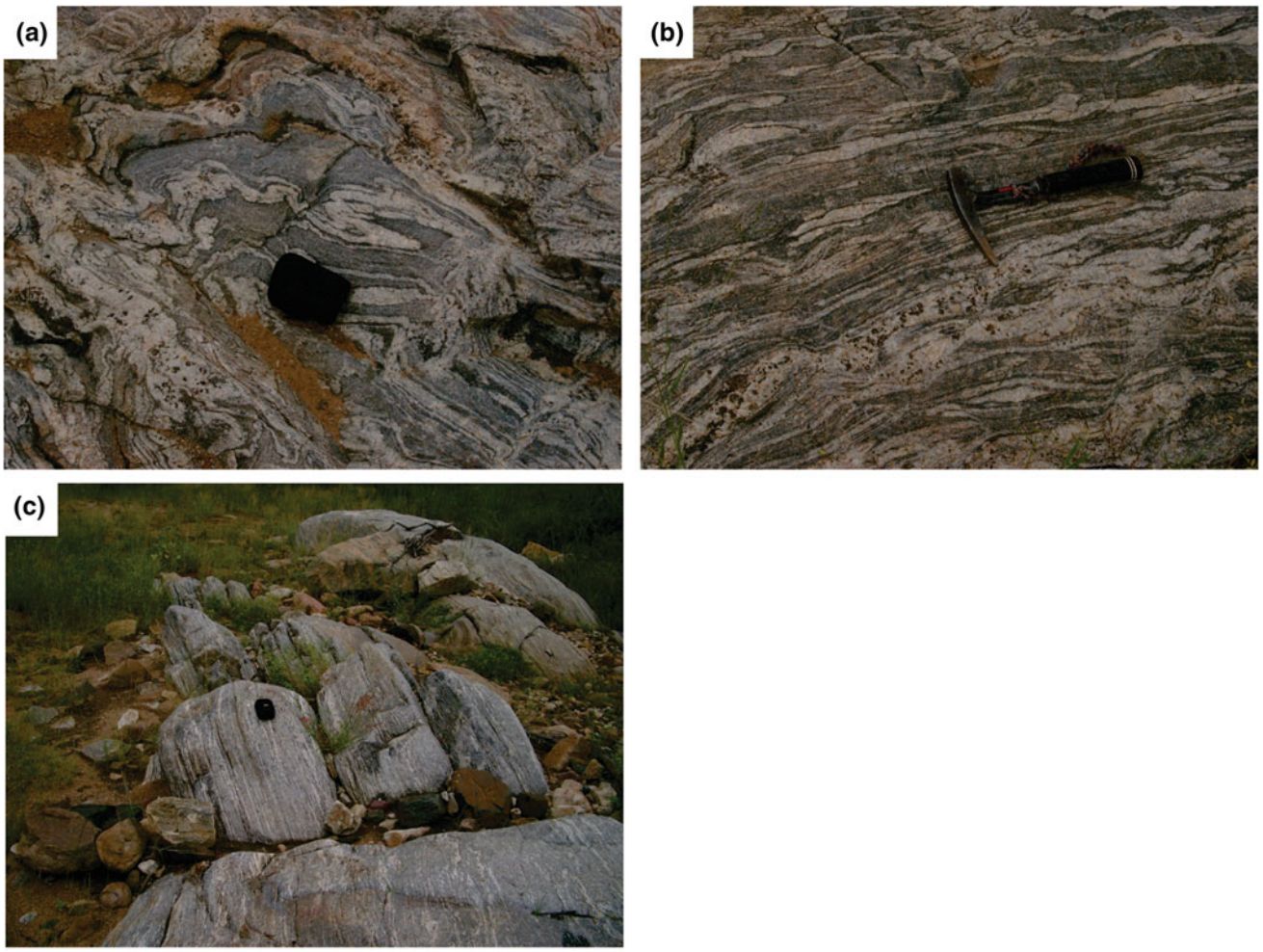

Fig. 8.20 South-north traverse across the rim of the Bellevue closed structure (Fig. 8.19) exposes continuous outcrops of grey tonalitic gneiss. The traverse starts in folded migmatitic gneiss associated with isoclinal folding (**a**) outside the closed structure, and demonstrates the progressive transposition (**b**) of the earlier folds into parallelism with the intense shear fabric developed in the rim (**c**) of the closed structure. This instructive example demonstrates the principle of heterogeneous deformation that controlled the formation and preservation of distinct granulite assemblages respectively, associated with isoclinal folds (**a**) and with closed structures (**c**) and of the TSZ. Gneisses associated with isoclinal folds (**a**) are granoblastic in thin sections in contrast with highly sheared gneisses (**b**, **c**) associated with closed structures. The principal of heterogeneous deformation allowed the construction of the two-stage D-*P-T-t* evolution of the CZ (e.g. TOV13-I, II in Fig. 8.17) metapelitic granulite in the rim of Tshanzi closed structure where an early granoblastic fabric is also overprinted by the younger shear fabric (Perchuk et al. 2008b; Mahan et al. 2011; Smit et al. 2011)

outer rims of the closed structures are high-temperature sheared rocks (straight gneisses) characterized by kinematic elements (Fig. 8.21) and differ significantly from annealed granoblastic rocks associated with isoclinal folds and dome-like structures that are largely devoid of kinematic elements. All *P-T* paths constructed for closed structures document nearly identical maximum *P-T* conditions of ca. 6 kbar and ca. 700 °C for the onset of shear deformation and related granitic diapirism and minimum *P-T* conditions of ca. 4.5 kbar and ca. 600 °C (Fig. 8.17) during emplacement into the upper crust. The latter being constrained to before intrusion of the Bulai pluton at ca. 2.61 Ga (Millonig et al. 2008; Smit et al. 2011). Sheared metapelitic gneisses associated with major circular structures retain no *P-T* memory of the early exhumation history (TOV13-I in Fig. 8.17), which is defined by the development of isoclinal folds and dome-like structures (Perchuk et al. 2008a, b; Smit et al. 2011). This is due to reworking of the early granoblastic fabric during the superimposed high-grade shear-deformational event (Fig. 8.20a–c).

The direct link between the onset of granitic diapirism and the formation of major closed structures is illustrated by the Avoca and Tshansi structures (Figs. 8.16 and 8.22) (Boshoff et al. 2006; Perchuk et al. 2008b; van Reenen et al. 2008; Smit et al. 2011). The steeply southwest-plunging oval-shaped closed Avoca structure (Fig. 8.22) located

Fig. 8.21 Steeply southwest-dipping planar shear fabric of migmatitic gneiss defining the rim of the Bellevue closed structure (Fig. 8.19). See text for discussion

northwest of the town of Alldays (Fig. 8.16) is cored by a ca. 2.63 Ga trondhjemitic L-tectonite (Fig. 8.23a) that intrudes (Fig. 8.23c) ca. 2.65 Ga penetrative foliated and lineated Singelele-type gneiss in the rim (Fig. 8.23b) (e.g. Boshoff et al. 2006). This relationship provides a precise link between granitic diapirism and the onset of the shear deformation at 2.65–2.62 Ga that controlled the final steep exhumation of the CZ during the Neoarchaean Limpopo orogeny (TOV13-II in Fig. 8.17) (Perchuk et al. 2008a; van Reenen et al. 2008; Smit et al. 2011). Superimposition of shear deformation onto previously folded lithologies is revealed by a south–north traverse that starts in strongly folded Alldays gneiss exposed directly south of the closed structure (Fig. 8.22), continues across intensely sheared and lineated Singelele-type granite in the rim of the circular structure (Fig. 8.23b) and ends in non-foliated but penetratively lineated trondhjemite in the core of the Avoca closed structure (Fig. 8.23a) (e.g. Boshoff et al. 2006; van Reenen et al. 2008; Smit et al. 2011). The origin and mechanism of emplacement of melt-cored diapirs in the CZ have been numerically modelled (Perchuk et al. 2008b), explaining the relationship between the onset of granitic diapirism and the development of closed structures associated with intense shear deformation.

The Tshanzi closed structure (Fig. 8.16) demonstrates the critical role of heterogeneous strain in the construction of two-stage *P-T-t* paths from distinct reaction textures preserved in a single thin section (TOV 13-I, II in Fig. 8.17) of a metapelitic granulite (Perchuk et al. 2008a; Mahan et al. 2011; Smit et al. 2011). The role of widespread granitic diapirism reflected by mega closed structures during the near-vertical exhumation of the CZ is furthermore documented by emplacement of large volumes of Singelele-type granitoid after 2.69 Ga.

The only examples of regional-scale Neoarchaean lineaments associated with shear deformation in the CZ are represented by the Triangle Shear Zone and Tshipise Straightening Zone (here identified by the acronym TSZ) that respectively bound the CZ in the north and in the south (Fig. 8.1). The 35 km wide southwest–northeast striking and steeply southeast-dipping high-grade TSZ (Fig. 8.1) separates the CZ from the SMZ. Sheared gneisses associated with this major shear zone are characterized by a steep to moderate southwest-plunging lineation and shear sense indicators (Horrocks 1983; Smit et al. 2011) that document reverse-sinistral displacement of the CZ rocks to the northeast (Smit et al. 2011), parallel to the direction of movement indicated by the plunge of mega-scale closed structures in the CZ. Decompression-cooling *P-T* paths (Perchuk et al. 2008a; Smit et al. 2011) derived from highly sheared metapelitic gneiss records *P-T* data that are almost identical to decompression-cooling *P-T* paths constructed for mega-scale closed structures in the CZ (TOV13-II in Fig. 8.17). Sheared rocks from the TSZ also retain no memory of the early stage of exhumation (TOV13-I in Fig. 8.17) recorded by their granoblastic equivalents associated with isoclinal folds. The similar direction of exhumation and *P-T-t* evolution of the TSZ and of closed

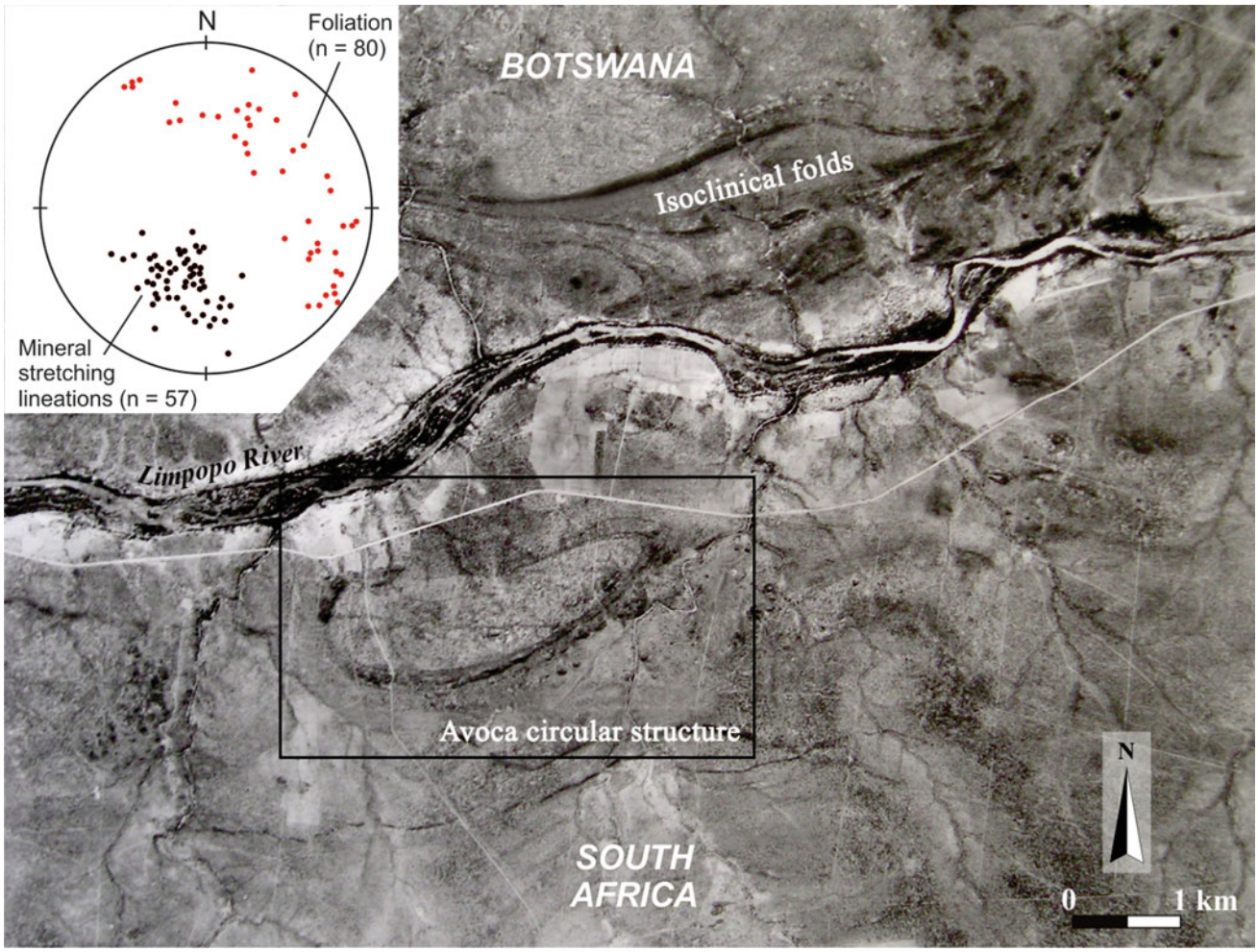

Fig. 8.22 Aerial photograph of the ca. 2.5 km in length southwest–northeast-directed oval-shaped closed Avoca structure located west of Alldays (Fig. 8.16) (modified after Boshoff et al. 2006). This sheared closed structure is closely associated with isoclinal folds of which the regional-scale isoclinal fold developed in Alldays tonalitic gneiss across the Limpopo River in Botswana is an example. The rim of the moderately southwest-plunging structure (inset structural stereogram) comprises penetrative lineated and foliated Singelele-type leucogranite dated at ca. 2.65 Ga. The core comprises unfoliated but intensely lineated (L-tectonite) leucotonalite dated at ca. 2.63 Ga that intrudes Singelele-type leucogranite (Fig. 8.23) (Boshoff et al. 2006; Smit et al. 2011). See text for discussion

structures within the CZ is strong evidence for the steep northeast-directed exhumation of the entire CZ at 2.65–2.62 Ga (e.g. Perchuk et al. 2008b; Smit et al. 2011).

Successful linking *P-T* data (TOV13-I, II in Fig. 8.17) obtained from high-grade metapelitic gneisses associated with distinct regional structural elements in the CZ (respectively, isoclinal folds and mega closed shear-related structures) (Figs. 8.16, 8.17 and 8.21) with time (*D-P-T-t* paths) is supported by field data. These data show that isoclinal folds are deformed by younger mega-scale closed shear-related structures (Figs. 8.16, 8.19 and 8.22). These younger structural features document kinematic, metamorphic and geochronological (Figs. 8.17, 8.19, 8.21 and 8.22) evidence for the final steep northeast-directed exhumation of the CZ at 2.65–2.62 Ga. Integrated geological data thus provides unequivocal evidence that argues against the proposal by Brandt et al. (2018) for a counterclockwise *P-T* path associated with the burial of rocks and prograde heating at exactly the same time and from the same general area.

It can thus be concluded that during initial exhumation proto-CZ and proto-SMZ material were both characterized by isoclinal folds and large dome-like structures (compare Figs. 8.2 and 8.16) that formed at ca. 2.72 Ga under peak metamorphic conditions in the lower crust. This melt-weakened crust (e.g. Jamieson et al. 2011) reflected by migmatitic gneisses in both the CZ (e.g. Figs. 8.20a–c) and the SMZ (Figs. 8.7a–c and 8.8a, b) documents evidence for steep exhumation of granulites at post-peak metamorphic

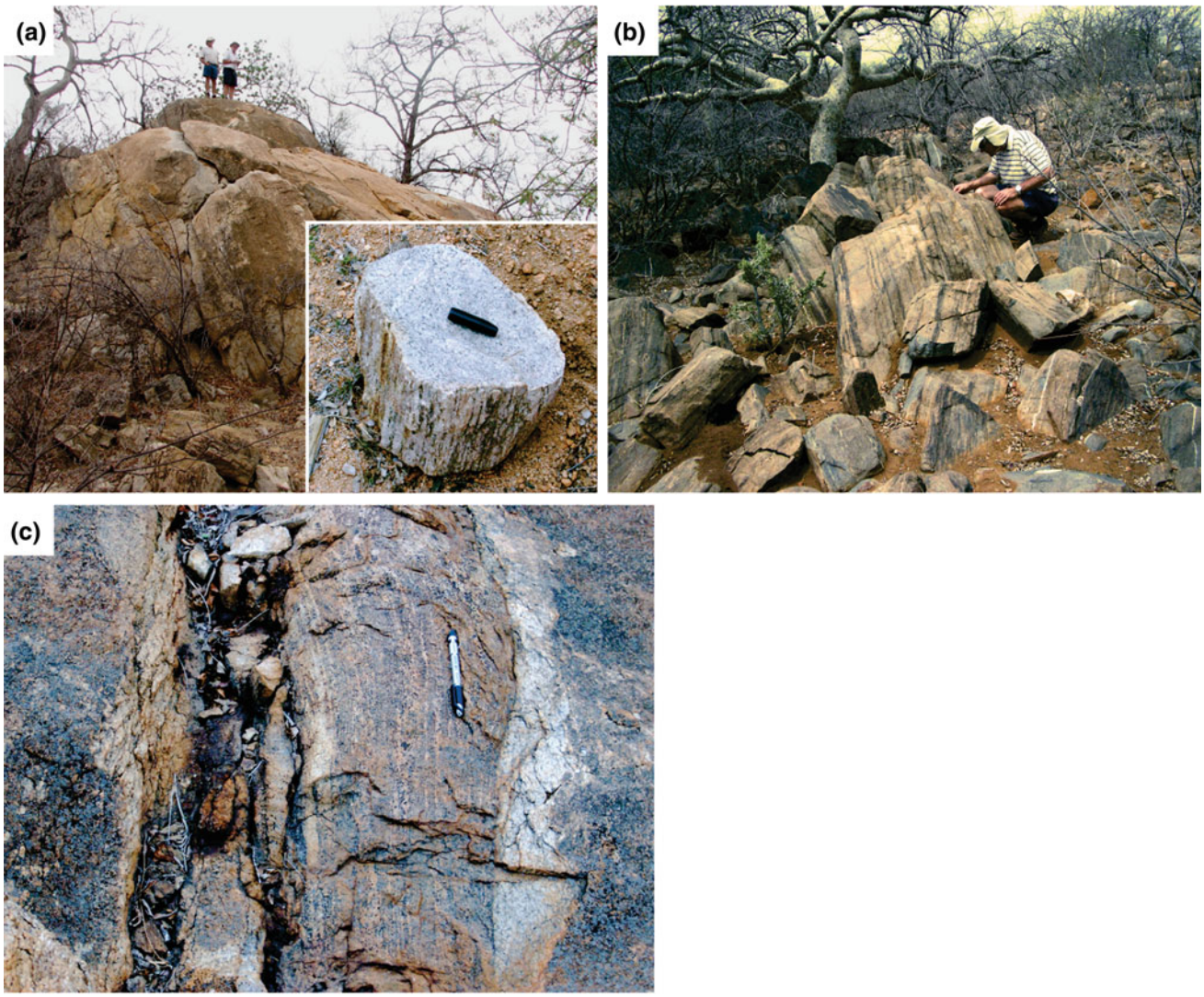

Fig. 8.23 **a** Humpback outcrop of ca. 2.63 Ga Avoca L-tectonite developed in tonalite that comprises the core of the oval-shaped closed structure. A penetrative lineation defined by quartz rodding and mineral elongation lineations is demonstrated in sections parallel to the plunge (inset photo). **b** Sheared and lineated Avoca granitic gneiss (ca. 2.65 Ga) in rim of the oval structure. **c.** Xenolith of ca. 2.65 Ga Avoca granitic gneiss enclosed by the ca. 2.63 Ga L-tectonic in the core of the structure. This important diapiric structural feature accurately constrains the timing of regional shear deformation at 2.65–2.62 Ga associated with final steep NE-directed exhumation of the CZ (Fig. 8.16). See text for further discussion

conditions (DR45-I in Fig. 8.11, TOV 13-I in Fig. 8.17) to the mid-crustal level (6 kbar, ca. 20 km level) before ca. 2.65 Ga (formation of mega closed structures). At this crustal level, the hot rocks cooled and annealed, resulting in widespread development of granoblastic textures that characterize much of the CZ and SMZ. The SMZ with its imbedded steeply plunging folds and steep shear zones (Fig. 8.4) was then extruded onto and over the NKVC while the CZ (and northern part of the SMZ north of Annaskraal Shear Zone) still resided at the mid-crustal level. At this level granitic diapirism accompanied by the formation of major closed structures (Figs. 8.19 and 8.22) controlled the final steep northeast-directed emplacement of the CZ at the 15 km (ca. 4.5 kbar) crustal level at 2.65–2.61 Ga (Fig. 8.17) (Smit et al. 2011). At this time the hot SMZ nappe interacted with infiltrating water-bearing fluids that resulted in widespread retrograde hydration (Figs. 8.3 and 8.9c–e).

The CZ was finally exhumed to the upper crustal level in the Palaeoproterozoic at ca. 2.01 Ga as the result of a superimposed high-grade shear event linked to discrete (metres-wide) fabric-parallel shear zones associated with widespread thermal overprint (e.g. Perchuk et al. 2008a; Perchuk and van Reenen 2008; van Reenen et al. 2008; Kramers and Zeh 2011; Mahan et al. 2011; Smit et al. 2011).

8.6 Linked Exhumation Histories of the SMZ and CZ at 2.72–2.62 Ga

Distinct *P-T-t* paths (Figs. 8.11 and 8.17) deduced for metapelitic granulite with similar principal mineral assemblages (Grt + Opx/Sil + Crd + Bt + Kfs + Qz) from the SMZ and CZ using a single methodology (e.g. Perchuk et al. 2000a; Smit et al. 2001, 2011; Perchuk and van Reenen 2008; Perchuk 2011) support a linked post-peak metamorphic evolution of the SMZ and CZ at ca 2.72–2.62 Ga that is supported by geophysical data (Fig. 8.15). Two-stage decompression-cooling *P-T* paths constructed for metapelitic gneisses from the CZ and the SMZ north of the Annaskraal Shear Zone (Figs. 8.1 and 8.2) are characterized by distinct gaps (Figs. 8.11 and 8.17). These gaps are in each case located at a pressure of 6-6.5 kbar (Figs. 8.11 and 8.17) and separate two distinct stages of decompression-cooling. In the case of the CZ, the first stage of decompression-cooling at 2.69–2.65 Ga is documented by emplacement of regional-scale isoclinal folds and dome-like structures cored by migmatitic gneisses at the mid-crustal level (Fig. 8.17), followed by cooling and annealing. Exactly the same situation applies to the SMZ north of Annaskraal Shear Zone (Figs. 8.3 and 8.11). The second decompression-cooling stage of steep exhumation of the CZ at ca. 2.65–2.62 Ga (Fig. 8.17) is documented by granitic diapirism that was accompanied by the formation of mega-scale closed structures associated with intensely sheared high-grade gneisses and the establishment of the TSZ. Sheared granulite (Figs. 8.20a–c and 8.21) associated with major closed structures and with the TSZ (Figs. 8.1 and 8.16) has no *P-T* memory of the early decompression-cooling stage due to intense shear deformation and high-temperature reworking of granoblastic gneisses (e.g. Fig. 8.20a–c) that resulted in intensely sheared high-grade gneisses (e.g. Figs. 8.20c and 8.21) (e.g. Perchuk et al. 2008a, b; Perchuk and van Reenen 2008; van Reenen et al. 2008; Mahan et al. 2011; Smit et al. 2011).

In contrast to the situation described for the CZ and for the SMZ north of the Annaskraal Shear Zone (Figs. 8.3 and 8.4), metapelitic granulites that outcrop south of this shear zone in the SMZ document evidence for near-isobaric cooling that commenced at exactly the same mid-crustal level (Figs. 8.11 and 8.16). In keeping with the rocks of the CZ, however, these granulites have little memory of an earlier decompression-cooling stage that accompanied emplacement at the mid-crustal level. Belyanin et al. (2014) and Safonov et al. (2014, 2018a, b) have shown that near-isobaric cooling of the SMZ nappe probably started at ultrahigh-temperatures above 900 °C and at 6–7 kbar pressure (Fig. 8.11).

Evidence for the near-isobaric cooling *P-T* path is supported by field, structural (Fig. 8.4) and geophysical data (Fig. 8.15) showing that the hot nappe was southwards transported over a distance of ca. 35 km along a near-isobaric (ca. 6 kbar) crustal plane (Fig. 8.11) underlain by relative cool granite-greenstone material (inset map in Fig. 8.3) against and over the adjacent NKVC at ca. 2.72 Ga. The near-isobaric crustal plane is defined by the flat section of the HRSZ (Fig. 8.4). The timing is constrained by metamorphism related to the hot-iron effect in the footwall of the HRSZ at 2.72–2.69 Ga (Kreissig et al. 2001; Kramers et al. 2014) and by the time of emplacement of the Matok pluton at ca. 2.68 Ga (Laurent et al. 2013).

The observation that a hot granulite nappe with its imbedded steeply plunging folds and steeply dipping shear zones is allochthonous with respect to the underlying near-horizontal shear fabric associated with the flat section of the HRSZ (Figs. 8.4 and 8.8a–c) has important constraints on the concept of a conveyor belt mechanism linked to steep tectonics in the CZ. Firstly, it demonstrates that the granulite-facies nappe could not have been formed and been exhumed in situ at mid-crustal level above the flat-lying HRSZ that is underlain by cooler greenstone belt material (inset map in Fig. 8.3). Second, the conveyor belt mechanism requires that the SMZ nappe be transported from a position in the core of the orogen below the present CZ in the north. The implication that proto CZ lower crustal material with a large metasedimentary component was underlain by proto-SMZ crustal material dominated by magmatic granulites (Fig. 8.24a) is supported by geophysical data (Fig. 8.15).

The evolution of the hot nappe after emplacement at 2.68 Ga is expressed by widespread retrograde hydration that established the Ath-in isograd and the regional zone of retrograde hydrated granulite (Figs. 8.3 and 8.4). The evolution of the CZ after emplacement at the mid-crustal level at 2.65–2.62 Ga (Kröner et al. 2018) was controlled by granitic diapirism and the formation of major closed structures associated with intense shear deformation.

The time difference between emplacement of the mainly undeformed Bulai pluton at ca. 2.61 Ga in the CZ (Millonig et al. 2008), and of the mainly undeformed Matok pluton at ca. 2.68 Ga in the SMZ (Laurent et al. 2013) is interpreted to be the direct result of the linked evolution of these two high-grade terranes. Whereas emplacement of the Bulai pluton signifies the end of steep granitic diapirism at ca. 2.61 Ga in the CZ, emplacement of the Matok pluton, at ca. 2.68 Ga occurred after southwards horizontal channelling of a hot SMZ nappe from underneath the CZ, prior to granitic diapirism. Granitic diapirism in the CZ at 2.65–2.63 Ga was thus complemented by a static high-temperature widespread

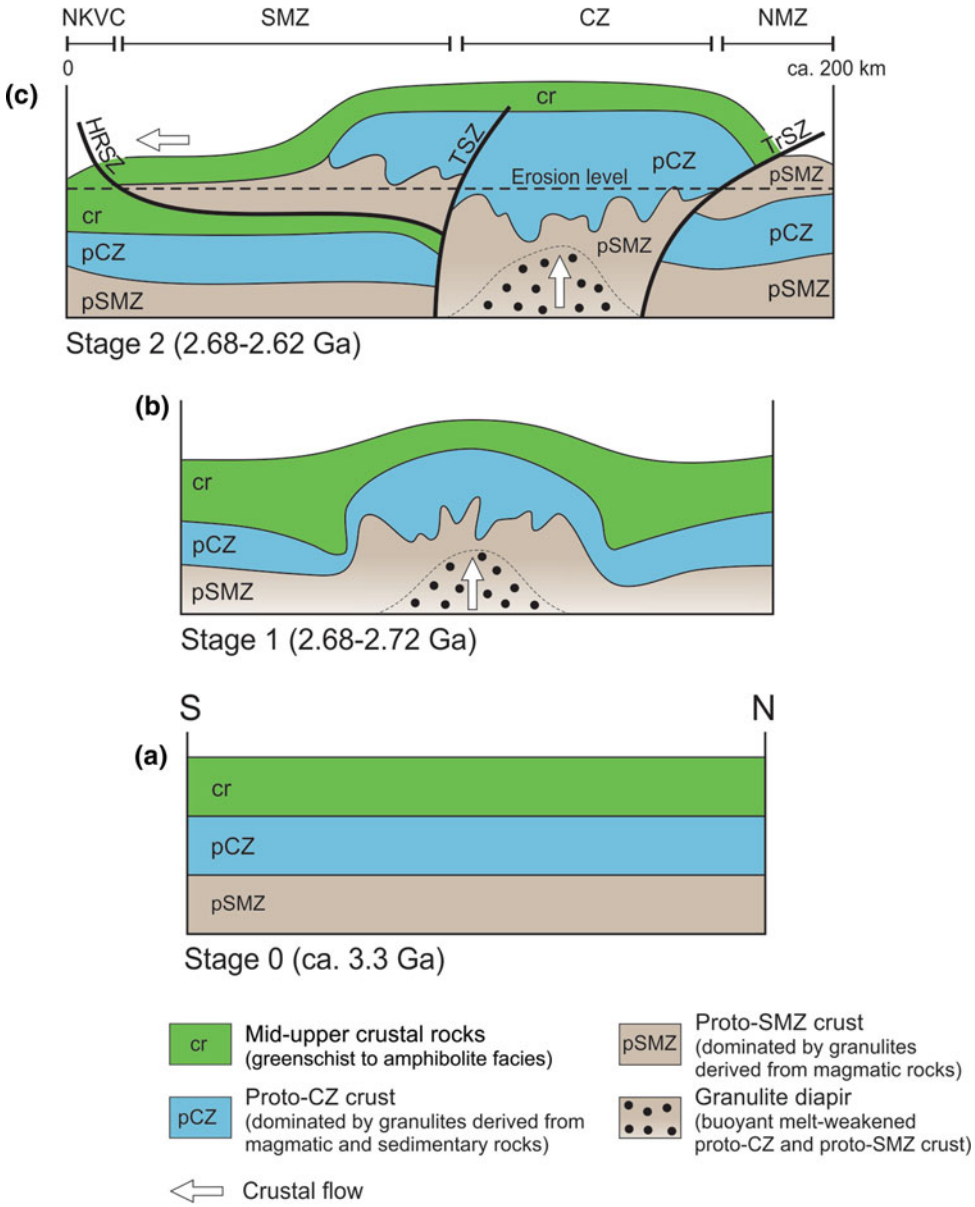

Fig. 8.24 Cartoon showing a crustal-scale granulite diapir penetrating into the upper crust at 2.72–2.62 Ga. **a** Stage 0: rhythmic layered successions reflecting a hypothetical granite-greenstone crustal section formed at ca. 3.3. Ga. **b** Stage 1: penetrating granulite diapir triggered steep exhumation of proto-SMZ and proto-CZ granulite-facies rocks at the mid-crustal section at 2.72–2.68 Ga (Fig. 8.17). **c** Stage 2: regional-scale gravitational crustal overturn of complex morphologies and dynamics that controlled the southwards channelling of a hot SMZ nappe along a near-isobaric crustal section (HRSZ) against and over the adjacent NKVC before 2.68 Ga (Fig. 8.4). Final steep exhumation of the CZ to the upper crustal level at 2.65–2.62 Ga was controlled by granitic diapirism associated with the formation of closed structures before emplacement of the Bulai pluton at ca. 2.61 Ga. HRSZ: Hout River Shear Zone; TSZ: Thipise Straightening Zone; TrSZ: Triangle Shear Zone. See text for further discussion

retrograde hydration event that established the Ath-in isograd in the SMZ after ca. 2.68 Ga. The two high-grade terranes were therefore subjected to different but temporally related processes during the final stages of the same orogenic event.

An important conclusion that follows from this discussion is that the SMZ conveyor belt mechanism (Fig. 8.4) was not driven by granitic diapirism in the CZ as proposed by Smit et al. (2014). Granitic diapirism only controlled the final emplacement of the CZ i.e., after ca. 2.65 Ga (Fig. 8.17), while tectonism in. the SMZ already stopped before emplacement of Matok pluton at ca. 2.68 Ga. Diapirism in the CZ and regional rehydration of the SMZ occurred at the same time.

In the section to follow we examine a proposed link between the conveyor belt mechanism (Fig. 8.4) and the action of a crustal-scale granulite diapir triggered by mantle heat-fluid flow that penetrated the upper crust underneath the present CZ (Fig. 8.24) at or before ca. 2.72 Ga.

8.7 Conveyor Belt Tectonic Mechanism and the Link with a Crustal-Scale Granulite Diapir

The numerical gravitational redistribution model for the LC proposed by Gerya et al. (2000) discusses important data that supports the concept of a conveyer belt mechanism (Fig. 8.4) that controlled emplacement of a hot SMZ nappe against and over the adjacent NKVC before ca. 2.68 Ga. The model of Gerya et al. (2000) explains the buoyant

exhumation of a granulite complex separated from two granite-greenstone cratons by inward-dipping crustal-scale shear zones up to 10 km wide and several hundred kilometres long via gravitational redistribution linked to the action of a granulite diaper within metastable hot and soft early Precambrian crust that was subjected to HT and UHT metamorphism. This scenario, where two stiff cratons are separated by a weak pre-existing zone developed within relatively thin (ca. 30 km thick) crust, produces an asymmetrical exhumation pattern (Perchuk and Gerya 2011) that accurately describes an analogue to thrusting the near-horizontal SMZ granulite-facies terrane (granulite nappe) against and onto the adjacent NKVC. It explains important aspects of the SMZ and its relationship with the NKVC (see Kramers et al. 2011). This asymmetrical numerical model (Perchuk and Gerya 2011) strongly supports the proposed conveyor belt mechanism as it pertains to the SMZ and contact with the NKVC (Fig. 8.4) but does not explain the linked evolution of the magmatic dominated SMZ and the CZ with large volumes of metasedimentary rocks as is suggested by the conveyor belt mechanism (Fig. 8.4).

A revision of the Gerya et al. (2000) gravitational redistribution model by Perchuk and Gerya (2011) discusses a different scenario in which relatively thick (ca. 40 km thick) sedimentary-dominated crust is overlain by dense greenstone material as part of a single crustal plate affected by mantle-derived fluid-heat flow (crustal-scale granulite diapir). In this scenario, near-vertical exhumation dominates and hot granulite-facies rocks are transported from a depth of ca. 40 km to mid- and upper crustal levels. Due to the absence of pre-existing weak zones, lateral channelling of hot granulite (representing the SMZ granulite nappe) is subordinate (Perchuk and Gerya 2011). The model illustrates the gravitational redistribution in multi-layered crust in which a crustal-scale granulite diapir penetrates into the upper crust.

We propose that the Perchuk and Gerya (2011) model offers a credible explanation for the exhumation of the CZ, with its large metasedimentary component and widespread granitic diapirism (Roering et al. 1992b; Perchuk et al. 2008a). It also offers an explanation for the Venetia Klippen, (Zeh et al. 2004; Perchuk and Gerya 2011) where sagduction enclosed typical low-grade Archaean greenschist-facies rocks within granulite-facies CZ lithologies. However, the Perchuk and Gerya (2011) numerical model does not explain the southward spreading of a hot SMZ nappe dominated by magmatic-derived granulites from underneath the CZ against and over the adjacent NKVC along a near-isobaric (ca. 6 kbar) crustal section, and the 'hot-iron' relationship with the NKVC (Fig. 8.11).

8.8 Gravity-Driven Geodynamic Model for Exhumation of the LC

We address the issue of the joint evolution of the SMZ (and NMZ) and CZ by considering a combination of the Gerya et al. (2000) and Perchuk and Gerya (2011) numerical gravitational models that link the action of a crustal-scale granulite diaper triggered by heat-fluid flow that penetrated the crust underneath the CZ at or before ca. 2.72 Ga.

8.8.1 Pre-Limpopo Complex Crustal Architecture

The assumption that the Mesoarchaean Kaapvaal Craton was underlain by granulite-facies rocks is supported by different data. First, the tilted crustal section through the Mesoarchaean Basement Complex in the core of the Vredefort Dome exposes the transition from upper amphibolite to granulite-facies rocks at 3130–3080 Ma (e.g. Gibson 2019, this volume). Second, Schmitz and Bowring (2003) suggested that much of the central KVC outside the Vredefort Dome is underlain by ca. 2.72 Ga ultrahigh-temperature granulite-facies rocks including metasedimentary varieties that were exhumed as xenoliths in kimberlites. Thirdly, the hypothetical crustal section that includes a significant volume of metasedimentary rocks at depth is supported by the results of thermomechanical numerical modelling of a Precambrian ultra-hot accretionary orogen (Perchuk et al. 2018) that suggests a link between the formation of the extensive Paleoarchaean granite-greenstone terrane of the central Kaapvaal craton and ultrahigh-temperature granulites at the base of the crust.

The pre-Limpopo Complex crustal architecture shown in Fig. 8.24a is, therefore, adapted from the crustal section of an ultrahot orogeny modelled by Perchuk et al. (2018). Our hypothetical ca. 35 km thick crustal section comprises (1) an igneous-dominated lower granulite-facies unit (termed proto-SMZ crustal material) unit at the base of the crust, followed by (2) a crustal unit still at granulite grade that includes large volumes of metasedimentary rocks (termed proto CZ crustal material), and (3) upper crustal section of greenschist-amphibolite-facies upper crustal material forming a granitoid-greenstone terrane. We propose that the igneous-dominated lower granulite-facies unit represents proto-SMZ crustal rocks, which on the surface today is represented by tonalitic orthogneisses (Baviaanskloof Gneiss) with minor volumes of metapelitic, mafic and ultramafic granulites (Bandelierkop Complex) (Fig. 8.2). The overlying granulite-facies metasedimentary component is interpreted to represent proto-CZ crustal material, while

part of the mid- to upper crustal material represents the granite-greenstone terrane presently exposed at surface on both the Kaapvaal and Zimbabwe Cratons.

The hypothetical crustal section (Fig. 8.24a) suggests that a pre-LC Archaean granite-greenstone terrane that included both the KVC and ZC (De Wit et al. 1992b) was underlain at depth by granulite-facies rocks that were exhumed at ca. 2.72 Ga and today are exposed at the surface as the LC.

8.8.2 Gravity-Driven Geodynamic Model of the Limpopo Complex

We speculate that the hypothetical pre-Limpopo crustal architecture (Fig. 8.24a) was disrupted at or before ca. 2.72 Ga by mantle fluid-heat flow that triggered a buoyant crustal-scale granulite diapir that penetrated the pre-Limpopo Complex crustal architecture underneath the present CZ.

8.8.2.1 Early Exhumation Stage Prior to ca 2.68 Ga

Fluid-heat flow enhanced by crustal radiogenic decay (e.g. Andreoli et al. 2011) and the release of hydrous fluid from metamorphic minerals at or before ca. 2.72 Ga resulted in partial melting of rocks at lower crustal levels with formation of melt-weakened migmatitic crust with reduced viscosity (e.g. Jamieson et al. 2011; Lexa et al. 2011). The resultant buoyant crustal-scale granulite diapir comprising hot lower (proto-SMZ) crustal material overlain by cooler proto-CZ crustal material (Fig. 8.24b) systematically disrupted the pre-existing stratigraphy and penetrated the mid- to upper crust (e.g. Perchuk and Gerya 2011) (Fig. 8.24a). The ascending melt-weakened migmatitic crust initially resulted in the formation of melt-weakened gneiss domes and associated steeply plunging regional isoclinal folds that currently characterize both the SMZ and CZ at the surface (compare Figs. 8.2 and 8.16). They eventually cooled at a depth of ca. 20 km (ca. 6 kbar) (Figs. 8.17 and 8.24b) beneath a stiffer mid- to upper crust before ca. 2.68 Ga (constrained by emplacement of the Matok pluton into the extruded the SMZ nappe). At this crucial crustal level, hot granulites cooled and were annealed as demonstrated by regionally developed granoblastic textures.

Metamorphic temperatures conditions of at least 900 °C at a pressure of 9 kbar (Tsunogae et al. 2004; Tsunogae and van Reenen 2011; Belyanin et al. 2014) were reached at the base of the crustal section (Fig. 8.24). This resulted in the production of large volumes of leuco-granitoid that intruded CZ migmatitic crust at 2.69–2.62 Ga (Singelele-type) (e.g. Kröner et al. 1999; Smit et al. 2011). This process further affected density, crustal strength, and tectonic style of the melt-weakened migmatitc crust (e.g. Jamieson et al. 2011; Lexa et al. 2011; Sawyer et al. 2011).

8.8.2.2 Second Exhumation Stage at 2.65–2.62 Ga Driven by Granitic Diapirism

The early exhumation stage (TOV 13-I in Fig. 8.17) was followed by final exhumation of the CZ to the upper crustal level, a process driven by granitic diapirism and associated with the formation of mega-scale closed structures dated at 2.65–2.62 Ga (Figs. 8.16, 8.19 and 8.22) and intensely sheared high-grade gneisses. Closed structures cored by granitoids are developed throughout the entire CZ in South Africa (Fig. 8.16) and are all characterized by similar features. These include evidence for intense shear deformation (Figs. 8.20c and 8.21), constant steep southwest-plunging fold axes that support exhumation towards the northeast (Figs. 8.19 and 8.22), and the fact that sheared metapelitic gneisses have no memory of the early decompression-cooling stagthe e of exhumation but only record *P-T-t* evidence for decompression-cooling after emplacement at the mid-crustal level (TOV13-II in Fig. 8.17) (e.g. Smit et al. 2011). The timing of a major event at ca. 2.65–2.62 Ga was recently confirmed by a detailed study of highly deformed high-grade gneisses from an enclave within the ca. 2.61 Ga Bulai pluton (Kröner et al. 2018).

8.8.2.3 Regional-Scale Gravitational Crustal Overturn of Complex Morphology and Tectonics Before ca. 2.68 Ga

Granulites comprising the proto-SMZ cooled after emplacement at the mid-crustal level (Fig. 8.11) underneath cooler and stiffer CZ material (Fig. 8.24b) and cover rocks before ca. 2.68 Ga. We proposed that rheological differences at this crustal level between hot underlying proto-SMZ rocks and cooler and stiffer overlying proto-CZ rocks facilitated regional-scale gravitational crustal overturn of complex dynamics and morphology (Figs. 8.4 and 8.24b) that initiated and controlled the southward channelling of a hot and denser granulite nappe with imbedded steep structures (the SMZ underlain by the sub-horizontal HRSZ) from underneath CZ material.

Near-horizontal channelling of a hot SMZ nappe at the mid-crustal level is supported by geophysical (Fig. 8.15a) and structural data (Fig. 8.6b–d) and constrained by *P-T-t* data (Fig. 8.11). It explains the preserved (imbedded) steeply plunging folds and steeply dipping shear zones that currently characterize the SMZ granulite nappe. These steeply dipping imbedded structures, that are allochthonous with respect to the younger near-horizontal underlying HRSZ (Figs. 8.6 and 8.8), preserve evidence for the initial near-vertical stage of exhumation of the SMZ from underneath the CZ (Figs. 8.11 and 8.24b). The timing of

near-horizontal channelling of the hot SMZ nappe is accurately constrained by different lines of evidence. First, thermal and dynamic interaction at 2.72–2.69 Ga of overriding hot granulite with underlying relatively cool greenschist along the contact of the steeply north-dipping HRSZ with the adjacent NKVC (e.g. Figs. 8.5a and 8.6a). Secondly, emplacement of the mainly undeformed Matok granite into already deformed and metamorphosed SMZ granulites at ca. 2.68 Ga (Fig. 8.3) (Laurent et al. 2013).

Jamieson et al. (2011) used the analogue 'of pressing on an egg sandwich' to explain a similar process that operated in the Moldanubian region of the Bohemian Massif in the Variscan Orogen of central Europe. In this example, melt-weakened migmatitic crust flowed outwards onto the lower foreland area, a process described as mid-crustal heterogeneous channel flow (Schulman et al. 2008). In the channel flow model, the tongue of melt-weakened crust is often bounded above and below by ductile shear zones and often preserves its imbedded structures such as shear zones and their initial orientation within the nappe (Jameson et al. 2011).

8.8.2.4 Regional Retrograde Hydration of the Hot SMZ Nappe at ca. 2.68–2.62 Ga

Emplacement of hot granulite for a distance of at least 35 km over cool underthrust greenschists (inset map in Figs. 8.3, 8.4 and 8.15) of the NKVC resulted in devolatilization of the underlying greenschist and the persistent production of large volumes of fluids at 2.72–2.68 Ga as long as the conveyor mechanism operated (Fig. 8.4) (Koons and Craw 1991; Koons et al. 1998; Yardley 2009). Fluids thus derived (e.g. van Reenen et al. 2014) infiltrated and interacted with cooling SMZ granulites in the overriding nappe, establishing the retrograde Ath-in isograd and the zone of retrograde hydrated granulite that bounds the SMZ in the south (yellow and orange areas in Fig. 8.3).

Retrograde hydration occurred at 2.68–2.62 Ga after emplacement of the nappe and during the same general time interval as granitic diapirism that controlled final emplacement of the CZ after ca. 2.65 Ga. Different processes operating at different times in the different zones of the LC are therefore linked to different stages of the same orogeny that controlled the Neoarchaean evolution of this granulite-facies terrane.

8.9 Conclusions

Published geological, geochronological and geophysical data show that the complexly deformed and intensely metamorphosed LC is separated from lower grade large continuous linear greenstone belts that outcrop on the adjacent KC and ZC cratons (Fig. 8.1) by inward-dipping crustal-scale Northern Marginal Thrust Zone and the HRSZ (Fig. 8.1). These inward-dipping dip-slip crustal-scale shear zones controlled thrusting high-grade LC rocks onto adjacent lower grade granite-greenstone lithologies during the Limpopo orogeny. In the case of the SMZ, the timing of this event is accurately constrained at 2.72–2.69 Ga. The entire LC (Fig. 8.1) is furthermore characterized by steeply plunging folds and steeply dipping high-grade shear zones linked to decompression-cooling *P-T* paths (e.g. Blenkinsop 2011; Smit et al. 2011; van Reenen et al. 2011) that attest to initial regional steep exhumation of the LC before 2.65 Ga. A hot granulite nappe with imbedded steep tectonic features comprising the SMZ south of Annaskraal Shear Zone was channelled southwards against and over the NKVC at the mid-crustal level before ca. 2.68 Ga along the sub-horizontal HRSZ. Evidence for low-angle tectonic features in the LC are restricted to the deeply eroded central and eastern parts of the SMZ that expose sheared flat-lying retrograde hydrated former granulites that are closely associated with the flat-lying section of the HRSZ (orange area in Figs. 8.3 and 8.4). Metamorphic, structural and geochronological data provide credible evidence only for a linked post-peak metamorphic decompression-cooling metamorphic evolution directed by steep tectonic features that affected both the CZ and SMZ at 2.72–2.62 Ga. On the other hand, both the NKVC and the ZC (Figs. 8.1 and 8.2) are typical low- to medium grade granite greenstone terrains with no evidence for shallow north-verging structures that might have been associated with crustal thickening related to continent–continent collision at ca. 2.72 Ga (Kramers et al. 2014). In fact, only the most northern edge of the NKVC in the immediate footwall of the HRSZ documents evidence for interaction with the SMZ during the ca. 2.72 Ga Limpopo orogeny (McCourt and van Reenen 1992; Roering et al. 1992a; Kramers et al. 2014). Finally, the most significant feature that characterizes the entire LC is the coherent and dramatic difference between the style of deformation and intensity of metamorphism compared with the adjacent lower grade granite-greenstone cratons (Fig. 8.1).

There is no credible published data that argues against the proposed linked tectono-metamorphic evolution of the SMZ and CZ at 2.72–262 Ga. Evidence for the timing of peak metamorphism in the SMZ at ca. 2.72 Ga is in the first place constrained by emplacement of the undeformed Matok granitoid pluton (Laurent et al. 2013) and Petronella anatectic tonalite (Belyanin et al. 2014) at ca. 2.68 Ga into already deformed and metamorphosed granulite gneisses. Metamorphic age data obtained directly from granulite gneisses precisely date the peak metamorphic event in the SMZ at ca. 2.72 Ga (Rajesh et al. 2014; Taylor et al. 2014; Nicoli et al. 2015). In the case of the CZ, Kröner et al. (1999, 2018) dated anatectic Singelele-type granite that intrudes already deformed and metamorphosed high-grade supracrustal

gneisses at ca 2.68 Ga. Furthermore, the same authors provide age data for a granoblastic quartzofeldspathic gneiss dated at ca. 2.72 Ga. Finally, the results of a detailed geochronological study of a large supracrustal enclave in the ca. 2.61 Ga Bulai pluton that predominantly records evidence for a high-grade metamorphic event at 2.64–2.62 Ga (Kröner et al. 2018) is in good agreement with our published *P-T-t* data for the final steep northeast-directed exhumation of the CZ associated with formation of mega closed structures (e.g. Smit et al. 2011). This contradicts linking the Neoarchaean evolution of the CZ to a counterclockwise *P-T* loop associated with burial and prograde metamorphism (Brandt et al. 2018). We thus propose that published data on the SMZ and CZ strongly support the working hypothesis of an intracrustal Limpopo orogeny at 2.72–2.62 Ga that is linked to the action of a granulite diapir.

This proposed gravity-driven intracrustal orogenic model is demonstrated with reference to a hypothetical crustal section (Fig. 8.24a) that comprises magmatic dominated lower crustal (proto-SMZ) granulites overlain by a crust that includes a large volume of metasedimentary granulites (proto-CZ rocks) and capped by mid-upper crustal greenschist-amphibolite grade granite-greenstone lithologies. The proposed crustal section is supported by published data on the nature of the Mesoarchaean Kaapvaal crust (e.g. Gibson 2019, this volume), and is not in conflict with published geophysical data on the LC (e.g. De Beer and Stettler 1992). The model is also supported by the results of thermomechanical numerical modelling of a Precambrian ultra-hot accretionary orogen that explains the formation of an extensive granite-greenstone terrane linked to the formation of ultrahigh-temperature granulite at the base of the crust (Perchuk et al. 2018).

The hypothetical Archaean crustal section (Fig. 8.24a) was disrupted at ca. 2.72 Ga by a buoyant crustal-scale granulite diapir that penetrated the upper crust underneath the present CZ. This diaper, triggered by mantle fluid-heat flow, resulted in emplacement of melt-weakened migmatitic crust characterized by large dome-like structures and regional isoclinal folds at the mid-crustal level before ca. 2.68 Ga. Regional-scale gravitational crustal overturn of complex morphology and dynamics at this crucial mid-crustal level directed southwards near-horizontal channelling of a hot SMZ nappe from underneath the CZ and along the flat-lying HRSZ against and over the adjacent NKVC for a distance of ca. 35 km before ca. 2.68 Ga (time of emplacement of the Matok pluton). The subsequent exhumation of the CZ at 2.65–2.61 Ga to the upper crustal level was controlled by extensive granitic diapirism associated with the formation of steep SW-plunging mega closed structures characterized by intensely sheared gneisses.

After southward thrusting, the hot SMZ nappe experienced static high-temperature retrograde hydration at 2.68–2.62 Ga related to infiltration of aqueous-carbonic fluids along the underlying flat-lying HRSZ and derived from devolatilization of lower grade greenstone material that underlies more than 60% of the SMZ (inset map in Fig. 8.3). The observation that high-grade SMZ lithologies and typical granite-greenstone lithologies of the NKVC share similar geochemical signatures (Kreissig et al. 2000) is a direct consequence of the proposed orogenic model that links the exhumation history of the SMZ to a pre-existing granite-greenstone-type crust.

Although this paper focuses on evidence for a linked evolution of the SMZ and CZ at 2.72–2.61 Ga, and the relationship of the SMZ with the NKVC, the proposed crustal-scale granulite diapir can be easily expanded (Fig. 8.24) to include exhumation of the NMZ, that is shown to also have been driven by extensive granitic diapirism in the interval 2.74–2.57 Ga (Blenkinsop 2011).

The proposed gravity-driven Neoarchaean Limpopo orogeny reflected by exhumation and regional-scale gravitational crustal overturn of complex morphology and dynamics might also be applicable to the evolution of other Archaean granulite-facies terranes located within granite-greenstone cratons. Data presented and discussed in this paper argues against the concept of a continental collision at ca. 2.72 Ga associated with burial and crustal thickening.

Acknowledgements This study was supported by grants from the National Science Foundation (NRF) of South Africa (GUN: 81040 to DvR), the University of Johannesburg (DvR), and James Cook University (JMH). The authors would like to thank Steve McCourt and Leonid Aranovich for their time and effort to produce highly informed objective and critical reviews of the manuscript. Steve McCourt is especially thanked for being willing to review a completely restructured version of the paper.

References

Andreoli MAC, Brandl G, Kramers JD, Mouri H (2011) Intracrustal radioactivity as an important heat source for Neoarchean metamorphism in the Central Zone of the Limpopo complex. In: van Reenen DD, Kramers JD, McCourt S, Perchuk LL (eds) Origin and evolution of Precambrian high grade gneiss terranes, with special emphasis on the Limpopo complex of Southern Africa, vol 207. Geological Society of America memoirs, pp 143–161

Aranovich LY, Newton RC (1999) Experimental determination of CO2–H2O activity-composition relations at 600–1000 °C and 6–14 kbar by reversed decarbonation and dehydration reactions. Am Mineral 84:1319–1332

Armstrong RA, Wilson AH (2000) SHRIMP U-Pb study of zircons from the layered sequence of the Great Dyke, Zimbabwe, and a granitoid anatectic dyke. Earth Planet Sci Lett 180:1–12

Bahnemann KP (1972) A review of the structure, the stratigraphy and the metamorphism of the basement rocks of the Messina District, Northern Transvaal. Dissertation, University of Pretoria

Baker J, van Reenen DD, Van Schalkwyk JF, Newton RC (1992) Constraints on the composition of fluids involved in retrograde anthophyllite formation in the Limpopo Belt, South Africa. Precambr Res 55:327–336

Barton JM Jr, van Reenen DD (1992) When was the Limpopo Orogeny? Precambr Res 55:7–16

Belyanin G, van Reenen DD, Safonov OG (2014) Response to comments on "ultrahigh-temperature metamorphism from an unusual corundum-orthopyroxene intergrowth bearing Al-Mg granulite from the southern Marginal Zone, Limpopo complex, South Africa (Belyanin et al. 2012)" by Nicoli et al. (2014). Contrib Mineral Petrol 167:1–5

Belyanin GA, Kramers JD, Vorster C, Knoper MD (2015) The timing of successive fluid events in the Southern Marginal Zone of the Limpopo complex, South Africa: constraints from ^{40}Ar-^{39}Ar geochronology. Precambr Res 254:169–193

Blenkinsop TG, Mkweli, S, Rollinson H, Fedo CM, Paya BK, Kamber BS, Kramers JD, Berger M (1995) The North Limpopo Thrust Zone (NLTZ): the northern boundary of the Limpopo belt in Zimbabwe and Botswana. In: Extended abstracts, Centennial Geocongress 95, geological society of South Africa, pp 174–177

Blenkinsop TG, Kröner A, Chiwara V (2004) Single stage, late Archaean exhumation of granulites in the Northern Marginal Zone, Limpopo Belt, Zimbabwe, and relevance to gold mineralization at Renco Mine. S Afr J Geol 107:377–396

Blenkinsop TG (2011) Archean magmatic granulites, diapirism, and Proterozoic reworking in the Northern Marginal Zone of the Limpopo Belt. In: van Reenen DD, Kramers JD, McCourt S, Perchuk LL (eds) Origin and evolution of precambrian high grade gneiss terranes, with special emphasis on the Limpopo complex of Southern Africa, vol 207. Geological society of America memoirs, pp 245–267

Bohlender F, van Reenen DD, Barton JM Jr (1992) Evidence for metamorphic and igneous charnockites in the Southern Marginal Zone of the Limpopo Belt. Precambr Res 55:429–449

Boshoff R, van Reenen DD, Smit CA, Perchuk LL, Kramers JD, Armstrong R (2006) Geologic history of the central zone of the Limpopo complex: the west Alldays area. J Geol 114:699–716

Brown M (2007) Crustal melting and melt extraction, ascent and emplacement in orogens: mechanisms and consequences. J Geol Soc Lond 164:709–730

Brandt S, Klemd R, Li Q, Kröner A, Brandl G, Fischer A, Bobek P, Zhou T (2018) Pressure-temperature evolution during two granulite-facies metamorphic events (2.62 and 2.02 Ga) in rocks from the central zone of the Limpopo Belt. South Africa Precambr Res 310:471–506

Cagnard F, Barbey P, Gapais D (2011) Transition between "Archaean-type" and "modern-type" tectonics: insights from the Finnish Lapland Granulite Belt. Precambr Res 187:127–142

Chardon D, Gapais D, Cagnard F (2009) Flow and ultra-hot orogens: a view from the Precambrian, clues for the Phanerozoic. Tectonophysics 477:105–118

De Beer JH, Stettler EH (1988) Geophysical characteristics of the southern African Continental Crust. J Petrol 1:163–184

De Beer JH, Stettler EH (1992) The deep structure of the Limpopo Belt from geophysical studies. Precambr Res 55:173–186

De Beer JH, Le Roux CL, Hanstein T, Stack KM (1991) DC resistivity and LOTEM model for the deep structure of the northern edge of the Kaapvaal craton, South Africa. Phys Earth Planet Inter 66:51–61

De Wit MJ, Jones MG, Buchanan DL (1992a) The geology and tectonic evolution of the Pietersburg greenstone belt, South Africa. Precambr Res 55:123–153

De Wit MJ, van Reenen DD, Roering C (1992b) Geologic observations across a tectono-metamorphic boundary in the Babangu area, Giyani (Sutherland) greenstone belt, South Africa. Precambr Res 55:111–122

De Wit MJ, Roering C, Hart RJ, Armstrong RA, De Ronde CEJ, Green RWE, Tredoux M, Peberdy E, Hart RA (1992c) Formation of an Archean continent. Nature 357:553–562

Dorland HC, Beukes NJ, Gutzmer J, Evans DAD, Armstrong RA (2004) Trends in detrital zircon provenance from Neoarchaean Paleoproterozoic sedimentary successions in the Kaapvaal Craton. Geoscience Africa 2004, Abstract Volume, University of the Witwatersrand, Johannesburg, South Africa, pp 176–177

Du Toit MC, van Reenen DD, Roering C (1983) Some aspects of the geology, structure and metamorphism of the Southern Marginal Zone of the Limpopo metamorphic complex. Spec Publ Geol Soc S Afr 8:89–102

Dubinina EO, Aranovich LYA, van Reenen DD, Avdeenco AS, Varlamov DA, Kurdyukov EB, Shaposhnikov VV (2015) Oxygen isotope systematics of the high-grade rocks of the Southern Marginal Zone of the Limpopo complex. Precambr Res 256:48–61

Durrheim RJ, Barker WH, Green RWE (1992) Seismic studies in the Limpopo belt. Precambr Res 55:187–200

Ellis DJ (1987) Origin and evolution of granulites in normal and in thickened crust. Geology 15:167–170

England PC, Thompson AB (1984) Pressure-temperature-time paths of regional metamorphism. I. Heat transfer during the evolution of regions of thickened continental crust. J Petrol 25:894–928

Fripp REP, Lilly PA, Barton JM Jr (1979) The structure and origin of the Singelele Gneiss, Limpopo mobile belt, South Africa. Trans Geol Soc S Afr 82:161–167

Gerya TV, Perchuk LL, van Reenen DD, Smit CA (2000) Two-dimensional numerical modeling of pressure-temperature-time paths for the exhumation of some granulite facies terranes in the Precambrian. J Geodyn 30:17–35

Gan SF, van Reenen DD (1995) Geology of gold deposits in the Southern Marginal Zone of the Limpopo Belt and the adjacent Sutherland Greenstone Belt, South Africa: Franke mine. S Afr J Geol 98:263–275

Gan SF, van Reenen DD (1997) Geology of gold deposits in the Southern Marginal Zone of the Limpopo Belt and adjacent Sutherland Greenstone Belt, South Africa: Klein Letaba. S Afr J Geol 100:73–83

Gibson RL (2019) The Mesoarchaean Basement Complex of the Vredefort Dome—A Mid-Crustal Section Through the Central Kaapvaal Craton Exposed by Impact. In: Kröner A, Hofmann A (eds) The Archaean Geology of the Kaapvaal Craton, Southern Africa. Regional geology reviews. Springer International Publishing AG

Hoernes S, van Reenen DD (1992) The oxygen isotopic composition of granulites and retrogressed granulites from the Limpopo Belt as a monitor of fluid-rock interaction. Precambr Res 55:353–364

Hoernes S, Lichtenstein U, van Reenen DD, Mokgatla KP (1995) Whole rock/mineral O-isotope fractionations as a tool to model fluid-rock interaction. Precambr Res 55:353–364

Hofmann A, Kröner A, Brandl G (1998) Field relationships of mid-to late Archaean high-grade gneisses of igneous and sedimentary parentage in the Sand River, Central Zone of the Limpopo Belt, South Africa. S Afr J Geol 101:185–200

Holland TJB, Powell R (1998) An internally consistent thermodynamic data set for phases of petrological interest. J Metamorph Geol 16:309–343

Horrocks PC (1983) The Precambrian geology of an area between Messina and Tshipise, Limpopo mobile belt. In: Van Biljon WJ, Legg JH (eds) The Limpopo Mobile Belt, vol 8. Special publication of the geological society of South Africa, pp 81–88

Huizenga JM, Perchuk LL, van Reenen DD, Varlamov DA, Smit CA, Gerya TV (2011) Granite emplacement and the retrograde P-T-fluid evolution of Neoarchean granulites from the CZ of the Limpopo complex. Geol Soc Am Mem 207:125–142

Huizenga JM, van Reenen DD, Touret JLR (2014) Fluid-rock interaction in retrograde granulites of the Southern Marginal Zone, Limpopo high-grade terrain, South Africa. Geosci Front 5:673–682

Jaguin J, Gapais D, Poujol M, Boulvais P, Moyen J-F (2012) The Murchison greenstone belt (South Africa): a general tectonic framework. S Afr J Geol 115:65–76

Jamieson RA, Unsworth MJ, Harris NB, Rosenberg CL, Schulmann K (2011) Crustal melting and the flow of mountains. Elements 7:253–260

Klemperer SL (1992) Introduction: deep crustal probing. Precambr Res 55:169–172

Kleywegt RJ (1988) Gravity signature of the Limpopo-Kaapvaal fossil plate boundary in southern Africa-discussion. Tectonophysics 145:349–350

Kleywegt RJ, De Beer JH, Stettler EH, Brandl G, Duvenhage AWA, Day RW (1987) The structure of the Giyani greenstone belt, as derived from geophysical studies. S Afr J Geol 90:282–295

Koizumi T, Tsunogae T, van Reenen DD (2014) Fluid evolution of partially retrogressed pelitic granulite from the Southern Marginal Zone of the Neoarchean Limpopo complex, South Africa: Evidence from phase equilibrium modelling. Precambr Res 253:146–156

Koons PO, Craw D (1991) Evolution of fluid driving forces and composition within collisional orogens. Geophys Res Lett 280: 935–938

Koons PO, Craw D, Cox S, Upton P, Templeton A, Chamberlain CP (1998) Fluid flow during active oblique convergence: a Southern Alps model from mechanical and geochemical observations. Geology 26:159–162

Kramers JD, Mouri H (2011) The geochronology of the Limpopo complex: a controversy solved. In: van Reenen DD, Kramers JD, McCourt S, Perchuk LL (eds) Origin and evolution of Precambrian high grade gneiss terranes, with special emphasis on the Limpopo complex of Southern Africa, vol 207. Geological Society of America Memoirs, pp 85–106

Kramers JD, Zeh A (2011) A review of Sm-Nd and Lu-Hf isotope studies in the Limpopo complex and adjacent cratonic areas, and their bearing on models of crustal evolution and tectonism. In: van Reenen DD, Kramers JD, McCourt S, Perchuk LL (eds) Origin and evolution of Precambrian high grade gneiss Terranes, with special emphasis on the Limpopo complex of Southern Africa, vol 207. Geological Society of America memoirs, pp 163–188

Kramers JD, Henzen M, Steidle L (2014) Greenstone belts at the northernmost edge of the Kaapvaal Craton: timing of tectonic events and a possible crustal fluid source. Precambr Res 253:96–113

Kramers JD, McCourt S, van Reenen DD (2006) The Limpopo Belt. In: Johnson MR, Anhaeusser CR, Thomas RJ (eds) The geology of South Africa. Geological Society of South Africa, Council for Geoscience, Johannesburg, Pretoria, pp 209–236

Kramers JD, McCourt S, Roering C, Smit CA, van Reenen DD (2011) Tectonic models proposed for the Limpopo complex: mutual compatibilities and constraints. In: van Reenen DD, Kramers JD, McCourt S, Perchuk LL (eds) Origin and evolution of Precambrian high grade gneiss Terranes, with special emphasis on the Limpopo complex of Southern Africa, vol 207. Geological Society of America memoirs, pp 311–324

Kreissig K, Nägler TF, Kramers JD, van Reenen DD, Smit CA (2000) An isotopic and geochemical study of the northern Kaapvaal craton and the Southern marginal zone of the Limpopo Belt: are they juxtaposed terranes? Lithos 50:1–25

Kreissig K, Holzer L, Frei IM, Villa JD, Kramers JD, Kröner A, Smit CA, van Reenen DD (2001) Geochronology of the Hout River Shear Zone and the metamorphism in the Southern Marginal Zone of the Limpopo belt, Southern Africa. Precambr Res 109:145–173

Kröner A, Jaeckel P, Brandl G (2000) Single zircon ages for felsic to intermediate rocks from the Pietersburg and Giyani greenstone belts and bordering granitoid orthogneisses, northern Kaapvaal Craton, South Africa. J Afr Earth Sci 30:773–793

Kröner A, Jaeckel P, Hofmann A, Nemchin AA, Brandl G (1998) Field relationships and age of supracrustal Beit Bridge complex and associated granitoid gneisses in the central zone of the Limpopo Belt, South Africa. S Afr J Geol 101:201–213

Kröner A, Jaeckel P, Brandl G, Nemchin AA, Pidgeon RT (1999) Single zircon ages for granitoids gneisses in the central zone of the Limpopo belt, southern Africa and geodynamic significance. Precambr Res 93:299–337

Kröner A, Brandl G, Brandt S, Klemd R, Xie H (2018) Geochronological evidence for three granulite-facies tectono-metamorphic events in the central zone of the Limpopo Belt, South Africa. Precambr Res 310:320–347

Laurent O, Paquette JL, Doucelance R, Martin H, Moyen JF (2013) Crustal growth and evolution in the northern Kaapvaal craton inferred by LA-ICP-MS dating of zircons from Meso- and Neoarchaean granitoids. Precambr Res 230:209–226

Laurent O, Zeh A, Brandl G, Vezinet A, Wilson A (2019) Granitoids and Greenstone Belts of the Pietersburg Block—Witnesses of an Archaean Accretionary Orogeny Along the Northern Edge of the Kaapvaal Craton. In: Kröner A, Hofmann A (eds) The Archaean Kaapvaal Craton, Southern Africa. Regional Geology Reviews. Springer International Publishing AG

Lexa O, Schulmann K, Janoušek V, Štípská P, Guy A, Racek M (2011) Heat sources and trigger mechanisms of exhumation of HP granulites in Variscan orogenic root. J Metamorph Geol 29:79–102

Light MPR (1982) The Limpopo Belt, Southern Africa: a result of continental collision. Tectonics 1:325–342

Mahan KH, Smit CA, Williams ML, Dumond G, van Reenen DD (2011) Scales of heterogeneous strain and polymetamorphism in high-grade terranes: insight from the Athabasca Granulite Terrane, western Canada and the Limpopo complex, southern Africa. In: van Reenen DD, Kramers JD, McCourt S, Perchuk LL (eds) Origin and evolution of Precambrian high-grade gneiss terranes, with special emphasis on the Limpopo complex of Southern Africa, vol 207. Geological Society of America memoirs, pp 269–287

Mason R (1973) The Limpopo mobile belt: southern Africa. Philos Trans R Soc Lond Series A 273:463–485

McCourt S, van Reenen DD (1992) Structural geology and tectonic setting of the Sutherland greenstone belt, Kaapvaal Craton, South Africa. Precambr Res 55:93–110

Millonig L, Zeh A, Gerdes R, Klemd R (2008) Neoarchaean high-grade metamorphism in the central zone of the Limpopo Belt (South Africa): Combined petrological and geochronological evidence from the Bulai pluton. Lithos 103:333–351

Miyano T, Ogata H, van Reenen DD, Van Schalkwyk JF, Arawaka Y (1992) Peak metamorphic conditions of sapphirine-bearing rocks in the Rhenosterkoppies greenstone belt, Northern Kaapvaal Craton, South Africa. In: Clover JE, Ho SE (eds) The Archean terranes, processes and metallogeny, vol 27. Geology Department (Key Centre), the University of Western Australia, pp 73–87

Nicoli G, Stevens G, Moyen JF, Frei D (2015) Rapid evolution from sediment to anatectic granulite in an Archean continental collision zone: the example of the Bandelierkop Formation metapelites, South Marginal Zone, Limpopo Belt, South Africa. J Metamorph Geol 33:177–202

Passeraub M, Wuest T, Kreissig K, Smit CA, Kramers JD (1999) Structure, metamorphism, and geochronology of the Rhenosterkoppies greenstone belt, South Africa. S Afr J Geol 102:323–334

Perchuk AL, Safonov OG, Smit CA, van Reenen DD, Zakharov VS, Gerya TV (2018) Precambrian ultra-hot orogenic factory: making and reworking of continental crust. Tectonophysics 746:572–586

Perchuk LL (2011) Local mineral equilibria and P-T paths: fundamental principles and their application for high-grade metamorphic terrains. In: van Reenen DD, Kramers JD, McCourt S, Perchuk LL (eds) Origin and evolution of Precambrian high-grade gneiss terranes, with special emphasis on the Limpopo complex of Southern Africa, vol 207. Geological Society of America memoirs, pp 61–84

Perchuk LL, van Reenen DD (2008) Reply to "comments on "P–T record of two high-grade metamorphic events in the central zone of the Limpopo complex, South Africa" by A Zeh and R Klemd. Lithos 106:403–410

Perchuk LL, Gerya TV (2011) Formation and evolution of Precambrian granulite terranes: a gravitational redistribution model. In: van Reenen DD, Kramers JD, McCourt S, Perchuk LL (eds) Origin and evolution of Precambrian high grade gneiss terranes, with special emphasis on the Limpopo complex of Southern Africa, vol 207. Geological Society of America memoirs, pp 289–310

Perchuk LL, Gerya TV, van Reenen DD, Safanov OG, Smit CA (1996) The Limpopo metamorphic complex, South Africa: 2 decompression/cooling regimes of granulites and adjacent rocks of the Kaapvaal Craton. Petrology 4:571–599

Perchuk LL, Gerya TV, van Reenen DD, Krotov AV, Safonov OG, Smit CA, Shur MYu (2000a) Comparative petrology and metamorphic evolution of the Limpopo (South Africa) and Lapland (Fennoscandia) high-grade terrains. Mineral Petrol 69:69–107

Perchuk LL, Gerya TV, van Reenen DD, Smit CA, Krotov AV (2000b) P-T paths and tectonic evolution of shear zones separating high-grade terrains from cratons, examples from Kola Peninsula (Russia) and Limpopo region (South Africa). Mineral Petrol 69:109–142

Perchuk LL, van Reenen DD, Smit CA, Boshoff R, Belyanin GA, Yapaskurt VO (2008a) Role of granite intrusions for the formation of ring structures in granulite complexes: examples from the Limpopo Belt, South Africa. Petrology 16:652–678

Perchuk LL, van Reenen DD, Varlamov DA, van Kal SM, Boshoff R (2008b) P-T record of two high-grade metamorphic events in the central zone of the Limpopo complex, South Africa. Lithos 103:70–105

Pili E, Shepard SMF, Lardeaux JM, Martelat JF, Nicollete C (1997) Fluid flow versus scale of shear zones in the lower continental crust and the granulite paradox. Geology 25:15–18

Pretorius JM (1988) BIF-hosted gold mineralization at the Fumani Mine, Sutherland greenstone belt, South Africa. S Afr J Geol 91:429–438

Rajesh HM, Santosh M, Wan Y, Liu SJ, Belyanin GA (2014) Ultrahigh temperature granulites and magnesium charnockites: evidence for Neoarchean accretion along the northern margin of the Kaapvaal Craton. Precambr Res 246:150–159

Retief EA, Compston W, Armstrong RA, Williams IS (1990) Characteristics and preliminary U-Pb ages of zircons from Limpopo Belt lithologies. In: Barton JM Jr (ed) Extended abstract volume, the Limpopo Belt: a field workshop on granulites and deep crustal tectonites, pp 100–101

Rey PF, Teyssier C, Whitney DL (2009) Extension rates, crustal melting, and core complex dynamics. Geology 37:391–394

Roering C, De Beer JH, van Reenen DD, Wolhuter LE, Baton JM Jr, Smit CA, McCourt S, Du Plessis A, Stettler EH, Brandl G, Pretorius SJ, Van Schalkwyk JF, Geerthsen K (1990) A geotransect across the Limpopo belt. In: Barton JM Jr (ed) Extended abstract volume, the Limpopo Belt: a field workshop on granulites and deep crustal tectonites, pp 105–106

Roering C, van Reenen DD, De Wit MJ, Smit CA, De Beer JH, Van Schalkwyk JF (1992a) Structural geological and metamorphic significance of the Kaapvaal Craton/Limpopo Belt contact. Precambr Res 55:69–80

Roering C, van Reenen DD, Smit CA, Barton JM Jr, De Beer JH, De Wit MJ, Stettler EH, Van Schalkwyk JF, Stevens G, Pretorius S (1992b) Tectonic model for the evolution of the Limpopo Belt. Precambr Res 55:539–552

Roering C, van Reenen DD, Smit CA, Du Toit R (1995) Deep crustal embrittlement and fluid flow during granulite metamorphism in the Limpopo Belt, South Africa. J Geol 103:673–686

Safonov OG, Tatarinova DS, van Reenen DD, Golunova MA, Yapaskurt VO (2014) Fluid-assisted interaction of peraluminous metapelites with tonalitic magma in the Southern Marginal Zone of the Limpopo complex. Precambr Res 253:114–145

Safonov OG, Tatarinova DS, Japaskurt WO, van Reenen DD, Gognova, MA, Varlamov DA, Smit CA (2018a) In source melting of metapelite from the Petronella shear zone, Limpopo complex South Africa: constraints from petrological studies and experiments. J Petrol. https://doi:10.1093/petrology/egy052

Safonov OG, Vadim N, Reutsky VN, Varlamov DA, Yapaskurt VA, Golunova MA, Shcherbakov VD, van Reenen DD, Smit CA, Butvina VG (2018b) Composition and source of fluids in high-temperature graphite-bearing granitoids associated with granulites: examples from the Southern Marginal Zone, Limpopo complex, South Africa. Gondwana Res 60:129–152

Sawyer EW, Cesare B, Brown M (2011) When the continental crust melts. Elements 7:229–234

Schmitz MD, Bowring SA (2003) Utrahigh-temperature metamorphism in the lower crust during Neoarchean Ventersdorp rifting and magmatism, Kaapvaal Craton, southern Africa. GSA Bull 115:533–548

Schulmann K, Lexa O, Štípská P, Racek M, Tajčmanová L, Konopásek J, Edel JB, Pechler A, Lehmann J (2008) Vertical extrusion and horizontal channel flow of orogenic lower crust: key exhumation mechanisms in large hot orogens? J Metamorph Geol 26:273–297

Smit CA, van Reenen DD (1997) Deep crustal shear zones, high-grade tectonites and associated alteration in the Limpopo belt, South Africa: implication for deep crustal processes. J Geol 105:37–57

Smit CA, Roering C, van Reenen DD (1992) The structural framework of the southern margin of the Limpopo Belt, South Africa. Precambr Res 55:51–67

Smit CA, van Reenen DD, Roering C (2014) Role of fluids in the exhumation of the Southern Marginal Zone of the Limpopo complex, South Africa. Precambr Res 253:81–95

Smit CA, van Reenen DD, Gerya TV, Perchuk LL (2001) P-T conditions of decompression of the Limpopo high-grade terrain: record from shear zones. J Metamorph Geol 19:249–268

Smit CA, van Reenen DD, Roering C, Boshoff R, Perchuk LL (2011) Neoarchean to Paleoproterozoic evolution of the polymetamorphic central zone of the Limpopo complex. In: van Reenen DD, Kramers JD, McCourt S, Perchuk LL (eds) Origin and evolution of Precambrian high grade gneiss terranes, with special emphasis on the Limpopo complex of Southern Africa, vol 207. Geological Society of America memoirs, pp 213–244

Stettler EH, De Beer JH, Blom MP (1989) Crustal domains in the northern Kaapvaal Craton as defined by magnetic lineaments. Precambr Res 45:263–276

Stuart GW, Zengeni T (1987) Seismic crustal structure of the Limpopo mobile belt, Zimbabwe. Tectonophysics 144:323–335

Taylor J, Nicole G, Stevens G, Fry ED, Moyne JF (2014) A process that controls leucosome composition in metasedimentary granulites: perspective from the Southern Marginal Zone, Limpopo complex, South Africa. J Metamorph Geol 32:713–742

Thompson AB (1990) Heat, fluids and melting in the granulite facies. In: Vielzeuf D, Vidal PH (eds) Granulites and crustal evolution. Kluwer Academic Publishers, pp 37–57

Treloar P, Coward MP, Harris NBW (1992) Himalayan-Tibetan analogies for the evolution of the Zimbabwe Craton and the Limpopo Belt. Precambr Res 55:571–587

Tsunogae T, van Reenen DD (2011) High-pressure and high-temperature metamorphism of Precambrian high-grade terranes: case study of the Limpopo Complex. In: van Reenen DD, Kramers JD, McCourt S, Perchuk LL (eds) Origin and evolution of Precambrian high grade gneiss terranes, with special emphasis on the Limpopo complex of Southern Africa, vol 207. Geological Society of America memoirs, pp 107–1214

Tsunogae T, van Reenen DD (2014) High- to ultrahigh-temperature metasomatism related to brine infiltration in the Neoarchaean Limpopo complex. Petrology and phase equilibrium modeling. Precambr Res 253:157–170

Tsunogae T, Miyano T, van Reenen DD, Smit CA (2004) Ultrahigh-temperature metamorphism of the southern marginal zone of the Archean Limpopo Belt, South Africa. J Miner Petrol Sci 99:213–224

van Reenen DD (1983) Cordierite+garnet+hyperthene+biotite-bearing assemblages as a function of changing metamorphic conditions in the Southern Marginal Zone of the Limpopo metamorphic complex, South Africa. In: Van Biljon WJ, Leg JH (eds) The Limpopo Belt, vol 8. Special publication of the Geological Society of South Africa, pp 143–167

van Reenen DD (1986) Hydration of cordierite and hypersthenes and description of the retrograde orthoamphibole isograd in the Limpopo Belt, South Africa. Am Mineral 71:900–915

van Reenen DD, Du Toit MC (1977) Mineral reactions and the timing of metamorphic events in the Limpopo Metamorphic complex south of the Soutpansberg. Bull Bots Geol Surv 12:107–128

van Reenen DD, Hollister LS (1988) Fluid inclusions in hydrated granulite facies rocks, Southern Marginal Zone of the Limpopo Belt, South Africa. Geochim Cosmochim Acta 52:1057–1064

van Reenen DD, McCourt S, Smit CA (1995) Are the Southern and Northern Marginal Zones of the Limpopo Belt related to a single continental collisional event? S Afr J Geol 98:489–504

van Reenen DD, Barton JM Jr, Roering C, Smit CA, Van Schalkwyk JF (1987) Deep crustal response to continental collision: the Limpopo Belt of South Africa. Geology 15:11–14

van Reenen DD, Roering C, Brandl G, Smit CA, Barton JM Jr (1990) The granulite facies rocks of the Limpopo Belt, southern Africa. In: Vielzeuf D, Vidal PH (eds) Granulites and crustal evolution. Kluwer Academic Publishers, pp 257–289

van Reenen DD, Boshoff R, Smit CA, Perchuk LL, Kramers JD, McCourt SM, Armstrong RA (2008) Geochronological problems related to polymetamorphism in the Limpopo Complex, South Africa. Gondwana Res 14:644–662

van Reenen DD, Smit CA, Perchuk LL, Roering C, Boshoff R (2011) Thrust exhumation of the Neoarchean ultrahigh-temperature Southern Marginal Zone, Limpopo Complex: Convergence of decompression-cooling paths in the hanging wall and prograde P-T paths in the footwall. In: van Reenen DD, Kramers JD, McCourt S, Perchuk LL (eds) Origin and evolution of precambrian high grade gneiss terranes, with special emphasis on the Limpopo Complex of Southern Africa, vol 207. Geological Society of America memoirs, pp 189–212

van Reenen DD, Huizenga JM, Smit CA, Roering C (2014) High-temperature fluid-rock interaction: instructive examples from the Southern Marginal Zone of the Limpopo complex. Precambr Res 253:63–80

Van Schalkwyk JF (1991) Metamorphism of ultramafic rocks during the Limpopo orogeny: evidence from the timing and significance of CO_2-rich fluids. Rand Afrikaans University

Van Schalkwyk JF, van Reenen DD (1992) High temperature hydration of ultramafic granulites from the Southern Marginal Zone of the Limpopo Belt by infiltration of CO_2-rich fluid. Precambr Res 55:337–352

Vezinet A, Moyen JF, Stevens G, Gautier N, Laurent O, Couzinié S, Frei D (2018) A record of 0.5 Ga of evolution of the continental crust along the northern edge of the Kaapvaal Craton, South Africa: consequences for the understanding of Archean geodynamic processes. Precambr Res 305:310–326

Watkeys MK, Light MPR, Broderick RJ (1983) A retrospective view of the central zone of the Limpopo Belt, Zimbabwe. In: Van Biljon WJ, Leg JH (eds) The Limpopo Belt, Special publication of the Geological Society of South Africa, vol 8, pp 65–80

Whitney DL, Evans BW (2010) Abbreviations for names of rock-forming minerals. Am Mineral 95:185–187

Yardley BWD (2009) The role of water in crustal evolution. J Geol Soc Lond 166:585–600

Zeh A, Klemd R, Buhlmann S, Barton JM (2004) Prograde-retrograde P-T evolution of granulites of the Beit Bridge Complex (Limpopo Belt, South Africa): Constraints from quantitative phase diagrams and geotectonic implications. J Metamorph Geol 22:79–95

Zeh A, Klemd R (2008) Comments on "P-T record of two high-grade metamorphic events in the central zone of the Limpopo complex, South Africa" by LL Perchuk, DD van Reenen, DA Varlamov, SM van Kal, Tabatabaeimanesh. R Boshoff Lithos 106:403–410

Zeh A, Jaguin J, Poujol M, Boulvais P, Block S, Paquette JL (2013) Juvenile crust formation in the Northeastern Kaapvaal Craton at 2.97 Ga, implications for Archean terrane accretion, and the source of the Petersburg gold. Precambr Res 233:2–43